SOME EFFECTS OF MICROSTRUCTURE ON THE FRACTURE OF STEEL

SOME EFFECTS OF MICROSTRUCTURE ON THE FRACTURE OF STEEL

By

DONALD EARL OSBORNE, B.A.Sc.

A Thesis

Submitted to the School of Graduate Studies

in Partial Fulfilment of the Requirements

for the Degree

Master of Engineering

McMaster University

May, 1972

MASTER OF ENGINEERING (1972)
(Metallurgy and Materials Science)

McMASTER UNIVERSITY
Hamilton, Ontario

TITLE: Some Effects of Microstructure on the Fracture of Steel

AUTHOR: Donald Earl Osborne, B. A. Sc. (University of Windsor)

SUPERVISOR: Professor J. D. Embury

NUMBER OF PAGES: vii; 156

ABSTRACT

The fracture behaviour of a medium strength bainitic steel (SAE 4340 in the "as transformed and in the "warm rolled" condition) and four carbon-manganese structural steels (in the hot rolled ferrite-pearlite condition) was investigated. The purpose was to isolate those features of the microstructure which exert control over the fracture properties.

The detailed nature of the microstructure of the steels was studied with transmission and scanning electron microscopy, qualitative x-ray analysis and quantitative metallography. An attempt was made to correlate the fracture behaviour with the microstructure through models which relate the fracture properties to the unnotched tensile properties.

In the case of the bainitic steels it was found that the carbide morphology, dislocation substructure and prior austenite grain size have the major influence on fracture properties. In contrast, the fracture properties of the structural steels were controlled by the volume fraction of inclusions and to some extent by the shape of the inclusions.

ACKNOWLEDGMENTS

It is a pleasure to express gratitude to those members of the Department of Metallurgy and Materials Science who assisted in this work. The author is sincerely grateful to Dr. J. D. Embury for his advice and encouragement throughout the duration of the program.

Special thanks are due to Mrs. A. S. Miltimore for rapidly and accurately typing this thesis; to Mr. M. van Oosten for his work on the drawings; and to Mr. J. Whorwood for his work on the photographs.

The author is also grateful to Mr. D. McCutcheon and members of the Research Centre of the Steel Company of Canada Limited for their help with the quantitative metallography and for supplying much of the data for the structural steels.

The financial support of the National Research Council of Canada is gratefully acknowledged.

Finally, the author is indebted to the members of the "deformation group": Malcolm Brown, Jack Morrison, Nabil Ibrahim and Gerry Moan for their advice and criticism through the months.

TABLE OF CONTENTS

CHAPTER I

INTRODUCTION: A DEFINITION OF THE PROBLEM

1.1 Survey of the Literature

Increasing recognition is being given to the economic advantages that high-strength low-alloy steels have to offer. Some of these advantages include lower cost structural components, increased resistance to brittle failure, and ease of forming welding and other fabrication procedures. Service conditions require that the steel exhibits good toughness at service temperatures.

The development of the strength properties of steels can be illustrated by use of a diagram such as that shown in Figure 1. The base line in the diagram is the relationship between yield strength and grain size obtained by Pickering and Gladman.

During the first half of this century, much of the steel produced for use as hot-rolled products consisted of plain carbon and carbon-manganese steels having a ferrite-pearlite microstructure. Because of concern over fabrication problems, carbon contents were limited to about .25%. Yield strengths were of the order of 50 ksi. It has been shown that the base strength of these steels is determined by the ferrite grain size and the lattice friction stress of iron. (Petch 1953) Additional strength is derived from pearlite and solid solution hardening. (Pickering 1963, Grozier 1967)

Over the past ten years, high-strength niobium and vanadium grades of carbon-manganese steels have been developed. The use of niobium and vanadium increased the yield strength of these hot-rolled steels to about

65 ksi. This is due to their ability to refine grain size and to produce precipitation hardening with fine dispersions of carbides, nitrides and carbonitrides. (Gray 1965)

By adding small amounts of molybdenum and boron to low-carbon base steels, it is possible to achieve yield strengths in the range of 70 ksi in hot-rolled products. These low-carbon moly-boron steels derive their strength from bainitic microstructures, with the amount of strengthening related to the transformation temperature (Irvine 1957). During the past ten years there has been considerable progress in the understanding of the transformation structures in steel and in the correlation of the microstructural features with mechanical properties. As a result, it has become possible to improve the properties of steel and to determine the preferred method of obtaining the improved property when many methods are available.

An increase in one property can usually only be achieved at the expense of another. This is particularly so when increases in strength are made. There is usually an accompanying reduction in ductility and toughness.

As strength levels in steels are increased, experience has shown that two of the most important material properties for component reliability are resistance to crack propagation (fracture toughness) and resistance to environmentally induced delayed failure (stress corrosion) (Ault 1967). At high strength levels, unnotched tensile properties such as yield strength and reduction in area have little bearing on component reliability. High strength steels are susceptible to catastrophic failure at design stresses considerably below their yield strength.

This growing understanding of the factors controlling the mechanical properties of steels (such as those of high strength steels which contribute to the behaviour mentioned above) has led to a variety of ways of achieving desired strength and toughness properties. There are a number of continuous cooling and controlled cooling methods to control microstructure and thus the

mechanical properties of steels. However, often these "conventional" heat treatments of low alloy and alloy steels cannot always meet current engineering requirements for improved strength without sacrifice of ductility and toughness. One of the avenues available for achieving improved mechanical properties and thus improved reliability in high strength steel is the use of combined thermal and mechanical treatments.

Thermal-mechanical treatments can be divided into three basic groups. The optimum in material properties are generally obtained by using high deformations and a balanced alloy composition consistent with developing the strength required with each thermal-mechanical treatment.

The first of these groups is "deformation before transformation" which includes low temperature thermal-mechanical treatment (ausforming) and high temperature thermal-mechanical treatment. Ausforming can lead to improved strength without deterioration of ductility or impact strength (Duckworth 1964), or alternatively, for a given strength level, steels processed this way may be significantly tougher than conventionally treated steel for a given strength level. The strength increase obtained by high temperature thermal-mechanical treatment is not as great as in ausforming, but ductility and fatigue properties may be significantly increased.

The second of these groups is "deformation during transformation" (isoforming). Small improvements in strength may be achieved by isoforming (depending on the subgrain size) but the main advantage is the considerable increase in toughness developed in low-alloy steels with low subzero impact transition temperatures.

The third of these groups is "deformation following transformation" which includes dynamic strain ageing and warm rolling. Dynamic strain ageing produces considerable increases in strength in both quenched and tempered steels and ausformed steels, however it appears to lower the fracture toughness (Zackay 1965). The advantages of warm rolling vary with steel composition and deformation temperature. Warm rolling usually

produces an increase in yield and tensile strengths, however ductility and impact properties may increase or decrease. (Peterson 1963, Uvira 1970).

As was stated at the outset of this literature review, low carbon-low alloy steels have recently been developed which derive their increased strength from bainitic microstructures. These steels represent the next "step up" with respect to strength level in hot rolled continuously produced steels. Before discussing the benefits of thermal-mechanical and bainitic microstructures, it would be useful to make some comments on the relative merits of the bainitic transformation as a strengthening mechanism.

Normally a homogeneous bainite transformation is difficult to achieve in a low carbon steel because the bainite "C" curve is masked by the ferrite curve. Molybdenum and boron have a greater effect in retarding the ferrite transformation than the bainite transformation. Elements such as chromium depress the bainite transformation curve. Thus with specific alloy combinations, it is possible to control the transformation characteristics to obtain uniform properties over a reasonable range of cooling rates.

If steels of roughly the same carbon content and with a reasonable combination of strength and impact properties are compared, diagrams such as that shown in Figure 2 can be constructed which illustrates the combination of impact and yield strength properties obtainable. This diagram indicates that the properties obtained from a bainitic steel are challenged at the low end by ferrite-pearlite steels and at the high end by quenched and tempered steels.

In comparing the strength and impact properties of bainitic steels, it is necessary to separate the upper bainite from the lower bainite. This is due to the microstructural features which control the impact resistance. The impact resistance of the upper bainite structure is controlled mainly by the prior austenite grain size whereas that of the lower bainite structure

depends more on the bainitic ferrite grain size and the nature of the carbides precipitated in the ferrite. The prospects for improvement of bainitic steels then appear to lie mainly with thermal-mechanical treatments. As far as upper bainitic steels are concerned, refinements in austenite grain size and/or changes in carbide morphology and dislocation substructure should produce improvements in impact properties. The effects of controlled rolling are illustrated in Figure 3. With this comparison it can be seen that for certain property combinations, there is a choice of steel to obtain these properties. Controlled rolled bainites offer intermediate strength properties with the added economic advantage of continuous production.

The effects of thermal-mechanical treatments on D6-AC steel (modified 4340) have been investigated by Ault (1967). An investigation into thermal-mechanical treatments applied to bainitic steels was conducted by Kalish (1965). An excellent review article concerning the effects of thermal-mechanical treatments on engineering and tool steels by Latham (1970) reflects the improvements that these treatments can bring about.

1.2 Approach of the Present Study

As the strength of commercial steels is increased, increasing emphasis must be placed on obtaining reliable estimates of the materials resistance to crack propagation. The resistance to crack propagation (or fracture toughness) and Charpy impact energies offer ways in which to include the material toughness in specifications and design procedures.

Just as the other mechanical properties of steel are related to the detailed microstructure, so are the fracture toughness and Charpy impact energy. Some limited experiments have been conducted in order

to determine which features of the microstructure exert control over the toughness and which of these features exert the most effective control for a given steel.

The salient microstructural features which influence the fracture behaviour of steels appear to be grain size, carbide morphology and distribution, dislocation substructure, and inclusions. The effects of grain size on the cleavage stress of iron was originally studied by Cottrell (1958). Carbide morphology and distribution has been studied to some extent by McMahon (1965), Danko (1957) and Timbres (1970). Turkalo (1958) and Embury (1966) have conducted studies into the effects of dislocation substructure on mechanical properties; however, knowledge of its effect on fracture properties is sketchy. Inclusions have a marked effect on the true fracture strain and Charpy shelf energy of steels. Their effects have been reported by a number of people, in particular, Sims (1959), Lichy (1965), and Birkle (1966). However, quantitative information about the effects of complex microstructures on the fracture properties of steels is quite limited.

There have been a number of models proposed which attempt to relate the plane strain fracture toughness to unnotched tensile properties and a "size" which is related to the microstructure (Krafft 1964, Hahn 1967, Malkin 1971). There have also been attempts to determine empirical relations between the Charpy shelf energy and unnotched tensile properties (Rosenfield 1971). The attractive features of these models and empirical relations are that unnotched tensile data can be easily and economically generated (as compared to plane strain fracture toughness data) and that the large body of information relating the microstructure to unnotched tensile properties can be used to assist in the development of tougher alloys.

The purpose of this present work is to obtain more quantitative information about the effects of microstructural variables on toughness through their effects on the unnotched tensile properties. The investigation

is divided into two parts. Part A includes work on a high strength steel (SAE 4340) in the upper bainitic condition and Part B, work on four structural steels in the hot rolled ferrite-pearlite condition.

PART A

Bainitic steels can be produced either by isothermal transformation or by continuous cooling. The continuously cooled bainites form and probably will continue to form the bulk of commercially produced bainitic steels. However, with continuously cooled bainites, there is almost a limitless number of microstructures which can be produced through variations in austenitizing temperature, rolling practice and cooling rate. (Habraken 1967, Irvine 1969). To produce a reasonably uniform and reproducible structure, the bainites investigated here were produced by isothermal transformation. A subsequent thermal-mechanical treatment was used to effect the desired changes in carbide morphology and distribution, and dislocation substructure. Unnotched tensile and fracture toughness data were determined for the "as transformed" and for the "warm rolled" bainitic steels. This data was correlated with microstructural observations in an attempt to isolate the variables responsible for changes in the unnotched tensile properties and thus in the fracture toughness.

PART B

With lower strength steels (the structural steels), transition temperature effects become more pronounced. The measurement of fracture toughness becomes extremely difficult in the transition temperature region because of the problems in maintaining constraint, inherent in low strength material fracture toughness specimens (ASTM 1970). In this work, fracture toughness tests were conducted below the transition temperature range. Charpy impact tests were conducted over a range of temperatures and transition curves plotted. The Charpy shelf energy was used as a measure of the material toughness above the transition temperature.

It has been known for some time that the shelf energy of steels is affected by the inclusion content. As mentioned before, there have been some attempts to derive empirical relations between the shelf energy and the unnotched tensile properties. An attempt has been made here to relate the Charpy shelf energy to the inclusion content by first relating the fracture strain to the inclusion content through a model for ductile rupture and then relating the shelf energy to the fracture strain (Rosenfield 1971). Again, evidence from microstructural observations is drawn upon to support the predictions of the models.

CHAPTER 2

MATERIALS AND EXPERIMENTAL METHOD

2.1 SAE 4340

2.1.1 Heat Treatment

The SAE 4340 steel was received from United States Steel in the form of 1x6x36 inch hot-rolled plate. The plate was cut into smaller test samples 1/2x2x6 inches with the long axis of these test samples parallel to the original plate rolling direction. This was done to eliminate any cross rolling effects in the subsequent thermal-mechanical treatments.

The heat treatment schedule used to put the SAE 4340 samples into the upper bainitic condition is given in Figure 4. The samples were austenitized at 1000°C for 30 minutes. The samples were then quenched in a molten salt bath at 450°C. Approximate heat transfer calculations indicate that an average cooling rate of about 60°C/sec could be expected with these samples. The salt bath consisted of a 50 wt. % $NaNO_3$ - 50 wt. % KNO_3 mixture. The samples were isothermally transformed in the salt bath for 1 week. After transformation, the samples were air cooled. The IT diagram indicates that this treatment should produce almost 100% upper bainite in the samples. Transmission electron micrographs of foils made from these samples support this prediction (Shackleton 1965, Oblak 1967, Irvine 1965).

2.1.2 Thermal-Mechanical Treatment

Several experiments were conducted using different rolling

temperatures to determine the warm rolling conditions for the 4340. The warm rolling schedule used in this work is given in Figure 5. It was chosen because it produced the desired microstructural changes, was compatible with rolling mill capacity and produced a final test sample thickness that was adequate for specimen machining requirements.

The 1/2x2x6 inch test samples were soaked for 15 minutes at 650°C in an electric furnace. The samples were then rolled in Stanat 6" rolling mill. The rolling schedule consisted of 12 passes with a 3 to 4 minute soak after each pass to maintain the sample temperature as near to 650°C as possible. The samples were reduced approximately 35% in thickness resulting in a final sample thickness of 0.350 inches. The samples were then air cooled. The total thermal-mechanical treatment time for each test sample was roughly 1 hour.

Oblak and Hehemann (1967) produced upper bainite in 5140 steel at 540°C and then up quenched the material to 580°C and held it for 4 hours. They found that the bainite lath interfaces were relatively immobile at this temperature and that the high dislocation density of the laths was not reduced significantly. Thus the 15 minute soak used here should not have much of an effect on the bainitic structure.

2.1.3 Chemistry

The SAE 4340 steel used in this work was supplied by United States Steel in the form of plate 1x6x36 inches. The plate was hot rolled from a 300 lb air-induction melted heat. The chemistry of the steel is given in Table I.

2.1.4 Microstructure, Carbide Morphology and Substructure

Transformation of the SAE 4340 to upper bainite was effected by an

isothermal transformation followed by air cooling. The detailed microstructure of the material in the upper bainitic condition is given in the scanning electron micrograph in Figure 6 and the transmission electron micrograph of Figure 7. As reported in the literature (Kelly 1961, Shackleton 1965, Oblak 1967), the classical upper bainitic structure forms as an aggregate of ferrite laths with carbides precipitated parallel to and between the laths. The ferrite laths contain an extremely high dislocation density. The crystallographic relationship between the ferrite and carbide components of upper bainite indicate that the carbide in upper bainite precipitates from carbon enriched austenite trapped between the ferrite laths (Irvine 1965, Shackleton 1965).

Oblak and Hehemann (1967) conducted transformation studies with a series of steels including SAE 1040, 5140, 2340 and two high carbon high silicon steels. They concluded that the lath structure of the upper bainite produced in the SAE 1040 steel was identical to that observed in the SAE 5140 and 2340 steels. Transformation in the upper bainitic region of the high carbon high silicon steels did not always result in lath-like arrangements. Some of the bainites in these steels were characterized by massive regions of ferrite with embedded carbides similar to those reported by Shackleton and Kelly (1965). Upper bainite in the SAE 4340 steel exhibits this lath structure with the carbides precipitated at the lath boundaries. The carbides have a rod-like shape and are of the order of 1 μ in length. Substantial dislocation substructure is evident in the material. (Figure 7)

The subsequent thermal-mechanical treatment (warm rolling) given to the upper bainitic 4340 resulted in significant changes in the microstructure of the material. The microstructure is illustrated in Figures 8 and 9. Rapid and almost complete spheroidization of the carbides has taken place. Conventional spheroidizing anneals for steel usually require from 10 to 48 hours at temperatures near 700^{o}C (Harrigan 1967) as opposed to the 1 hour

warm rolling treatment at 650°C given to the SAE 4340. Comparison of Figures 6 and 8 reveals that there is a refinement in carbide dispersion and a marked reduction in the carbide aspect ratio. Rapid spheroidization of carbides and refinements in carbide dispersions in steels as a result of concurrent straining has been reported by Uvira 1970, Harrigan 1967, and Sherby 1969. This effect is quite evident in the 4340 as revealed by its response to warm rolling treatments.

Comparison of the transmission micrographs of Figures 7 and 9 indicates a further change in structure. In addition to changes in carbide dispersion and aspect ratio, the warm rolling induces in the material a well developed and clearly defined dislocation cell structure of about 1 micron in size. Carbides in the material are located mainly at the cell boundaries.

Determination of the prior austenite grain size in the material was attempted using an isothermal transformation technique to decorate the prior austenite grain boundaries with proeutectoid ferrite, or to selectively nucleate ferrite in prior austenite grains. The results of one of these isotherma treatments on the 4340 are shown in Figure 10. The darker areas in the micrograph are ferrite and the lighter areas martensite. The prior austenite grain boundaries are readily visible. These tests indicate a prior austenite grain size of 10-15 μ.

2.1.5 Banding

After the heat treatment used to put the 4340 in the upper bainitic condition, marked banding was observed in the microstructure (Figure 11). The bands in the case of upper bainite consist of regions of high carbide concentration and regions of low carbide concentration.

There has been general agreement that banded structures in steels arise from the effects of alloy segregation on carbon location. This segregation originates in normal interdendritic segregation during ingot

solidification and persists in some form into the final product as a laminar distribution (Jatczak 1952, Kirkaldy 1962, Grange 1971). The reason for the banded structure in 4340 comes about from the opposing effects of solution elements and carbide formers on the location of carbon in austenite (during soaking, cooling and transformation) through their effect on carbon activity (Jatczak 1952). The activity of carbon is increased in regions rich in silicon, nickel and phosphorous and decreased in regions rich in manganese and chromium (Kirkaldy 1962).

Another reason for the banded structure in as transformed 4340 is the constitutional effect of the alloying elements on shifting the A_3 temperature, resulting in premature or delayed nucleation of ferrite in certain regions (Bastien 1957). That is, the regions lower in carbon content nucleate ferrite first and reject carbon to the regions already higher in carbon content, further delaying the nucleation of ferrite in the high carbon region.

Other factors influence the degree, type and form of banding by their influence on the degree of chemical segregation. Some of these may be austenitizing temperature and time, diffusion rates of carbon and alloy elements, cooling rates and the rates of nucleation and growth of the austenite decomposition products (Jatczak 1952).

Studies by Jatczak (1952) on SAE 4340 indicated that isothermal treatment at the ferrite pearlite nose (650^{o}C) was more sensitive for developing banded structures than continuous cooling treatments. In this work, a series of samples of 4340 (see Table 2) were austenitized, isothermally transformed for various periods of time and then water quenched. The effects of the isothermal transformation for 30 minutes are shown in Figure 12. The dark regions in the micrograph are ferrite and the light regions martensite. The bands appear to be in long strips parallel to the rolling direction and perpendicular to the plate thickness.

The heterogeneous ferrite nucleation and its effects on subsequent transformation is responsible for the banding observed both in the ferrite-

pearlite transformation and in the bainite transformation.

The warm rolling treatment tends to remove most of the microscopic evidence of banding as illustrated in Figure 13. This is due primarily to refinements in the carbide dispersion effected by warm rolling.

Examination of the as transformed and the warm rolled SAE 4340 with the electron probe was conducted to determine if any alloy segregation existed. The probe traverses on both materials indicated that there was no detectable alloy segregation.

2.2 Structural Steels

2.2.1 Chemistry

The structural steels used in this work were supplied by the Steel Company of Canada in the form of hot-rolled plates 1/2x3x24 inches. The heat number, chemistry, heat type and transformation characteristics are given in Table 3.

2.2.2 Microstructure

The microstructures of heats 3441, 3450, 3458 and X65 are given in Figures 14, 15, 16, 17 respectively. The grain size and pearlite content of the four steels is given in Table 4.

The steels exhibit pearlite banding with the bands oriented in the rolling direction. The pearlite in the bands is very fine scale pearlite. The bands in heats 3450 and 3458 have a centre to centre separation of roughly 20 microns. The bands in heats 3441 and X65 have a centre to centre separation of roughly 50 microns.

The banding in the structural steels comes about from the effects of the alloying and impurity elements on the location of carbon in austenite

through their effect on carbon activity (Jatczak 1952). The carbon activity would be increased in the regions rich in silicon and phosphorous and decreased in the regions rich in manganese (Kirkaldy 1962). Again, the constitutional effect of the alloying elements on the position of the A_3 temperature could be involved in the banding phenomena (Bastien 1957). In the case of the structural steels the regions lower in carbon content nucleate ferrite first and reject carbon to the regions higher in carbon content. The higher carbon content requires that ferrite and pearlite nucleate in these regions. The result is the banded structure observed. There are other factors which control the degree of banding and these along with the two mentioned here are discussed in detail in section 2.1.5.

Examination of the four materials with the scanning microscope revealed that there were inclusion stringers oriented inthe rolling direction in heats 3441, 3450 and 3458. Information obtained from x-ray analysis equipment coupled to the SEM indicated that the stringers were manganese-iron-sulphur compounds. In addition to the stringers in heat 3441, there were also some globular inclusions. These were examined with the x-ray equipment. The particles had a very high aluminum concentration and so are probably aluminum oxide inclusions. This finding would be consistent with the chemistry of heat 3441 (Table 3).

There were no inclusion stringers observed in the X65 material as such. The inclusions present were in the form of small isolated spheres or in rows of small spheres. Examination of these particles with the x-ray equipment indicated that they were manganese-iron-sulphur compounds. Quantitative information about inclusions in the materials is given in the next section.

2.2.3 QTM Data

Detailed inclusion analysis of the four steels was performed by the Steel Company of Canada with their Quantimet. The Quantimet obtains

quantitative data on inclusions by electronically making point counts over a given frame area. Each frame is divided into 160,000 picture points, and the information is obtained from the picture point intensities.

The results for the steels used in this work are given in Table 5. The data are consistent with the chemistry of the steels listed in Table 3. That is, the steel with the highest total inclusion area (3441) has the highest sulphur content.

2.3 Mechanical Tests

2.3.1 Compact Tension Tests

The fracture toughness specimens chosen for this investigation were compact tension specimens (Wessel 1968, ASTM 1970). The details of this specimen are given in Appendix A.

The compact tension specimen was chosen for a number of reasons. One of the most important was size. The final dimensions of the warm rolled SAE 4340 plate test samples were 0.350 x 2 x 6 inches, which put a limit on the specimen thickness. The compact tension specimens used were 2 inches square by 0.25 inches thick. This allowed about 0.050 inches of material for machining the sample faces. The test plates were cut into blanks 0.25 x 2 x 2 inches. The surfaces of these blanks were left "as milled". The notch was then cut into the blanks. The notch was made with a 0.125 inch mill cutter. The cutter was ground to form a 30 degree included notch angle and a notch root radius of 0.002 inches. The notch orientation with respect to the rolling direction of the plate test samples is given in Figure 18. This notch orientation is termed "crack divider" (Embury 1967) with respect to the banding in the plate samples. After the notch was cut, the samples were mounted in a special jig and the pin loading holes were drilled and reamed. The jig

insured that the pin loading holes were drilled in the correct position with respect to the notch and that their axis was perpendicular to the sample faces.

The specimen thickness is the critical dimension in determining the testing capacity of the compact tension specimen. The ASTM minimum thickness requirement for plane strain fracture toughness testing is given by the equation

$$B \geq 2.5 \left(\frac{K_{Ic}}{\sigma_y}\right)^2 \quad \text{(ASTM 1970)}$$

where B = specimen thickness.

This ASTM requirement can be expressed in terms of Irwin's plane strain β_{Ic} value (Irwin 1960)

$$\beta_{Ic} = \frac{1}{B} \left(\frac{K_{Ic}}{\sigma_y}\right)^2 \leq 0.4$$

that is, a true plane strain fracture toughness value can be obtained from a compact tension specimen if $\beta_{Ic} \leq 0.4$. The ASTM requirement places a very severe limitation on the minimum specimen thickness. There are some data from the literature which suggest that the limitation should not be as severe. Data from fracture toughness investigations of A517-F steel made by Barson and Rolfel(Barsom 1971) indicate that plane strain conditions exist in this material for $\beta_{Ic} = 0.6$. Hahn and Rosenfield conclude that there is a significant shift away from plane strain conditions when $\beta_{Ic} > 1.3$ (Hahn 1967). If this β_{Ic} value and a thickness of 0.25 inches are used, the maximum plane strain capacity of the 4340 specimens would be about 60 ksi $\sqrt{\text{in}}$ (assuming a yield stress of 100,000 psi) and the maximum plane strain capacity of the structural steel specimens would be about 40 ksi $\sqrt{\text{in}}$ (assuming a yield stress of 60,000 psi).

The compact tension specimens were fatigue pre-cracked according to

ASTM specifications. The specimen surfaces at the root of the notch were polished so that the growth of the cracks could be monitored. The specimens were fatigue pre-cracked with an MTS closed loop electro-hydraulic fatigue rig using tension-zero-tension loading. Cracks of 0.060 to 0.080 inches in length were grown in about 40,000 cycles. The crack growth rate was about 10^{-6} inches/cycle. This corresponds to a stress intensity of less than 20 ksi$\sqrt{in.}$ (Tetelman 1967) for both the 4340 and the structural steels, which is within the ASTM recommended limits for fatigue cracking (ASTM 1970). Because of the severe thickness restriction on the structural steels, it was planned to conduct tests on these materials over the range of temperatures from -120°C to -30°C. From these tests, it could be determined at which temperature sufficient loss of constraint occurred to make the test invalid. Other tests could then be conducted at more suitable temperatures. This method proved to be satisfactory. Fracture toughness tests were conducted on the X65 and 3458 from -120°C to -30°C, and on the 3441 and 3450 from -120°C to -60°C.

The fracture toughness tests on the SAE 4340 were conducted over the range of temperatures from -120°C to 25°C.

The low temperatures were obtained by using a liquid nitrogen spray cooling system. Copper spray tubes 0.25 inches in diameter and bent in the form of hoops, were fitted around the specimen grips. The spray tubes were connected to a large liquid nitrogen dewar. Liquid nitrogen was pumped through the spray tubes by pressurizing the dewar with nitrogen gas. The grips specimen and spray system were enclosed in a 4-inch thick styrofoam insulation box. Temperature control was obtained by controlling the flow of liquid nitrogen through the spray tubes. The temperature of the specimen was monitored by two copper-copper constantan thermocouples soldered to the specimen just above and below the fatigue pre-crack. The specimen temperature could be controlled to within $\pm$ 5°C during testing.

The compact tension specimens were loaded with an Instron universal

testing machine (Model TTC) at a crosshead speed of 0.005 inches/minute. Specimen opening displacements were monitored with an Instron extensometer mounted across the notch on two stainless steel L-shaped brackets. The brackets were attached to the specimen by means of small set screws. The low temperature response of the extensometer was checked prior to testing by immersing it in an ethanol and dry ice bath and using it to measure the displacements of a calibrating device. The results are shown in Figure 19. The extensometer response did not appear to be significantly affected by the low temperature.

After the fracture toughness tests had been completed, the broken halves of the compact tension specimens were removed from the grips as quickly as possible and immersed in methanol, to prevent condensation on the fracture surfaces. The specimens were dried, wrapped in tissue and stored in a desicator. Some of these specimens were examined later in the SEM.

The fracture toughness was calculated from both critical load measurements using the ASTM 5% secant intercept method (ASTM 1970) and from opening displacement measurements (Hoagland 1972).

2.3.2 Unnotched Tensile Tests

Small tensile specimens were machined from the plate test samples of both SAE 4340 and structural steels. The orientation of the tensile specimens with respect to the rolling direction is shown in Figure 18. The samples are 0.125 inches in diameter and have a gauge length of 1.1875 inches.

The tensile tests were conducted with an Instron universal testing machine (Model TTC) at a crosshead speed of 0.02 in/minute. The Instron crosshead was fitted with a cage that allowed tests to be conducted in various temperature baths. The tests were conducted over a temperature range of -196°C to 100°C. Strength data were determined from the load-extension curves

from each test. Accurate determinations of the diameters of the tensile specimens in the necked region were made using a "Shadow graph". The diameters were used to calculate true fracture strains.

2.3.3 Charpy Impact Tests (Structural Steels Only)

Standard size Charpy impact specimens were machined from the plate test samples of the structural steels. The notch orientation with respect to the rolling direction is shown in Figure 18. This notch orientation is termed "crack divider" with respect to the banding in the plate samples (Embury 1967).

Impact tests were conducted over the range of temperatures from -196°C to 170°C. The tests were conducted with a Tinius Olsen impact testing machine.

The data were plotted against test temperature to develop impact transition temperature curves for each of the four steels.

2.3.4 Notch Bend Tests (SAE 4340 Only)

Notch bend tests were conducted with sub-size Charpy specimens 6x6x44 mm in size machined from test plates samples of the as transformed and warm rolled SAE 4340. The notch orientation of these specimens with respect to the rolling direction is given in Figure 18.

The notch bend tests were conducted with an Instron universal testing machine (Model TTC) fitted with a three point bend jig and cage so that the tests could be conducted in temperature baths. The tests were conducted over the temperature range of -196°C to 100°C.

The nominal breaking stress and the general yield stress were calculated using the equations

$$\sigma_{nb} = \frac{3}{2} \cdot \frac{L}{Bd^2} \cdot P_{nb}$$

$$\sigma_{gy} = \frac{3}{2} \cdot \frac{L}{Bd^2} \cdot P_{gy} \qquad \text{(Allen 1965)}$$

where σ_{nb} = nominal breaking stress

P_{nb} = nominal breaking load

σ_{gy} = general yield stress

P_{by} = general yield load.

L = distance between support rollers of the three point bend jig.

B = width of specimen.

d = depth measured on the reduced area at the base of the notch.

In order to determine the fracture stress of the as transformed and the warm rolled SAE 4340, the results of the notch bend tests were plotted against test temperature. When fracture of the notch bend specimen occurs at general yield, the fracture stress can be expressed as:

$$\sigma_f = R\sigma_y \quad \text{(Uvira 1970)}$$

where σy = uniaxial yield stress at the temperature at which

$$\sigma_{nb} = \sigma_{gy}$$

R = constraint factor related to the notch angle.

For the specimen geometry used here, R is equal to 2.18.

2.4 Crack Growth Tests

2.4.1 Compact Tension Specimens (SAE 4340 Only)

The phenomenon of slow crack growth leading to catastrophic cleavage failure was observed in the warm rolled SAE 4340 at intermediate test temperatures ($\sim -70^{\circ}C$). In order to study slow crack growth in more detail, three compact tension specimens were pre-cracked and loaded at $-70^{\circ}C$. The load displacement records from the original fracture toughness tests were used to determine the maximum load to which the specimens could be subjected to achieve some slow growth without causing cleavage failure. The specimens were loaded to this predetermined point and then unloaded. Two of the specimens were then cooled to liquid nitrogen temperature and fractured to provide a cleaved surface distinct from the ductile slow growth surface. The third specimen was sectioned perpendicular to the specimen thickness at the specimen mid-thickness to provide a crack profile view.

The fractographic observations made with the scanning electron microscope came from the regions of the specimens illustrated in Figure 20.

2.4.2 Unnotched Tensile Specimens

An examination of the unnotched tensile specimens machined from the as transformed and warm rolled SAE 4340 and from the structural steels (3441) was conducted to determine the approximate magnitude of the strains necessary to initiate voids in the material. These tests would also help to indicate the void initiation sites and which sites were critical to the fracture process.

Two types of tensile tests were performed. In one, the tensile specimens were loaded until they had necked but had not failed; and in the other, the specimens were loaded until they had failed. The specimens were

sectioned at the specimen mid-thickness parallel to the tensile axis. The tensile tests with the SAE 4340 were conducted at 100°C and those with the structural steels (3441) were conducted at 0°C.

2.4.3 Charpy Impact Tests (Heat 3441 Only)

Examination of Charpy impact specimens machined from heat 3441 was conducted with the SEM.

To provide a crack profile view, several of the Charpy specimens were struck a blow (at room temperature) amounting to about 25 ft. lb. The shelf energy of this material was determined to be 33 ft. lb. The 25 ft. lb. blow produced a crack about half way through the specimens. The specimens were then sectioned at mid-thickness parallel to the specimen length and perpendicular to the notch root. The specimens were polished and then etched with Picral.

"Two surface specimens" (Embury 1971) were prepared from the Charpy specimens, which had been broken at room temperature, in the following way.

The broken Charpy specimen was sectioned parallel to the specimen length and perpendicular to the fracture surface. (That is, the section was parallel to the original plate width and perpendicular to the rolling direction.) The fracture surface was covered with laquer (to protect the details of the surface) and then mounted, polished and etched with Picral. The specimens were broken out of the mounts and ultrasonically cleaned in Acetone. The polished and etched surface and the fracture surface could then be examined simultaneously with the scanning electron microscope. The "views" described above are illustrated schematically in Figure 21.

2.4.4 Notch Bend Tests (SAE 4340 Only)

Notch bend specimens machined from both the as transformed and the warm rolled material were examined in the SEM.

To provide a crack profile view, the load-extension curves obtained from the original notch bend tests were used to determine the load to which the specimens could be subjected without causing failure. The specimens were subjected to the predetermined load at two test temperatures -77°C and 100°C. The specimens were then sectioned at the mid-thickness parallel to the specimen length and perpendicular to the notch. The specimens were polished and then etched with Picral.

"Two surface specimens" were prepared from broken notch bend specimens tested at -196°C using the same method as described in the previous section. These were also examined in the scanning electron microscope. The "views" described above are shown in Figure 21.

2.5 Electron Microscopy

2.5.1 Transmission Electron Microscopy

Thin foils for the transmission electron microscope were prepared from the as transformed and the warm rolled SAE 4340.

Small sections about .050 x .5 x .5 inches were cut from the test plate samples of both materials. The sections were mechanically polished to a thickness of .005 inches. The sections were then chemically thinned in a solution of 80 vol. % H_2O_2, 18 vol. % H_2O and 2 vol. % HF. Final electropolishing was done in a 95 vol. % glacial acetic acid 5 vol. % perchloric acid solution with stainless steel cathodes at a potential of 30 volts.

The thin foils were examined with a Siemens Elmiskop I electron microscope.

2.5.2 Scanning Electron Microscopy

Fracture surfaces and polished and etched surfaces of the SAE 4340 and the structural steels were examined in the scanning electron microscope.

Sections of the fracture surface were cut from compact tension specimens and Charpy specimens with a diamond saw. The sections were ultrasonically cleaned in methanol, then washed with methanol and dried. The sections were then mounted on aluminum studs with conducting paint and examined with a Cambridge Stereoscan scanning electron microscope.

The samples of material that were polished and etched were rough polished with a series of emery papers and final polished with 1μ diamond paste. The surface was washed and then etched with a 5% picral solution. The picral etch proved to be more satisfactory than nital because its slower etching rate allowed better control of the degree to which the surfaces were etched.

The samples were ultrasonically cleaned in methanol then washed with methanol and dried. The samples were mounted on aluminum studs with conducting paint and examined with the scanning electron microscope.

2.5.3 X-ray Analysis

A Nuclear Diodes Edax x-ray analyser was used in conjunction with the scanning electron microscope to obtain qualitative information on the inclusions present in the steels.

CHAPTER 3

RESULTS AND OBSERVATIONS

The study of the fra cture behaviour of the SAE 4340 and of the structural steels involved a variety of mechanical tests and experimental techniques which are described in the Materials and Experimental Method section. For the sake of clarity in reporting the data, the results and observations of this investigation will be reported in two parts. Part A for the SAE 4340 steel and Part B for the structural steels. Each part will be subdivided into Mechanical properties, Fracture topography and Crack growth observations.

Many of the formulations of the plane strain fracture toughness given in the literature are written as a function of the unnotched tensile properties and/or the cleavage stress. Some of these relations will be used in the analysis of the fracture toughness data in an attempt to explain the effect of microstructure on the mechanical properties and thus on the fracture toughness of the steels.

Thus tensile tests and fracture toughness tests were conducted on the SAE 4340 and on the structural steels over a range of temperatures. In the case of the SAE 4340, the tensile tests were used to determine the UTS, the yield strength, the work hardening exponent and the true fracture strain all as a function of test temperature. For the structural steels, the tensile tests were used to determine the UTS, the yield strength and the true fracture strain again as a function of temperature.

Notch bend tests were conducted over a range of temperatures to determine the cleavage stress of the 4340.

Because of the difficulty in obtaining valid plane strain fracture

toughness data for the structural steels above -50°C due to specimen thickness limitations, Charpy impact tests were conducted on the structural steels over a range of temperatures. Impact transition curves were obtained and the shelf energies used as a measure of the toughness above the transition temperature.

The fracture topography of the steels was examined extensively with the scanning electron microscope. Only the micrographs showing features considered pertinent to the discussion are given. Scanning electron micrographs of the as transformed and the warm rolled 4340 compact tension specimens tested at -120°C and 25°C are given. These represent the extreme in fracture topography, provide a comparison of the two treatments and indicate the changes that are taking place in the fracture mode. Scanning electron micrographs of the structural steel compact tension specimens tested at -120°C are given. Fracture toughness data from these materials indicated that -120°C was the temperature at which all the specimens were subject to a maximum of plane strain at the crack tip and should thus provide a reasonable basis for comparison of their respective topographies.

The crack growth observations reported for both grades of steel consist of a series of scanning micrographs which reveal the detailed nature of the failure mechanisms in the materials. The orientation of the plane of the micrographs with respect to the original test plate dimensions is indicated in the figures. The significance of the micrographs can best be understood by referring to Figures 20 and 21 which show the orientation of the various "views" presented.

PART A: SAE 4340

3.1 Mechanical Properties

3.1.1 Unnotched Tensile Properties

The results of tensile tests conducted on the 4340 both in the as transformed to upper bainite condition and after warm rolling are given in the following figures. The tests were conducted over the range of temperatures from -196°C to 100°C. Each point on the graphs represents a single test result.

The UTS and yield stress values are given in Figure 22. The tests results show that the thermal mechanical treatment produces a reduction in the UTS at all test temperatures. This amounts to about a 20,000 psi reduction at 100°C and about a 10,000 psi reduction at -196°C. The as transformed material did not exhibit a true yield point. Offset yield stress values (0.2%) were determined and they are plotted in Figure 22. The warm rolled material did exhibit upper and lower yield points. The data given in Figure 22 for this material condition are the lower yield stress values. The tensile data also indicates that the thermal-mechanical treatment does not significantly change the yield stress of the material over the range of test temperatures.

The work hardening exponent is given for both material conditions in Figure 23. Each data point again represents a single test. The work hardening exponent plotted here is defined by a true stress-true strain relationship of the form

$$\sigma = K\varepsilon^{n}$$ (Mendelson 1968, Tetelman 1967)

where σ = true stress

K = strength coefficient

ϵ = true strain

n = work hardening exponent

The data indicate that the thermal-mechanical treatment results in a reduction in the work hardening index over all test temperatures.

The true fracture strain is given in Figure 24 for both material conditions. As before, each data point represents a single test. The true fracture strain used in this analysis is defined as

$$\epsilon_f = \ln \frac{A_o}{A_f} \qquad \text{(Tetelman 1967)}$$

where A_o = initial cross sectional area

A_f = final cross sectional area

The test data show that the thermal-mechanical treatment increases the true fracture strain over all test temperatures.

3.1.2 Fracture Toughness Properties

Fracture toughness tests were conducted with samples of the as transformed and the warm rolled SAE 4340 over the temperature range from -120°C to 25°C. The samples used in the investigation were pre-cracked compact tension fracture toughness specimens, the details of which are given in Appendix A. Load displacement curves were generated from the tests and calculations of the fracture toughness were made from the load displacement curves. In the case of the SAE 4340, fracture toughness values were calculated in two ways. Determinations were made from both critical load measurements

(ASTM 1970) and from opening displacement measurements (Hoagland 1972).

The load displacement curves obtained in the tests with the 4340 can be grouped into four basic types and are illustrated schematically in Figure 25. The type of curve obtained was, of course, a function of test temperature and material condition (ie. as transformed or warm rolled). A type 1 load displacement curve consisted of an initial portion in which there was a linear relation between load and displacement. This was followed by a non-linear portion, followed by specimen failure. Subsequent examination of the fracture surfaces indicated that slow crack growth occurred before instability set in. Further discussion of this phenomenon is given in later sections.

Specimens exhibiting type 2 load displacement records, showed little if any linear load-displacement behaviour. In these cases, the tests were stopped when the extensometer range had been exhausted.

Type 3 and Type 4 load-displacement records were similar in that linear load-displacement behaviour was observed right up until crack "pop-in" occurred. In the case of Type 3 initial "pop-in" resulted in complete failure. Type 4 behaviour was the result of multiple crack "pop-in", before final failure.

The fracture toughness data obtained from these tests are plotted in Figure 26. The circles indicate data from critical load caluclations, and the crosses from opening displacement calculations.

The tests in which the maximum load at fracture was not within the ASTM 5% secant-intercept requirement for plane-strain behaviour (ASTM 1970) are indicated by full circles in Figure 26. These tests then, did not yield true plain strain fracture toughness values due to loss of constraint in the specimens. The other data satisfy the ASTM secant-intercept criterion and are given as plane strain fracture toughness values.

Only a few of the data points satisfy the ASTM requirement for

minimum specimen thickness in plane-strain fracture toughness testing (ASTM 1970) as given by the equation

$$B \geq 2.5 \left(\frac{K_{Ic}}{\sigma_y}\right)^2$$

where B = specimen thickness.

This ASTM requirement can be expressed in terms of Irwin's plane-strain β_{Ic} value (Irwin 1960)

$$\beta_{Ic} = \frac{1}{B} \left(\frac{K_{Ic}}{\sigma_y}\right)^2 \leq 0.4$$

Data compiled by Barsom and Rolfe (Barsom 1971) on grade A517-F steel showed the same type of behaviour as that observed here. That is, the test data satisfy the ASTM 5% secant-intercept requirement for plane-strain behaviour but do not satisfy the ASTM requirement for minimum specimen thickness. Analysis of the Barsom and Rolfe data indicate that plane strain behaviour exists for $\beta \approx 0.6$. Examination of the data obtained in the experiments conducted with the SAE 4340 indicates that a good percentage of the plastic zone is experiencing plane strain conditions for $\beta_{Ic} \approx 1.3$. Hahn and Rosenfield argue that there is a significant shift away from plane-strain conditions in the material when

$$\left(\frac{K_{Ic}}{\sigma_y}\right)^2 \frac{1}{B} > 1.3 \quad \text{i.e. when } \beta_{Ic} > 1.3 \quad \text{(Hahn 1967)}$$

Thus the data on 4340 appear to be consistent with the Hahn and Rosenfield approach to the stress state in the material. Also, the specimens in which plane strain conditions were assumed to be present, failed catastrophically.

Yield stress, fracture toughness and β_{Ic} values are listed in Table 6 for both the as transformed and warm rolled 4340. Along with this information is listed the type of load-displacement curve plotted for each test. In summary then, the ASTM 5% secant-intercept requirement would indicate that the values

obtained for warm rolled material at 25°C and -30°C are not true K_{Ic}. The Hahn and Rosenfield approach indicates that the values for the as transformed material at 25°C and for the warm rolled material at 25°C, -30°C and -70°C are not true K_{Ic}. The two determinations thus appear to be reasonably compatible in their indication of stress state.

3.1.3 Notch Bend Properties

The result of notch bend tests performed on the as transformed and warm rolled 4340 are in Figures 27 and 28 respectively.

When fracture of the specimens occurs at general yield, the cleavage stress of the material can be determined. The value for the as transformed material was 344 ksi and that for the warm rolled 364 ksi.

3.2 Fracture Topography

3.2.1 Test Temperature -120°C

The as transformed SAE 4340 compact tension specimens failed catastrophically at this test temperature. The specimens exhibited a type 3 load displacement record (see Figure 25). Initial pop-in led to complete specimen failure. There were no observable shear-lips on the fracture surfaces. A scanning electron micrograph of the failed as transformed SAE 4340 specimen is given in Figure 29. At this test temperature the as transformed steel exhibits a cleavage failure mode (Beachem 1965, 1968). Examination of the fracture surface with the scanning microscope indicated that the cleavage facets were of the order of 10 microns in size and that they exhibited river markings characteristic of cleavage failure in steels.

A scanning electron micrograph of the warm rolled SAE 4340 is given

in Figure 30. The specimens exhibited a type 1 load displacement record (see Figure 25). At this test temperature some slow crack growth preceded specimen failure. Scanning micrographs and discussion of this slow growth phenomenon will be given later. Macroscopic examination of the fracture surface revealed that there were no observable shear-lips; however, the fracture surface was very uneven as opposed to the flat fracture surface exhibited by the as transformed material.

At this test temperature the warm rolled material exhibits a fracture surface consisting of regions of ductile failure and of cleavage failure (Beachem 1965, 1968) lined up roughly parallel to the direction of crack propagation. Examination of the fracture surface with the scanning microscope indicated that the cleavage facets were of the order of 10 microns in size. Stereo scanning micrographs showed the ductile regions on the fracture surface were in fact regions in which the material had been sheared. These shear regions were inclined at roughly 45° to the surrounding cleaved regions and in general separated cleaved regions of different elevation. A composite scanning electron micrograph of this fracture surface was made, covering a section of surface about 800 microns square at 400X magnification. This study indicated that the sheared regions were isolated from one another and they occupied less than 20% of the total surface area.

3.2.2 Test Temperature $25^{\circ}C$

The as transformed SAE 4340 compact tension specimens failed by a series of "pop-in" steps (the multiple "pop-in" referred to before) followed by catastrophic specimen failure. The specimens exhibited a type 4 load displacement record (see Figure 25). Macroscopic examination of the specimens revealed shear-lips of approximately 1/4 the specimen thickness. The center of the specimen exhibited a flat fracture surface.

A scanning micrograph of the center flat protion of the as transformed material is given in Figure 31. At this test temperature the as transformed steel exhibits a fracture surface consisting of a uniform mixture of ductile and cleavage failure modes. Beachem and Pelloux use the term quasi-cleavage to describe this type of fracture surface (Beachem 1965). In steels containing fine precipitates (quenched and tempered steels), a quasi-cleavage fracture surface exhibits some of the features of cleavage in the initiation of facets and some of the features of plastic rupture in the linking of the microcracks. The proportion of these two modes depends on the steel chemistry, heat treatment and test conditions (e. g. test temperature). Examination of the shear lips with the scanning microscope revealed that the surfaces were covered with fine cusps characteristic of shear rupture (Beachem 1965).

A scanning electron micrograph of the warm rolled SAE 4340 is given in Figure 32. At this test temperature, the specimens exhibited a type 2 load displacement record (see Figure 25). The specimens did not fail catastrophically. Crack growth in these specimens was stable. Macroscopic examination of the fracture surface indicated that the crack had followed planes inclined at 45^{o} to the specimen thickness. This type of crack growth behaviour is characteristic of materials subject to plane stress conditions. The crack follows planes of maximum shear stress in which the most extensive slip and void formation occur (Broek 1970). Hahn and Rosenfield describe this type of crack growth as being characteristic of the "wedge-type" plastic zone associated with plane stress states (Hahn 1966). The load-displacement record and the value of $\beta_{I\,c}$ along with these macroscopic fra cture surface observations, indicate that very little of the plastic zone was subject to plane strain conditions.

The scanning micrograph in Figure 32 is from a small flat area of the fracture surface adjacent to the fatigue crack. The fracture surface is covered

in fine cusps 1 to 2 microns in size. There are also some larger cusps present 5 to 10 microns in size. This surface is characteristic of normal rupture (Beachem 1965). Examination of the shear lips of the specimen revealed that they were covered with fine cusps characteristic of shear rupture.

3.3 Crack Growth Observations

The nature of crack growth in the SAE 4340 was studied in detail using a series of controlled crack growth tests and sectioning techniques. (These are described in the Experimental Method section). The results and observations made from compact tension, notch bend and tensile specimens are given in the following three sections.

3.3.1 Compact Tension Specimens

The phenomenon of slow crack growth leading to catastrophic cleavage failure was observed in some of the warm rolled SAE 4340 compact tension specimens. The most extreme case occurred at a test temperature of $-70^{\circ}C$. The load-displacement record for this test exhibited a large non-linear portion before specimen failure occurred. A scanning electron micrograph of the fracture surface is given in Figure 33a. The micrograph at 20X shows the fatigue crack, the crescent shaped slow growth region and the cleaved region. The detailed nature of the fracture surface is shown in the higher magnification micrograph (Figure 33b). The slow growth region exhibits a ductile failure mode; (Beachem 1965, 1968) the fracture surface being covered in fine cusps roughly 1 micron in size. There are also larger cusps 5 to 10 microns in size, some of which have small inclusions at the centre.

Scanning micrographs of the cleaved regions show the cleavage facets to be of the order of 10 microns in size.

A scanning electron micrograph showing the fracture surface of one of the slow growth specimens is given in Figure 34a. Except for the difference in width, the slow growth region in this specimen is very similar to that of the original fracture toughness specimen shown in Figure 33a. The surface is covered in fine cusps roughly 1 micron in size. There are also larger cusps 5 to 10 microns in size, some of which have inclusions at the center.

Scanning electron micrographs of the slow growth specimens that were sectioned at mid-thickness (crack profile view) are given in Figures 35, 36, 37 and 38. Each section is about 30 microns below the preceding. Figure 39a shows that last section after it had been etched. It shows the carbide morphology and numerous voids associated with the crack tip. A higher magnification photograph is given in Figure 39b. The cusps on the fracture surface are quite evident. Some of these cusps have carbides laying in them.

3.3.2 Notch Bend Specimens

Results of the examination of the warm rolled SAE 4340 crack profile specimen loaded at -77^{o}C are given in Figure 40. There are numerous voids associated with the main crack which have been initiated around the carbides in the material. There is also a microcrack initiated ahead of the main crack front.

Scanning micrographs of the "two surface specimen" are given in Figure 41. There are a number of non-propagating microcracks visible.

3.3.3 Tensile Specimens

Scanning electron micrographs of the as transformed and the warm rolled SAE 4340 tensile specimens which had been pulled until necking had

started, are given in Figures 42 and 43 respectively. In both materials there is evidence of inclusion-matrix interface decohesion. However, there were no voids initiated at or around the carbides.

Figure 44 shows a scanning micrograph of the as transformed tensile specimen which had been pulled to failure. Voids have been initiated in the material at cracked carbides and are present only in the vicinity of the crack plane.

Scanning micrographs of the warm rolled tensile specimen which had been pulled to failure are given in Figure 45. The voids in the material are initiated around the carbides and are again present only in the vicinity of the crack plane. The voids are in rows which make an angle with the crack plane of about 45^{o}.

PART B: STRUCTURAL STEELS

3.4 Mechanical Properties

3.4.1 Unnotched Tensile Properties

For the reasons given at the beginning of this chapter a series of tensile tests were conducted on the structural steels over a range of temperatures. The range being from -196°C to 25°C. The results are given in Figures 46, 47, 48. Each data point given in these figures represents a single test. Some of the tensile data presented were courtesy of the Steel Company of Canada. This is also indicated on the figures.

The UTS values for the structural steels are given in Figure 46.

The yield stress values for the structural steels are given in Figure 47. The structural steels exhibited upper and lower yield points. The data presented in Figure 47 are lower yield stress values. The true fracture strain for the structural steels is given in Figure 48. The true fracture strain defined before as $\varepsilon_f = \ln \frac{A_o}{A_f}$ (Tetelman 1967), is plotted in this figure. The true fracture strain for alloys 3458, 3450 and 3441 is essentially independent of temperature above -120°C, whereas that for X65 varies continuously from -196°C to 25°C.

3.4.2 Charpy Impact Properties

In an attempt to correlate impact data on the structural steels with fracture toughness data, a series of standard full size Charpy impact tests were conducted on the structural steels. The tests were performed over the range of temperatures from -196°C to 170°C, so that transition curves could

be plotted. The results of the tests are given in Figure 49. Each data point shown represents a single test.

3.4.3 Fracture Toughness Properties

Fracture toughness tests were conducted with samples of the structural steels. The samples used in the investigation were pre-cracked compact tension specimens. These samples were of the same design as those used in the testing of the 4340, the details of which are given in Appendix A. Load displacement records were obtained from the tests and caluclations of the fracture toughness were made from these curves. The load displacement records from the tests with the structural steels can be grouped into two basic types. These are types 1 and 2 illustrated in Figure 25. The type of curve obtained was again a function of test temperature and material. A description of the type 1 and 2 curves is given in section 3.1.2.

Determinations of the fracture toughness were made using the ASTM 5% secant-intercept method (ASTM 1970). From these data, it would appear that constraint had broken down in the X65 and 3458 samples at about -55°C and in the 3441 and 3450 samples at about -90°C. The data are plotted in Figure 50. The tests conducted at -60°C with the 3441 and 3450 material yielded no useful results.

Yield stress, fracture toughness and β_{Ic} values for the structural steels are listed in Table 7. Also listed is the type of load displacement record associated with each test.

The Irwin (1960) β_{Ic} values indicate that full plane strain conditions did not exist in most of the test samples. Hahn and Rosenfield suggest that the plastic zone ahead of the crack is intermediate between plane stress and plain strain when $\beta_{Ic} \approx 2.6$ (Hahn 1967). This means that only the 3458 and X65 tests at -120°C satisfy both the β_{Ic} and the ASTM 5% secant intercept requirements for plane strain conditions.

As the value of $\beta_{I\,c}$ increases, an increasingly larger portion of the plastic zone is subject to plane stress conditions and the fracture toughness tests no longer yield valid $K_{I\,c}$ data.

Calculations of the fracture toughness were also made using opening displacement measurements (Hoagland 1972). In all cases except the X65 and 3458 tests at -120°C, the calculated K_I was higher, in some cases 30% higher, than the K_I calculated from the critical load. The discrepancy between the two calculations generally increased with increasing temperature.

3.5 Fracture Topography

3.5.1 Test Temperature -120°C

a) Heat 3441

The heat 3441 compact tension specimens exhibited a type 1 load-displacement record (see figure 25). Some slow crack growth preceded specimen failure as indicated by the load displacement record. Macroscopic examination of the fracture surface revealed that there were no observable shear lips.

Scanning electron micrographs of the fracture surface are given in Figure 51a. The low magnification photographs (200X) indicate that the fracture surface is very uneven. It appears as if the fracture surface is divided into sections roughly parallel to each other and roughly parallel to the crack growth direction, but at different elevation. Stereo scanning micrographs of this surface bear out the observation (Figure 51b). They also show that the cleaved regions are separated by very narrow regions that are perpendicular to the fracture surface. Often inclusion stringers were observed in the narrow separating regions; for example, Figure 51b shows an inclusion stringer laying in the separating region.

The fracture surface exhibits a cleavage failure mode (Beachem 1965, 1968). The cleavage facets are of the order of 10 microns in size.

b) Heats - 3450, 3458, X65

Much the same fractographic observations were obtained from the heats 3450, 3458, X65. For this reason, they will be grouped together.

The heat 3450, 3458 and X65 compact tension specimens exhibited type 1 load-displacement records (see Figure 25). Some slow crack growth preceded specimen failure as indicated by the load displacement records. Macroscopic examination revealed that there were no observable shear lips on any of the specimens.

Scanning electron micrographs of the fracture surfaces of heats 3450, 3458 and X65 are given in Figures 52, 53 and 54 respectively. In all cases the fracture surfaces exhibit cleavage failure modes (Beachem 1965, 1968) with the cleavage facets being of the order of 10μ in size.

Stereo scanning micrographs of the fracture surfaces did not reveal any of the sectioning and elevation differences exhibited by heat 3441.

3.6 Crack Growth Observations

3.6.1 Tensile Specimens

A scanning electron micrograph of a sectioned 3441 tensile specimen pulled to failure at $0^{\circ}C$ is given in Figure 55. The rolling direction is roughly perpendicular to the plane of these micrographs. These micrographs represent a view corresponding to the polished plane of the "two surface specimen" shown in Figure 21.

There are numerous voids in the material which are present only in

the vicinity of the crack plane. The voids do not appear to be related to the pearlite banding. Close examination of the voids revealed that some of them had inclusions at their centers. The micrograph indicates that the approximate void spacing is 75 microns.

3.6.2 Charpy Impact Specimens

A scanning electron micrograph of the crack profile view specimen is given in Figure 56. There are only a few voids ahead of the main crack. These voids appear to have been initiated around inclusions in the material.

Scanning electron micrographs of the two surface specimen are given in Figures 57a, b, c, d.

Low magnification micrographs (example Figure 57a) reveal two things. One is that the fracture surface is lined in the direction of crack propagation with deep grooves. The second is that between the deep grooves, there are much shallower grooves with a spacing that roughly corresponds to the pearlite band spacing. Higher magnification micrographs (Figures 57b, d) reveal that the deep grooves in the fracture surface correspond to regions of extensive tearing on the polished surface. Associated with the heavily torn regions are numerous voids which have been initiated at inclusions in the material. It would also appear from these micrographs that the inclusion and thus void density is much higher in the torn regions than in the surrounding material. (The plane of the micrographs of the tensile specimens shown in Figure 55 is the same as the polished surface of the two surface specimen shown here.)

Examination of the deep grooves on the fracture surface revealed that the walls of the grooves were made up of a series of small steps consisting of a mixture of cleavage and of shear rupture (Figure 57c). The depth of these grooves is closely related to the extent of tearing that is evident on the polished surface.

CHAPTER 4

ANALYSIS AND DISCUSSION

4.1 Proposed Method of Analysis

The data reported in this work from mechanical tests and from fractographic observations indicate that different failure mechanisms are involved in the fracture behaviour of these steels depending on temperature and composition. Fracture topography and crack growth studies best support this conclusion. The models used here to describe the failure mechanisms are a critical stress model, a critical strain model and a hole growth model. These will be described in more detail later.

The critical stress model is applicable when the tensile stress ahead of the crack is raised through plastic constraint and/or work hardening to the cleavage stress of the material. Catastrophic failure results. The model used here is that developed by Malkin and Tetelman. It expresses the fracture toughness in terms of the mechanical properties of the material. The effects of microstructure on these controlling properties will be examined and discussed.

The critical strain model becomes applicable when the stress concentration referred to above is not sufficient to generate stresses at the crack tip of the order of the cleavage stress. The criterion for fracture is that a critical strain be reached in a volume of material (called the "process zone") ahead of the crack. Two formulations of this model will be given; one based on energy considerations, and one based on plastic strain considerations. The models will be used to predict the size of the process zone. Evidence from the microstructure will be given in support of the predicted zone sizes. The effect of microstructure on the controlling parameters and thus on fracture toughness will be discussed.

The hole growth model is applicable to tough materials which fail

in a ductile fashion. The model will be used to correlate the fracture strain and Charpy shelf energy with volume fraction of inclusions.

Evidence based on microstructural observations will be given in support of the model prediction regarding hole initiation sites and the coalescence mechanism.

4.2. Pertinent Data in Support of the Method of Analysis

At the lowest test temperature, the as transformed and warm rolled SAE 4340 fail by a cleavage mode. Scanning electron micrographs of the as transformed 4340 broken at -120°C are given in Figure 29. The cleavage facets are roughly 10-15 μ in size which is about the same size as the prior austenite grains. The bainite ferrite plates are about 2 to 3 microns wide. The $K_{I\,c}$ value for this material and test temperature was found to be 32 ksi $\sqrt{in}$ (from Figure 26) and the calculated $G_{I\,c}$ value was 28 $\frac{in.\ lb}{in^2}$. A crack extension force of 28 $\frac{in.\ lb}{in^2}$ is consistent with the energy required to initiate plastically induced cleavage failure in steels (Tetelman 1967). Similar conclusions can be drawn concerning the warm rolled 4340 at this test temperature. There is a difference in fracture topography (see Figure 30) in that the fracture surface exhibits cleaved regions separated by narrow sheared regions. The sheared regions contribute to the higher fracture toughness of the warm rolled material. The $K_{I\,c}$ value for this temperature is 62 ksi $\sqrt{in}$ (from Figure 26) and the calculated $G_{I\,c}$ value is 114 $\frac{in.\ lb}{in^2}$. This $G_{I\,c}$ value is about midway between the energy required to initiate plastically induced cleavage failure and that to initiate plastically induced normal rupture in steels (Tetelman 1967).

The structural steels also exhibit a cleavage failure mode at a test temperature of -120°C (see Figures 51, 52, 53, and 54). However, since they have a lower yield stress than the 4340 at all test temperatures, they are

intrinsically tougher. Heats X65 and 3458 have K_{Ic} values of about 58 ksi $\sqrt{in}$ which lead to a G_{Ic} value that is about 110 $\frac{in.\ lb}{in^2}$. A crack extension force of 110 $\frac{in.\ lb.}{in^2}$ suggests that these two steels could be grouped with the warm rolled and the as transformed 4340 with respect to failure mechanism. That is failure in these materials could be described by a critical stress model. (It must be noted here that the cleavage stress, determined from notch bend data, was used as a measure of the critical stress for fracture).

The K_{Ic} value for heats 3450 and 3441 is about 75 ksi $\sqrt{in}$ at -120°C. This leads to a G_{Ic} of roughly 170 $\frac{in.\ lb}{in^2}$ which is about 2/3 the energy required to initiate plastically induced normal rupture in steels. These two steels are then, beyond the scope of the critical stress model.

The above calculations of K_{Ic} and G_{Ic} are based on the premise that plane strain conditions exist in the materials at the test temperature. The β_{Ic} values for the as transformed and warm rolled SAE 4340, Heats X65 and 3458 are 0.34, 1.04, 1.56 and 1.20 respectively. (These values are based on critical load determinations of K_{Ic}). These values suggest that almost full plane strain conditions exist in these materials at -120°C. Heats 3450 and 3441 have a β_{Ic} value of about 2.5 at this test temperature indicating a stress state intermediate between plane stress and plane strain in these materials at -120°C.

As the test temperature is raised, a point is reached when plastic constraint and work hardening are insufficient to raise the stress at the crack tip up to the cleavage stress of the material. When this happens, as long as plane strain conditions exist, a critical strain model for fracture can be applied. β_{Ic} values for the as transformed 4340 indicate that the stress state is essentially full plane strain to about 0°C.

Scanning electron micrographs of the as transformed SAE 4340 broken at 25°C are given in Figure 31. The steel exhibits a quasi-cleavage failure mode. The cleavage facets present are again of the order of the prior

austenite grain size (10-15μ). The K_{Ic} value for this test was 64 ksi $\sqrt{in}$ (from Figure 26). The calculated G_{Ic} value was 121 $\frac{in.\ lb}{in^2}$. This crack extension force is about midway between the energy required to initiate plastically induced cleavage failure (20 $\frac{in.\ lb}{in^2}$) and that for plastically induced normal rupture (240 $\frac{in.\ lb}{in^2}$) in steel (Tetelman 1967). Plane strain conditions in the warm rolled material appear to have broken down at about -50°C. Scanning electron micrographs of the warm rolled material tested at 25°C are given in Figure 32. Due to loss of constraint, true K_{Ic} values could not be determined.

Constraint in the structural steels breaks down at test temperatures of -60°C or less. Since the structural steels also exhibit a transition temperature (see Charpy data), the low temperature description of failure in these materials is further complicated by mixed mode failure in the transition temperature region. Above the transition temperature, the structural steels are relatively tough and thus plane strain conditions cannot be maintained in the compact tension specimens. The failure mechanism can best be described by a hole growth and coalescence model, which is sensitive to the stress state, the inclusion morphology and the inclusion content of the steels.

In summary then, the problem of describing the failure mechanism in the steels and relating the failure mechanisms to the detailed microstructure will be handled in the following way (see Table 8). A critical stress model for fracture will be applied to the as transformed 4340 over all test temperatures, and to the warm rolled 4340 from -120°C to about -50°C. Since the cleavage stress for the X65 and the 3458 heats of structural steel was not determined, the critical stress model could not be applied to these steels. The critical strain models will be applied to the as transformed and warm rolled 4340 over essentially the same temperature range as with the critical stress model. There is an overlap of the critical strain and critical stress models because it is difficult to decide at which temperature the stress

ahead of the crack tip can no longer reach the cleavage stress of the material. An attempt will be made later in the discussion to define the conditions for the change from critical stress to critical strain models. A hole coalescence model will be applied to the structural steels in the shelf energy temperature range.

4.3 Critical Stress Model

4.3.1 Details of the Model

Malkin and Tetelman have developed a simple model to determine $K_{I\,c}$ in terms of the microscopic cleavage stress σ_f^* (the localized fracture stress of microscopic regions, of the order of the grain size, near the crack tip), and the tensile yield stress σy for low temperature cleavage failure (Malkin 1971). Their model was developed for reactor grade steels, (room temperature yield stress of 50 ksi) and applies at sufficiently low temperatures where $\frac{\sigma f^*}{\sigma y} \leq 3.4$. When the critical displacement is small and the structure is large, unstable fracture occurs before general yield and fracture mechanics can be used to relate opening displacement to the critical plastic zone size (R_F) which is in turn, a function of stress intensity ($K_{I\,c}$) and of yield stress. The plastic zone size is determined by the criteria for localized fracture of microscopic regions near the crack tip. Cleavage occurs in steels when the tensile stress in the plastic zone ahead of the crack builds up to a critical value σ_f^* which is a function of grain size and other microscopic variables.

The Malkin and Tetelman model will be briefly described here. This model is based on Hill's (1950) expression for the longitudinal stress distribution in the plastic zone under plane strain conditions for rigid perfectly plastic materials. Under plane strain conditions, the plastic zone shape can be predicted by slip line field theory (see Figure 58).

$$\text{Then } \sigma_{yy}^{\text{max.}} = \sigma_y \left[1 + \ln\left(1 + \frac{x}{p}\right)\right] \qquad R \leq x \leq R_\beta$$

where $\sigma_{yy}^{\text{max.}}$ = maximum longitudinal tensile stress

p = root radius of notch.

By equating the external bending moment to the sum of the internal bending moments resulting from the longitudinal stress distribution (Wilshaw 1968), and by expressing the plastic zone size R as a function of the yield stress and the stress intensity parameter (McClintock 1965), Malkin and Tetelman have shown that

$$K_{Ic}(\rho) = 2.89\, \sigma_y \left[\exp\left(\frac{\sigma_{f^*}}{\sigma_y} - 1\right) - 1\right]^{1/2} \sqrt{\rho}$$

As reported in the literature, it has been shown that for $\rho \leq \rho_o$ (where ρ_o is the effective limiting root radius of the notch), the fracture toughness no longer decreases with decreasing ρ_o. (Cottrell 1965, Shoemaker 1965, Irwin 1964, Malkin 1971). That is, the effective limiting root radius sets a lower limit on K_{Ic} and prevents the toughness from becoming negligibly small in sharply cracked structures.

With this assumption then,

$$K_{Ic} = 2.89\, \sigma_y \left[\exp\left(\frac{\sigma_{f^*}}{\sigma_y} - 1\right) - 1\right]^{1/2} \sqrt{\rho_o}$$

4.3.2 Application of the Model to SAE 4340

The Malkin-Tetelman model outlined here can be applied to the as transformed and warm rolled SAE 4340. It is possible to predict values of fracture toughness from experimental measurements of the cleavage stress,

the yield stress and the effective limiting root radius.

The values of σf^* for the as transformed and warm rolled material as determined from notch bend data are 344 ksi and 364 ksi respectively. The yield stress as a function of temperature has been determined. The effective limiting root radius for the as transformed and warm rolled material can be estimated by substituting measured K_{Ic}, σf^* and σy values into the Malkin-Tetelman equation. Using these values for the 4340 at the test temperature -120°C, the value of ρ_o for the as transformed material is 2.5×10^{-3} in and for the warm rolled material 6×10^{-3} in. Malkin and Tetelman have determined ρ_o for a ferrite-pearlite steel. The value they obtained is 5×10^{-3} inches. Malkin and Tetelman also estimate ρ_o for A302B and A533 grade steels to be 2×10^{-3} inches. The estimates of ρ_o for the 4340 thus seem to be in accord with previous estimates.

If it is assumed that σ_f^* is essentially temperature independent at low temperatures (Knott 1966 , Oates 1968), the estimated values of ρ_o, yield stress data, and σ_f^* values can be used to predict K_{Ic} as a function of temperature. The predicted curves are plotted in Figure 59 along with measured K_{Ic} data.

Values of yield stress, fracture toughness, predicted fracture toughness, $\frac{\sigma f^*}{\sigma y}$ and G_{Ic} are given in Table 9 as a function of test temperature. The predicted K_{Ic} values are in reasonable agreement with the experimentally determined values for the as transformed material up to about -30°C. The $\frac{\sigma f^*}{\sigma y}$ value is 3.28 at this test temperature. The prediction for the warm rolled material is reasonably good up to about -70°C. The $\frac{\sigma f^*}{\sigma y}$ value for this temperature is 3.37.

Summarizing the data for the SAE 4340, it appears that the critical stress criterion for cleavage fracture applies when $\frac{\sigma f^*}{\sigma y} \lesssim 3.1$, when G_{Ic} is low and when the fracture surface exhibits a predominantly cleavage failure mode.

4.3.3 Controlling Parameters ($\sigma_f^*, \sigma_y, \rho_o$)

The material parameters that influence the fracture toughness at low temperatures according to the critical stress model are the cleavage stress, the tensile yield stress and the effective limiting root radius of the notch. In the analysis of the reactor grade steels, Malkin and Tetelman have assumed that ρ_o is a material constant and that it is not a function of temperature. They base this assumption on the fact that every class of materials appears to have a single value of ρ_o. They have also determined that the cleavage stress is independent of temperature over the temperature range for which the critical stress model is valid.

If these assumptions are made for the 4340, then for a given test temperature, the differences in fracture toughness between the as transformed and warm rolled material can be attributed to differences in the cleavage stress and in the effective limiting root radius. And, for a given material condition (either as transformed or warm rolled), the change in fracture toughness with temperature can be accounted for by the temperature dependence of the yield stress.

Then, in the temperature range in which the critical stress model is valid, it is possible to predict the temperature dependence of the fracture toughness of the 4340. It remains to examine the effect of microstructure on the controlling parameters of the critical stress model, in order to draw some conclusions as to the effects of microstructure on fracture toughness and the origin of the benefits of warm rolling.

4.3.4 Effect of Microstructure on the Yield Stress

The results of tensile tests conducted on the 4340 materials indicate that there is no significant difference between the yield stress of the as transformed material and the yield stress of the warm rolled material.

Transmission and scanning electron micrographs appear to be in disagreement with this data in that they reveal marked changes in both carbide morphology and dislocation substructure. This apparent contradiction can be rationalized by reference to some basic concepts of the theory of yielding in dispersed systems. The major theories of yielding in dispersed systems predict that the yield strength should vary as the reciprocal of the particle spacing or as the reciprocal square root of some effective grain size.

Transmission electron studies of the two materials indicate that the carbides in the as transformed material are rod shaped, whereas those in the warm rolled material have a much smaller aspect ratio. It also appears that the carbide spacing in the materials has not been significantly changed by warm rolling. It is of the order of 1 μ in both materials. If the as transformed 4340 had been given a spheroidizing anneal (instead of a warm rolling treatment), then a drop in the yield stress would be expected. This is due to the fact that spheroidized carbides are a less effective barrier to slip processes than are rod-shaped carbides. However, the warm rolling treatment produces a dislocation cell structure that is pinned by the carbides. Since the carbide spacing has not changed, the cell structure in the warm rolled material has roughly the dimensions of the carbide spacing in the as transformed material. Evidence in the literature indicates that cell walls of the type observed in the 4340 are effective barriers to slip. Turkalo (1958) observed that the carbides in spheroidite pin a dislocation cell structure similar to that observed in the warm rolled 4340. Embury (1966) showed that the flow stress of rolled and drawn pearlite varied as the reciprocal square root of the dislocation cell size.

The result is that the effective grain size has not changed appreciably and thus there is little change in the yield stress.

4.3.5 Effect of Microstructure on Cleavage Stress

The results of the notch bend tests were used to calculate the cleavage stresses of the as transformed and warm rolled 4340. The cleavage stress of the former is 344 ksi and of the latter 364 ksi.

The major theories of fracture predict that the cleavage stress should vary as the reciprocal square root of an effective grain size (Cottrell 1958), or as the reciprocal square root of the maximum particle size (Hodgson 1969).

Both the Cottrell model and the Hodgson-Tetelman model will be outlined here since they both give reasonable estimates of the cleavage stress of the 4340 based on microstructural observations. However, most of the fractographic and crack growth observations suggest that it is the mechanism described by the Cottrell model which is operative.

a) Hodgson-Tetelman Cleavage Stress Model

The tensile stress required to cause cracks to spread through carbides in steel can be expressed as:

$$\sigma_c = \frac{4 G_c \gamma}{k (D_s - \bar{d})^{1/2}} \qquad \text{(Cottrell-Petch model)}$$

where G_c = shear modulus of carbides

γ = work required to propagate a crack through the carbide

k = Petch constant

D_s = interparticle spacing

$\bar{d}$ = mean particle diameter

If the carbide cracks propagate into the matrix and cause the matrix to cleave, the cleavage strength will be given by σ_p, the stress required to propagate a crack in the matrix. This can be expressed as:

$$\sigma_p = \left[\frac{4 E \gamma_f}{(1-\nu^2)} \right]^{1/2} \cdot \frac{1}{\sqrt{d}} \qquad \text{(Hodgson 1969)}$$

where E = elastic modulus

γ_f = effective ferrite surface energy

ν = Poisson ratio

d = carbide size

Hodgson and Tetelman found from their experiments with carbon-manganese steels, that the cleavage strength of the steels increased as the particle size decreased even though the free interparticle spacing $(D_s - \bar{d})$ was maintained constant. This would suggest that σ_p was greater than σ_c and thus was responsible for the cleavage strength of the steels.

This carbide-size dependence of the cleavage stress could be taking place in the 4340. Transmission micrographs show that there is essentially no change in the carbide spacing on warm rolling; however, there is an increase in the cleavage stress accompanied by a decrease in the carbide size. If this is the case, then the ratio of the cleavage stress of the as transformed 4340 to that of the warm rolled 4340 should be roughly equal to the square root of the inverse of their respective carbide sizes.

That is

$$\frac{\sigma_f^* \text{ (as transformed)}}{\sigma_f^* \text{ (warm rolled)}} \approx \sqrt{\frac{d \text{ (warm rolled)}}{d \text{ (as transformed)}}}$$

Transmission microscopy indicates that the average carbide size for the warm rolled SAE 4340 is about 0.8 μ and that for the as transformed is about 1.1 μ.

Then

$$\sqrt{\frac{d_{(\text{warm rolled})}}{d_{(\text{as transformed})}}} = 0.85$$

The ratio of the observed cleavage stresses of the two materials is

$$\frac{\sigma_f^* \text{ (as transformed)}}{\sigma_f^* \text{ (warm rolled)}} = 0.94$$

The agreement is fair. Hodgson and Tetelman found that this model was good for structures containing carbides larger than 1 micron. They also found that when the carbides get smaller, the stress required to crack them becomes larger, and when σ_c approaches σ_p, the free interparticle spacing becomes important in determining the magnitude of the cleavage stress.

b) Cottrell Cleavage Stress Model

It was stated at the beginning of this section, that most of the fractographic and crack growth observations suggest that the Cottrell cleavage stress model is more applicable to the steels than is the Hodgson-Tetelman model. That is, there is some"effective grain size" controlling the cleavage stress rather than the particle size.

The Cottrell model (Cottrell (1958)) expresses the cleavage stress of a material as a function of the material's shear modulus, the effective surface energy, the Petch constant and the effective grain size.

That is:

$$\sigma_f^* = \frac{4 G \gamma_m}{k_y d^{1/2}}$$

where G = matrix shear modulus

γ_m = effective matrix surface energy

k_y = Petch constant

d = effective grain size.

The effective grain size of the 4340 materials appears to be the prior austenite grain size. Scanning electron micrographs of the as transformed and warm rolled compact tension specimens broken at low temperature exhibit cleaved fracture surfaces with cleavage facets of the order of the prior austenite grain size. There are no features on the fracture surface which relate to the particle size. Evidence of stopped microcracks, whose lengths are about 10-15 μ, appear in some of the scanning micrographs. Figure 60 shows some possible non-propagating microcracks in the warm rolled 4340. In order to verify the existence of stopped microcracks in the 4340, a "two surface specimen" was prepared from a notch bend sample which had been broken at -196°C. This low temperature would insure that a cleavage failure had occurred in the sample. Scanning electron micrographs of this sample are given in Figure 41. Stopped microcracks roughly 10 microns in length are present just below the fracture surface. Figure 41 also shows a series of microcracks about 10 microns in size connected to the fracture surface.

Using an effective grain size of approximately the prior austenite grain size (10 - 15 μ) and values for G of 10^{12} $\frac{\text{dynes}}{\text{cm}^2}$ (Cernica 1966), for γ_m of 10^4 $\frac{\text{ergs}}{\text{cm}^2}$ (Hodgson 1969) and for k_y of 1 $\frac{\text{kg}}{\text{mm}^{3/2}}$ (Embury 1971), the Cottrell model predicts a cleavage stress for the 4340 of about 350 ksi. This is in good agreement with the measured values of 344 ksi and 364 ksi for the as transformed and warm rolled materials respectively.

It has been known for some time that the fracture properties of

upper bainites are related to the prior austenite grain size (Irvine 1969), and the fracture behaviour of the 4340 is consistent with that reported in the literature. The reason that the prior austenite grain size is important is that cracks can propagate across the low angle boundaries of the parallel bainitic ferrite plates but are impeded by grain boundary carbides and the high angle boundaries. The warm rolling treatment produces changes in the microstructure which break up the path of easy propagation through the bainitic ferrite plates. In terms of the Cottrell model, the warm rolling raises the effective matrix surface energy. This could account for the higher measured cleavage stress of the warm rolled material.

In summary then, the Malkin-Tetelman model applies at sufficiently low temperatures or in irradiated steels where $\frac{\sigma_{f^*}}{\sigma_y} \leq 3.4$. The maximum ratio of $\frac{\sigma_{f^*}}{\sigma_y}$ according to elastic - perfectly plastic analysis for a sharp crack is about 2.6 (Shoemaker 1965). However, strain hardening in steels can raise the value of $\frac{\sigma_{f^*}}{\sigma_y}$ to over 3 (Rice 1968). The steels that were studied by Malkin and Tetelman in the development of this model had strain hardening exponents between 0.1 and 0.2. This leads to a value of $\frac{\sigma_{f^*}}{\sigma_y}$ of 3.4 at low temperature.

The as transformed and warm rolled SAE 4340 both have an n value of less than 0.1. From this value, the Rice and Rosengren analysis would predict a maximum value of $\frac{\sigma_{f^*}}{\sigma_y}$ of about 3.1. That is, the critical stress model for cleavage failure should apply to the SAE 4340 steels as long as $\frac{\sigma_{f^*}}{\sigma_y} \leq 3.1$.

The results of this investigation indicate that the critical stress model is capable of describing the fracture toughness behaviour of the 4340 at temperatures below about -30°C. The model predicts that for a given test temperature the fracture toughness of a material is governed by the cleavage stress and that for a given material, the fracture toughness variations with temperature are governed by the temperature dependence of

the yield stress, which is in good accord with the experimental data.

The mechanical properties of the material that determine the fracture toughness are the cleavage stress and the yield stress. These are in turn determined by the microstructure. In bainitic steels the cleavage stress is controlled by the prior austenite grain size. The warm rolling treatment appears to increase the cleavage stress by raising the effective surface energy of the ferrite matrix. The yield stress in the 4340 is controlled by carbide morphology and dislocation substructure. The warm rolling reduces the carbide aspect ratio. However the dislocation cell structure produced serves as an effective barrier to slip processes so that the yield stress remains essentially the same as that of the as transformed material.

The conclusion is that refinements in carbide morphology and the presence of dislocation cell structures are beneficial in that fracture toughness can be improved without an accompanying loss of strength.

4.4 Critical Strain Models

When plastic constraint and strain hardening are insufficient to raise the stress in the plastic zone up to the cleavage stress, unstable fracture in the material occurs when a critical plastic strain (ε_c) is achieved in a volume near the crack tip. This type of failure is best handled by a critical strain model rather than the critical stress model outlined before.

Many examples of critical strain models can be found in the literature (Krafft 1964, Hahn 1967, Malkin 1971). The basic problem is to correlate the stress intensity factor (the fracture toughness) to the plastic strain in the plastic zone. The plastic strain is in turn a function of microstructure. The region in front of the crack in which failure in the material occurs is that region in which the critical strain for fracture has

been attained. Krafft (1964) calls this region the "process zone".

In this work, two different approaches to the critical strain model have been taken. One is based on an energy criterion as outlined by Tetelman and the other is based on the plastic strain distribution in the plastic zone similar to that developed by Malkin and Tetelman (1971). The two will be briefly described and their applicability to the SAE 4340 will be discussed.

4.4.1 Model Based on Energy Considerations

In all of the critical strain models for fracture developed in the literature, the fracture criterion is related to the amount of plastic strain that occurs in the small region near the crack tip (the "process zone"). If plane strain conditions exist in the material, then plastic deformation at the crack tip is confined to narrow bands whose thickness is of the order of the diameter of the crack tip (see Figure 61). This is based on the "hinge-type"plastic zone described by Hahn and Rosenfield (1966). The displacement of the crack faces at the crack tip ($2\,V_{(c)}$) is

$$2\,V_{(c)} = 2\,\rho\,\varepsilon_{(c)}$$

(for plane strain)

where $\varepsilon_{(c)}$ = tensile strain in the region in front of the crack tip.

At the point of instability, the opening displacement has reached a critical value and the strain in the process zone has reached the fracture strain.

$$V^*_{(c)} = \rho\,\varepsilon^*_{(c)}$$

When $V_{(c)}$ has reached the critical value $V^*_{(c)}$, the stress required for unstable extension is given by

$$\sigma = \left[\frac{2E}{\pi c}\,\sigma_{(c)}\,V^*_{(c)}\right]^{1/2}$$

From an approximation made by Tetelman (1967) on an analysis by Goodier (1963).

where $\sigma_{(c)}$ can have a value from the yield stress up to the ultimate tensile stress. The term $2\sigma_{(c)}\,V^*_{(c)}$ is an energy factor and is the work required for crack propagation. In the notation of fracture mechanics, this work is termed the crack extension force $G_{I\,c}$

$$G_{I\,c} = 2\sigma_{(c)}\,V^*_{(c)} = 2\sigma_{(c)}\,\rho\,\varepsilon^*_{(c)}$$

From a fracture mechanics analysis of mode I (tensile) loading it may be shown that

$$K_{I\,c} = \left[\frac{E\,G_{I\,c}}{1-\nu^2}\right]^{1/2} \qquad \text{(Plane strain)}$$

That is, the crack extension force can be determined from fracture toughness values. Then an estimate of the process zone size can be obtained from this equation and the one previous.

$$\rho = \frac{G_{I\,c}}{2\sigma_{(c)}\,\varepsilon^*_{(c)}}$$

In the analysis of plastically induced cleavage failures $\sigma_{(c)}$ is roughly equal to σ_y. This model assumes small tensile specimens at the crack tip (that is, the stress state at the crack tip is the same as that in the neck of a tensile specimen), so that

$$\varepsilon^*_{(c)} = \varepsilon_f$$

Then

$$\rho = \frac{G_{I\,c}}{2\sigma_y \varepsilon_f}$$

4.4.2 Model Based on Plastic Strain Considerations

It is assumed, for the sake of simplicity, that the materials are rigid perfectly plastic. This is a reasonable assumption for these steels since the ratio of the yield stress to the UTS (over the temperature range of the fracture toughness tests) is about 0.8. Also the work hardening exponents of the steels are between 0.1 and 0.2.

It has been shown both theoretically (Rice 1968) and experimentally (Wilshaw 1966) that the strain distribution in the plastic zone ahead of the crack tip is of the form $\varepsilon(x) = \frac{K}{x}$.

Here a hyperbolic plastic strain distribution is assumed to exist in the plastic zone with the plastic strain varying from the yield strain (ε_y) at the elastic-plastic interface to a maximum (ε_m) at the crack tip. That is

$$\varepsilon(x) = \varepsilon_y \cdot \frac{R}{x} \qquad \text{(see Figure 62)}$$

where R = plastic zone size.

This strain distribution indicates that as $x \to 0$, $\varepsilon(x) \to \infty$. What really happens is that the maximum strain or the critical strain for fracture ε_m is attained over some region x_1, the process zone size. That is,

$$\varepsilon(x) = \varepsilon_m \quad 0 \leq x \leq x_1$$

Fracture mechanics analysis indicates that R is given by

$$R \approx \frac{1}{3\pi} \left(\frac{K_{Ic}}{\sigma_y}\right)^2$$

In this model the estimate of ε_m is the assumption which introduces the greatest error. McClintock (1968, 1969) has shown that the ductility (the fracture strain) of a deforming region was greatly reduced by the presence of triaxial stress states. Hahn and Rosenfield (Hahn 1967) have made calculations of the ratio of the fracture strain in plane strain to that in uniaxial tension. The results along with some experimental values are given in Table 10. This information is consistent with the McClintock calculations. In the development of their critical strain model, Hahn and Rosenfield assumed that $\varepsilon_m \approx \frac{\varepsilon_f}{3}$ for plane strain in view of experimental data and theoretical predictions. This same assumption will be used here.

Then the size of the process zone x_1 will be given by

$$x_1 = \frac{\varepsilon_y R}{\varepsilon_m} \approx \frac{\sigma_y}{E} \cdot \frac{1}{\frac{\varepsilon_f}{3}} \cdot \frac{1}{3\pi} \left(\frac{K_{Ic}}{\sigma_y}\right)^2 = \frac{K_{Ic}^2}{\pi E \varepsilon_f \sigma_y}$$

i.e. $$x_1 = \frac{K_{Ic}^2}{\pi E \varepsilon_f \sigma_y}$$

4.4.3 Calculation of the Process Zone Size

Values of ρ (from energy considerations) and values of x_1 (from plastic strain considerations) were calculated for the as transformed and warm rolled 4340 at the indicated temperature. The data are listed in Table 11. The agreement between the two models is good.

The size of the process zone predicted by the two critical strain criteria for the 4340 do not appear to represent the effective limiting root radius of the critical stress model. The effective limiting root radius for the

as transformed material is about 60 μ and that for the warm rolled material is about 150 μ . These are from 2 to 5 times larger than the process zones.

The process zones are probably related to the "stretch zones" reported in the literature, which are formed between the fatigue crack and the overload fracture region of the fracture toughness specimens. Gerberich and Hemmings (1969) observed stretch zones of from 2 to 5 microns in width in TRIPsteels. Beachem and Pelloux (1965) observed the same phenomenon in a Ti - 2.5 Al - 16V alloy. Spitzig (1968) observed stretch zones in a 0.45% carbon steel ($K_{I_c} \approx$ 60 ksi $\sqrt{in}$) of from 5 - 10 microns. Also, Broek (1970) has made observations of stretch zones in aluminum alloys.

The stretch zones reported in the literature are smaller than the process zones determined here due to differences in strength levels. The TRIPsteels investigated by Gerberich and Hemmings had yield strengths in the order of 250 ksi at the test temperature. For a given fracture toughness, increases in yield stress would produce a corresponding drop in the process zone size as predicted by the critical strain models. Thus it would be expected that the process zones of the steels investigated here are larger than those reported in the literature, in particular those reported by Gerberich and Hemmings.

It must be stated however, that Gerberich and Hemmings suggest that the stretch zone may not be related at all to the intrinsic toughness of the material, but related to the fatigue pre-cracking stress intensity. Whether this is the case for the 4340 and the structural steels is not known, since all the fatigue pre-cracking was done at the same stress intensity. Also, only extensive investigation of the process zone of the warm rolled 4340 broken at -70^{o}C was conducted, so that there is insufficient microscopic data on which to base any sound conclusions as to the nature of the stretch zones.

4.4.4 Microstructural Observations

(a) Process Zone Size

Slow crack growth leading to catastrophic cleavage failure was observed in some of the SAE 4340 warm rolled compact tension specimens. Scanning electron micrographs of the specimen tested at -70°C and of the slow growth specimen are given in Figure 33 and Figure 34 respectively. Examination of the fracture surfaces revealed that the interface between the slow growth region and the cleaved region was very irregular, indicating that void initiation and coalescence occurs in localized regions ahead of the main crack. When the slow growth specimens were pulled apart at -196°C, the intact regions ahead of the main crack and between the torn regions cleaved, resulting in the irregular interface.

Further study of these torn regions was conducted using the slow growth specimens sectioned at mid-thickness. A scanning micrograph of this specimen is given in Figure 35. Each of the three subsequent micrographs shown (Figures 36, 37, 38) were taken from sections approximately 30, 60 and 90 μ below the first section. Figure 35 indicates that substantial void formation and growth occurred ahead of the main crack. Examination of the micrographs of Figure 37 and 38 indicates that void growth has not occurred at these sections to the extent that it had in the section of Figure 35. Figure 39a shows a scanning micrograph of the same sections as that shown in Figure 38 after etching. It reveals small voids associated with the main crack. However, void growth is not nearly as extensive as that shown in Figure 35.

The sections shown in Figures 35 to 38 indicate that the regions of extensive void growth (the "process zone") are 20 to 30 microns in size at this test temperature (-70°C). They also suggest that void growth does not

occur uniformly ahead of this main crack in the crack plane but in localized regions. These observations are compatible with those made from the fracture surfaces of the other slow growth specimens. This microstructural evidence of the process zone size is also in good agreement with the size predicted by the two critical strain criteria for -70°C. That is $\rho = 30\mu$ and $x_1 = 23\mu$.

Higher magnification scanning micrographs of the crack and associated voids shown in Figure 39a are given in Figure 39b. These micrographs indicate that the voids are initiated at the carbides in the warm rolled material. Some carbides can be seen laying in the cusps on the fracture surface. Void initiation and growth at the carbides was also observed in the sectioned notch bend test specimens (Figure 40).

(b) Void Initiation Process

Microscopic observations from the compact tension specimens and from the notch bend specimens suggest that it is the carbides which are critical to slow crack growth and thus critical to the fracture process. The results obtained from microscopic examination of the sectioned tensile specimens are in agreement. These specimens reveal that voids are initiated first at inclusions, but the inclusion initiated voids do not appear to control the fracture process. The sectioned tensile specimens also reveal that the carbide shape determines the magnitude of the strains required and the mechanism involved in void formation in the materials.

Scanning electron micrographs of the as transformed and of the warm rolled sectioned tensile specimens are given in Figures 42 and 43 respectively. These specimens were pulled until necking had started. In both materials, voids had formed first at the matrix-inclusion interface. Interface decohesion had occurred around the whole inclusion but void growth appeared to be greatest in the direction of the tensile axis. This is to be expected. When the

particle has a higher stiffness than the matrix (as do carbides in steel), the matrix stress concentrations occur at the particle surfaces which are normal to the maximum principle stresses (Gurland 1963, Broek 1970, Low 1968). There was not evidence of cracked carbides or void formation at the carbides in the specimens.

As stated before, the studies with the tensile specimens indicate that voids are initiated first at inclusions in both the warm rolled and the as transformed materials. Whether these voids grow substantially during further straining was not adequately determined. However, inclusions observed in the specimens pulled to failure had voids associated with them that were not much larger than those in the necked specimens. Broek (1970) observed that elongated inclusions fail first prior to fracture, but growth of the so-formed cavities was hardly observed. Brindley (1968) reported that studies with tensile specimens revealed cracked particles but no void growth. From studies with magnesium alloys, Calhoun (1970) obtained results that confirm Broek's (1970) observation that the premature crack and void formation at large inclusions is irrelevant to the fracture process. They suggest that the initiation and growth of small voids does not occur until the onset of fracture.

Scanning electron micrographs of the as transformed and the warm rolled 4340 sectioned tensile specimens are shown in Figure 44 and 45 respectively. These specimens were pulled to failure. More voids are present in the warm rolled material than in the as transformed material.

Closer examination of the materials in the scanning microscope showed that many of the voids in the as transformed 4340 were initiated at cracked carbides, whereas the voids in the warm rolled 4340 were initiated around the carbides.

Many models have been developed to explain cavity or void formation at spherical particles in a matrix (Gurland 1963, Ashby 1966). Analysis of

the fracture of elongated particles by shear stresses from dislocation pileups has been made by Gurland (1963) and by Broek (1970).

The following argument from plasticity considerations can be advanced to explain void formation at particles. If a material is subjected to a uniaxial tensile stress, shear stresses inclined at 45^{o} to the tensile axis are developed. These shear stresses try to elongate the particles in the direction of the tensile axis. Since the particles are rigid, they resist this deformation resulting in tensile stresses at the particle-matrix interface which is normal to the tensile axis, and compressive stresses at the particle-matrix interface which is parallel to the tensile axis. The tensile stresses thus open voids at the particle matrix interface which is normal to the tensile axis. If the particles are rod-shaped, it is more difficult for the particles to get rid of the accumulated shear loops generated by the action of the shear stresses. The result is that the elongated particles crack instead of forming voids at their ends.

This appears to be the case in 4340 since void formation occurs at cracked carbides in the as transformed material and around carbides in the warm rolled material.

Carbide initiated voids in these tensile specimens were observed only near the crack plane. Voids in the compact tension specimens and the notch bend specimens were also observed only near the cracks. This supports the conclusion that the carbides are the particles critical to the fracture process.

4.5 Hole Growth Model

4.5.1 Ductile Fracture Criteria

Fundamental work on the phenomenon of ductile rupture has been

somewhat limited due to the theoretical complexity of the problem and in the difficulty in doing clear cut experiments. Criteria for initial yielding or for brittle fracture require only the current state of stress. In ductile fracture, changes in the size, shape and spacing of the voids will depend on the entire history of stress and strain. The actual process by which the voids coalesce to form the initial crack while the material as a whole is deforming, is extremely complicated.

The measurement of plane strain fracture toughness in low strength steels is very difficult. These materials are relatively tough so that specimens must be extremely thick in order to maintain plane strain conditions at the crack tip. (The measurement is further complicated in the transition temperature region due to mixed mode failures in and around the transition temperature.)

As long as the material is subject to plane strain, the opening displacement is directly related to the crack tip strain and the fracture toughness is in turn directly related to the opening displacement. When plane strain conditions break down, the opening displacement is still related to crack tip strain; however, there is presently no workable relationship between fracture toughness and opening displacement for plane stress conditions or for stress states intermediate between plane stress and plane strain.

Calculations of the fracture toughness made from critical load measurements and from opening displacement measurements for the structural steels differed in some cases by 30%. K_{Ic} values from opening displacement measurements were larger than those from critical load measurements. The discrepancy between the two generally increased with increasing temperature.

This can be explained by the fact that plane strain conditions were relaxed in the specimens as the test temperature increased, resulting in an increase in the fracture strain. Hahn and Rosenfield have made calculations of the ratio of the true fracture strain in plane stress and in plane strain to the true fracture strain in uniaxial tension. That is,

$\frac{\varepsilon_f}{\varepsilon_f \text{ (tensile)}}$. The results are given in Table 10 and indicate that the true fracture strain in plane strain is less than that in plane stress. The same conclusion was reached by McClintock (1969). The fracture toughness calculations based on opening displacement measurements are made with the assumption that plane strain conditions exist in the material. The β_{Ic} data (Table 7) on the structural steels indicate that this is not the case. The resulting increase in true fracture strain (and opening displacement) due to loss of constraint would produce a proportionately larger value of K_{Ic} than that obtained from critical load calculations.

The difficulties in measuring fracture toughness above the transition temperature can be by-passed by using the Charpy shelf energy as a measure of the material's toughness. Many material specifications involve a minimum Charpy impact energy at a given temperature. In the case of the structural steels tested here, the Charpy shelf energy was found to be sensitive to inclusion content, morphology and distribution. The data can be rationalized on the basis of a hole growth model and the factors contributing to the material toughness isolated.

4.5.2 Effect of Second Phase Particles on Ductile Fracture

Fracture by the growth of holes has been observed in ductile metals by a number of investigators (Tipper 1949, Puttick 1959, Rogers 1960, Bluhm 1966). Fractographic observations of the ductile fracture surfaces of metals have shown that the features of such surfaces are quite similar for a great variety of alloys (Gurland 1963). The frequent correspondence between inclusions and the dimples on fractographs, justifies the current view that inclusions, and second phase particles in general exert considerable influence on the process of ductile fracture (Gurland 1963, Rosenfield 1968).

The effect of second phase particles on the ductile fracture of copper has been well documented by Edelson (1962). Several important conclusions can be drawn from the Edelson work (Rosenfield 1968).

1. The nature of the particles does not matter. Edelson used particles ranging from hard refractory oxides to holes.
2. As the volume fraction of particles decreases, the ductility (as defined by $\varepsilon_f = \ln \frac{A_o}{A_f}$) or fracture strain increases.
3. The size of the particle does not matter. Edelson used a particle range from 1 to 200 μ.

There is not yet enough data to confirm the first and third points; however, there is considerable evidence in support of the second.

Studies of specimens which have been loaded short of fracture, and sectioned reveal that two main features dominate ductile fracture in metals. These are:

1. The formation and growth of voids around inclusions.
2. The concentration of shear in sharply defined bands.

Evidence for these two features consists of optical metallography (Gurland 1963, Rogers 1960), fractography (Beachem 1965) and transmission electron microscopy (Broek 1970, Palmer 1966).

The importance of non-metallic inclusions in steels is in their ability to affect the physical and mechanical properties of the materials. There is generally universal acceptance that sulphur has a deleterious effect on the properties of steel due to the formation of metal-sulphide inclusions. The effects of increasing amounts of sulphur on shelf energy in a variety of alloys is shown in Figure 63. In all cases, an increase in sulphur content produces a decrease in the shelf energy.

In addition to the total quantity of inclusions present affecting the mechanical properties, it has been shown that such factors as shape, size, distribution and properties of the inclusions themselves have an effect that is almost as important as the total quantity.

In wrought steels, sulphur contributes to the directional effects. The sulphides become elongated in the rolling direction resulting in marked differences in properties measured in the longitudinal direction and in the transverse direction. The effect of improved sulphide shape by additions of zirconium and titanium to low carbon steel was demonstrated by Lichy (1965). Cerium has much the same effect on sulphide shape. More oval sulphides are the result of these additions because (Mn, Zr)S, (Mn, Ti)S, and (Mn, Ce)S are less malleable and elongate less during hot rolling than does MnS. The result is improved mechanical properties for a given sulphur content. The effect of sulphide shape is demonstrated by heat X65. Heat X65 and 3441 have about the same sulphur content. The cerium additions to X65 improve the sulphide shape with the result that impact properties and ductility are improved. The effect of sulphur on tensile ductility and on impact properties was shown to vary with both the quantity of sulphur and with the type and distribution of the sulphides (Sims 1959).

4.5.3 Hole Growth Model

McClintock (1968) has developed a criterion for ductile fracture by the growth of holes. The analysis is based on solid mechanics and takes into account stress state, the influence of the geometric arrangement of holes and the influence of work hardening. It is also based on the premise that holes already exist in the material or that they form at essentially zero strain. This is certainly not the case in metals. Gurland's studies (1963) indicate that holes are formed initially at cracked particles and that hole formation occurs throughout the stress strain curve. Palmer (1966) has shown that in

copper-silica dispersions, the matrix particle interface remains partially bonded even at high strains. However at strains approaching the fracture strain where the particle matrix interface has broken and where triaxiality effects predominate, the McClintock analysis is satisfactory.

The most critical aspect of the ductile fracture process is the mechanism of hole coalescence (Rosenfield 1968). Bluhm and Morrissey (1965), using an extremely hard tensile machine, showed that hole formation and growth are gradual, while hole coalescence is rapid and catastrophic. When the holes begin to join together, crack propagation through the specimen follows closely behind.

The problem of hole coalescence can be understood on the basis of a simple model which relates the fracture strain to the volume fraction of second phase particles. (In the case of the structural steels, it will be the volume fraction of inclusions). At low strains, voids begin to appear around the second phase particles as shown schematically in Figure 64a. As the strain increases, the voids grow. The critical event for fracture is the coalescence of the holes. This occurs when the holes have grown out from the particle centers a distance of about $\frac{l_o}{2}$ (see Figure 64b). The fracture strain can then be written as

$$\varepsilon_f = \frac{l_o/2}{r_o}$$

where l_o = particle spacing

r_o = particle radius

i.e. $$\varepsilon_f = \frac{1}{2} \cdot \frac{l_o}{r_o}$$

This model indicates that fracture occurs when the strain over a region in size about equal to the initial particle spacing is equal to ε_f and that the fracture strain decreases as the particle density (volume fraction) increases. It does not however, take into account the effects of work

hardening nor does it take into account the effects of stress state or the localization of strain. The work hardening characteristics of the material undoubtedly have some control over the way in which the material between the particles is sheared to allow hole growth. Also, at strains approaching the fracture strain, triaxiality effects become important.

4.5.4 Application of the Model to the Structural Steels

If some simplifying assumptions are made, the hole growth model can be used to describe the fracture strain behaviour of the structural steels as a function of inclusion content.

The assumptions made in this analysis are:

1. The strain hardening exponents of the structural steels are approximately equal at a given temperature.
2. The stress state in the tensile samples is the same for all heats for a given test temperature and strain rate.
3. The inclusions are spherical in shape.

It is worth noting that this analysis tests only one orientation and so does not reflect the anisotropy in properties due to inclusion stringer effects.

Assumptions one and two appear to be quite reasonable. The strain hardening exponents of 3 of the 4 structural steels are given in Table 12. They are about the same. There is no reason to believe that the strain hardening exponent of heat 3450 should be drastically different from that of the other three. Since the tensile tests were performed at the same cross-head speed and with the same size tensile specimens, the stress state in the neck of the materials should be the same. Assumption three probably introduces the most error into the analysis. It is especially questionable for heat 3441, since the inclusions observed in this material were in the form

of long stringers.

With these assumptions in mind, the fracture strain then is given by the model.

$$\varepsilon_f = 1/2 \frac{\ell_o}{r_o}$$

By assuming that the inclusions are spherical, the volume fraction of inclusions can be expressed as

$$f = \frac{r_o^2}{\ell_o^2}$$

where r_o = particle radius

ℓ_o = particle spacing

Also the particle spacing can be expressed as

$$\ell = \frac{1}{\sqrt{N}}$$

where N = number of particles per unit area.

Then in terms of the QTM data

$$f = \frac{r_o^2}{\ell_o^2} = \frac{\ell^2 N}{4}$$

where ℓ = mean individual particle size

In this formulation, the mean individual particle size is used as a measure of the diameter of the inclusion.

Then from the hole growth model

$$\varepsilon_f = \frac{1}{2} \cdot \frac{\ell_o}{r_o} = \frac{1}{2} \cdot \frac{1}{\sqrt{f}} = \frac{1}{\ell\sqrt{N}}$$

That is, the fracture strain varies as one over twice the square root of the volume fraction. The data for the structural steels and data on copper dispersions (Edelson 1962, Zwilsky 1957), are plotted in Figure 65.

The data for both the copper dispersions and for the structural steels exhibit the predicted inverse relation between the fracture strain and the square root of the volume fraction. The data also indicate that the fracture strain depends only on the volume fraction and is independent of the particle size. The difference in slope and position of the copper data line and the steel data line is due to differences in the work hardening indices, the elastic moduli and possibly the stress state operative in the two sets of data.

Rosenfield, Hahn and Embury have performed statistical analyses on some data of Reinbolt and Harris on ferrite-pearlite steels and have shown that the Charpy shelf energy can be expressed as a function of the true fracture strain and the UTS. Their equation is:

$$C_v^{\text{max.}} \approx 1100 \frac{\varepsilon_f}{\sqrt{\text{UTS}}} \quad \text{(Rosenfield 1971)}$$

where the UTS is expressed in ksi.

This analysis indicates that the Charpy shelf energy should be proportional to the true fracture strain. Then according to the hole growth model, the shelf energy should also be proportional to one over the square root of the volume fraction. The Charpy shelf energy is plotted against fracture strain and one over the square root of the volume fraction ($\frac{1}{\ell\sqrt{N}}$) in Figure 66. The predicted linear relationship appears to be in accord with experimental data.

4.5.5 Microstructural Observations

(a) Hole Initiation Process

In the SAE 4340 the critical particles for slow crack growth leading to cleavage failure were the carbides. Although voids opened up first at the inclusions in the steel, the presence of inclusions appeared to be irrelevant to the fracture process.

Microscopic examination of the structural steels, indicates that the above is not the case for the structural steel. Scanning electron micrographs of a tensile specimen of heat 3441 sectioned at mid-thickness parallel to the plate thickness and perpendicular to the rolling direction are given in Figure 55. Holes in the material were found only near the crack plane (in the neck of the specimen) and were initiated around inclusions. Some of the inclusions were still present in the holes. The holes are not related in any way to the pearlite bands.

According to the hole growth model used here, the particles responsible for the fracture process should have a spacing of the order of $\frac{1}{\sqrt{N}}$.

The QTM data for heat 3441 show that N for this material is $174.1\ \text{mm}^{-2}$. That is, the critical particles should have a spacing of roughly 75 microns. Examination of the scanning micrograph indicates that the hole spacing in the material is, on the average, very close to 75 microns.

This microscopic evidence suggests that the inclusions are the particles critical to the fracture process since holes in the material are initiated at the inclusions. The pearlite banding and the ferrite grain size appear to have little to do with the hole initiation process. However, they probably have a significant influence on the hole growth and

coalescence mechanism because of their effect on the behaviour of the material between the holes.

(b) Fractographic Observations

Further evidence of the importance of the inclusions is given in Figures 57 a, b, c, d. These scanning micrographs of the "two surface specimens" reveal details of the fracture surface that bear direct relation to the microstructure.

The first observation is that the fracture surface is covered with grooves in the direction of crack propagation. That is the grooves are parallel to the rolling direction. The grooved appearance of the fracture surface is similar to that reported by Embury (1967) for a series of mild steel laminates. There are a number of deep grooves separated by fine grooves. The fine grooves have a spacing that corresponds roughly with the pearlite spacing on the polished surface. Higher magnification revealed that the deep grooves on the fracture surface were made up of a series of small steps consisting of a mixture of cleavage and of shear rupture. The depth of these grooves is closely related to the extent of tearing that is evident on the polished surface.

The inclusions in these photographs appear to be spherical. They are really in the form of stringers which run parallel to the fracture surface and perpendicular to the polished surface. Thus on the polished surface only the ends of the stringers are visible.

The fractographic observations further substantiate those made from the tensile specimens. It is apparent that the inclusions are the critical particles for fracture. It appears that some regions in the steel have a higher density of inclusions than do others. That is the distribution of inclusions in the material is not uniform. Extensive hole growth and

tearing take place during fracture in the regions of higher inclusion content.

CHAPTER 5

CONCLUSIONS

In keeping with the format of the rest of the thesis, the conclusions will be presented in two parts; Part A for the SAE 4340 and Part B for the structural steels.

Part A: SAE 4340

1) The warm rolled SAE 4340 upper bainite has a higher value of fracture toughness than the as transformed 4340 for the range of test temperatures used. The thermal-mechanical treatment (warm rolling) produces changes in the bainite microstructure (i.e., refinement of the carbide dispersion and development of a dislocation cell structure) which result in improved fracture toughness without an accompanying loss in strength.

2) The carbides appear to be the particles critical to the fracture process. In the as transformed 4340 voids are formed at cracked carbides, whereas in the warm rolled 4340 voids are formed around the carbides. In both cases it is the growth and coalescence of voids initiated at the carbides and not the voids initiated at inclusions which are critical to the fracture process.

3) At sufficiently low temperatures, the fracture toughness of the material is governed by the magnitude of the cleavage stress, and changes in fracture toughness with temperature are governed by the temperature dependence of the yield stress.

4) At higher temperatures, the fracture toughness becomes a function of the yield stress, the process zone size and the fracture strain in this process zone.

Part B: Structural Steels

1) The distribution of inclusions in the structural steels is not uniform. The heterogeneity in distribution results in the regions of extensive tearing which were observed in the Charpy "two surface" specimens.

2) Control of the inclusion shape improves mechanical properties. That is, for a given sulphur content, more spherical sulphides result in increased shelf energy and fracture strain.

3) The inclusions are the particles critical to the fracture process. The pearlite banding and the ferrite grain size have little to do with the hole initiation process; however, they probably exert considerable influence on the growth and coalescence of the holes.

4) On the basis of the proposed model, it appears that there is an inverse relationship between the square root of the volume fraction of inclusions and the true fracture strain. The same inverse relationship appears to hold for the Charpy shelf energy.

PROPOSALS FOR FUTURE WORK

The results of the experimental work on the 4340 indicate that thermal-mechanical treatments offer a method of increasing the fracture toughness without simultaneously decreasing the strength of steels in the upper bainitic condition. It is apparent that the fracture toughness of these steels could be further increased by selecting suitable rolling practices to refine the austenite grain size before transformation to bainite.

Since it has been shown that warm rolling can be a beneficial treatment for isothermal bainites, it would be interesting to apply the same type of treatment to continuously cooled bainites. Continuously cooled bainitic steels are a bit more challenging because of the variety of microstructures which can be produced by changing the rolling practice and cooling rate. However, the problem becomes a little less formidable now that it is known which microstructural changes are beneficial.

The structural steels pose a different problem again. The results of this work indicate that the inclusion content and the microstructural anisotropy of the material exert a marked influence on fracture properties. It has been shown that useful correlations can be made between the shelf energy, the fracture strain and the volume fraction of inclusions. However, care must be exercised in the use of these relations since they do not reflect the variation in properties with specimen orientation. In order to better isolate the effects of the heterogeneity in inclusion distribution, it would be interesting to make a study of the anisotropy of $C_v^{max.}$ and the tensile properties along with a careful assessment of inclusion shape and distribution. This would provide a basis for determining the relative merits of the analysis presented here, and if it can be used, with reasonable confidence, to assess the fracture properties of structural steels.

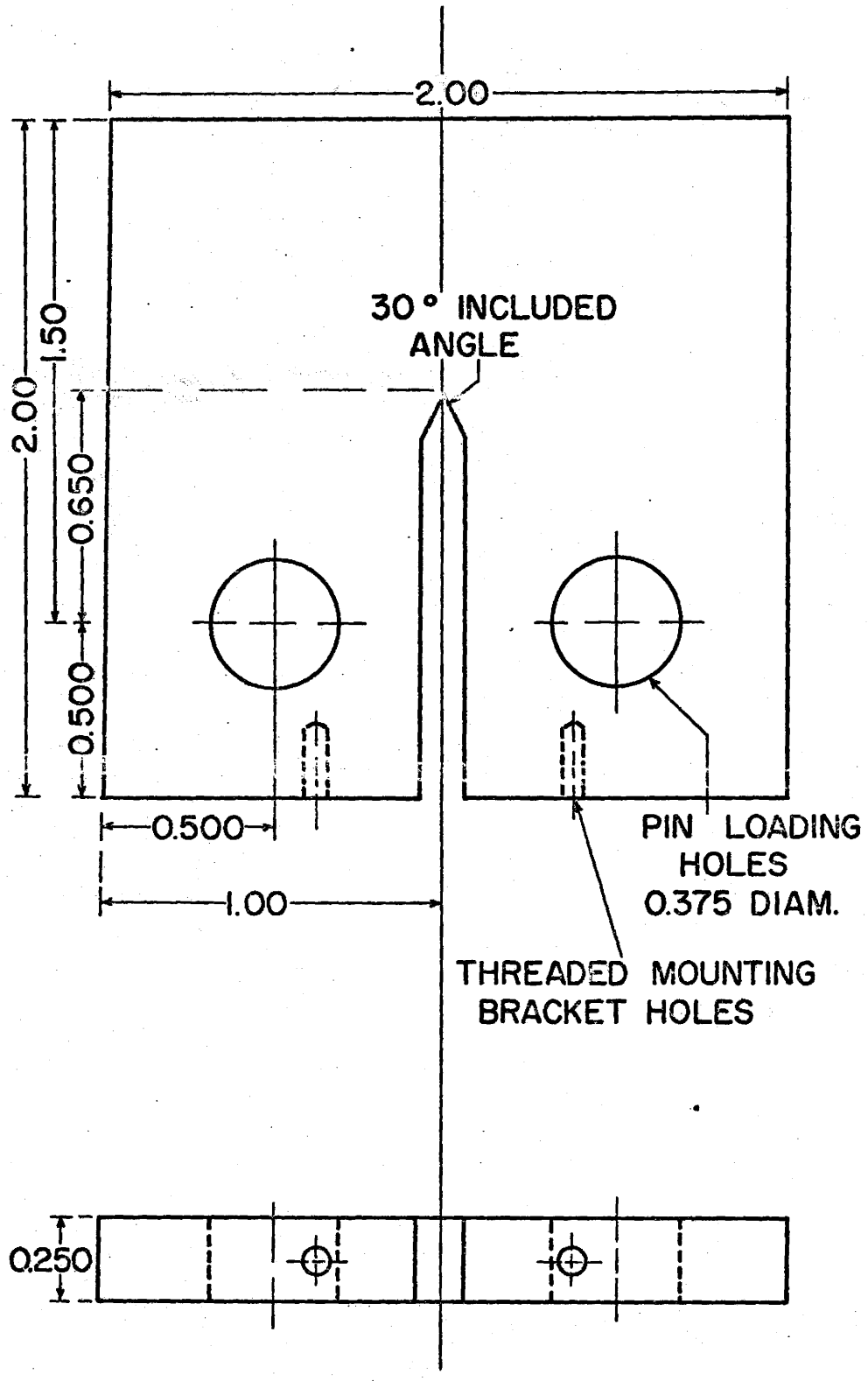

APPENDIX A . COMPACT TENSION SPECIMEN.
Scale 1" = 1/2".

REFERENCES

N. P. Allen, C. C. Earley, J. H. Rendall (1965); Proc. Roy. Soc., A285, 120.

M. F. Ashby (1966); Phil. Mag., 14, 1157.

ASTM (1970); Plane Strain Fracture Toughness of Metallic Materials, E399-70T.

R. T. Ault, K. O. McDowell, P. L. Hendricks, T. M. F. Ronald (1967); Trans. ASM, 60, 79.

J. Barsom, S. Rolfe (1971); Eng. Frac. Mech., 2, 341.

P. Bastien (1957); JISI, 187, 281.

C. Beachem, R. Pelloux (1965); "Electron Fractography - A Tool for the Study of the Micromechanisms of Fracturing Processes", Fracture Toughness Testing, ASTM STP 381.

C. Beachem (1968); "Microscopic Fracture Processes", Fracture: An Advanced Treatise, Vol. 1, Academic Press, New York.

A. J. Birkle, R. P. Wei, G. E. Pellissier (1966); Trans. ASM, 59, 981.

J. I. Bluhm, R. J. Morrissey (1966); Proceedings of First International Conference on Fracture, Sendai, Japan, Vol. III, 1739.

B. Brindley (1968); Acta. Met., 16, 587.

D. Broek (1970); "A Study on Ductile Fracture", National Aerospace Laboratories, Netherlands.

C. Calhoun, N. Stoloff (1970); Met. Trans., 1, 997.

J. N. Cernica (1966); Strength of Materials, Holt, Rinehart and Winston, New York.

A. H. Cottrell (1958); Trans. AIME, 212, 192.

A. H. Cottrell (1965); Proc. Roy. Soc., A285, 34.

J. C. Danko, R. D. Stout (1957); Trans. ASM, 49, 189.

W. E. Duckworth, P. R. Taylor, D. A. Leak (1964); JISI, 202, 135.

B. Edelson, W. Baldwin (1962); Trans. ASM, 55, 230.

B. Edelson (1963); Trans. ASM, 56, 82.

J. D. Embury, A. S. Keh, R. M. Fisher (1966); Trans. AIME, 236, 1252.

J. D. Embury, N. J. Petch, A. E. Wraith, E. S. Wright (1967); Trans. AIME, 239, 114.

J. D. Embury (1971); Strengthening Mechanisms in Crystals, (Amsterdam: Elsevier).

J. D. Embury, D. E. Osborne (1971); "Some Comments on the Use of the Scanning Electron Microscope in Fractography", International Materials Symposium, Berkely.

W. W. Gerberich, P. L. Hemmings (1969); Trans. ASM, 62, 540.

J. N. Goodier, F. A. Field (1963); Fracture of Solids, Gordon and Breach, New York.

R. A. Grange (1971); Met. Trans., 2, 417.

J. M. Gray, D. Webster, J. H. Woodhead (1965); JISI, 187, 292.

J. D. Grozier, J. H. Bucher (1967); J. Materials, 2, 393.

J. Gurland (1963); Trans. AIME, 227, 1146.

J. Gurland, J. Plateau (1963); Trans. ASM, 56, 442.

L. J. Habraken, M. Economopoulos (1967); "Bainitic Microstructures in Low-Carbon Alloy Steels and Their Mechanical Properties", Transformation and Hardenability in Steels, Symposium.

G. T. Hahn, A. R. Rosenfield (1966); "Mechanics and Metallurgy of Brittle Crack Extension", Ship Structure Committee, Battelle Columbus Laboratories.

G. T. Hahn, A. R. Rosenfield (1967); "Sources of Fracture Toughness: The Relation Between K_{Ic} and the Ordinary Tensile Properties of

Metals", presented at the ASTM Symposium, "Applications Related Phenomenon in Titanium and Its Alloys", Los Angeles.

M. Harrigan (1967); "Kinetics of Spheroidization of a Eutectic Composition Steel as Influenced by Concurrent Straining", 9th Technical Report to AISI.

R. Hill (1950); Mathematical Theory of Plasticity, Oxford University Press, London.

R. G. Hoagland, A. R. Rosenfield, G. T. Hahn (1972); Met. Trans., 3, 123.

D. Hodgson, A. S. Tetelman (1969); Fracture 1969, Brighton, Chapman and Hall.

K. J. Irvine, F. B. Pickering (1957); JISI, 187, 292.

K. J. Irvine, F. B. Pickering (1965); "High Carbon Bainitic Steels", Physical Properties of Martensite and Bainite, Special Report 93, Iron and Steel Institute.

K. J. Irvine (1969); "A Comparison of the Bainite Transformation with Other Strengthening Mechanisms in High-Strength Structural Steel", Steel Strengthening Mechanisms, Symposium, Zürich.

G. R. Irwin (1960); Trans. ASME, D82, 417.

G. R. Irwin (1964); Appl. Mater. Res., 3, 2.

C. Jatczak, D. Girardi, E. Rowland (1952); Trans. ASM, 48, 279.

D. Kalish, S. A. Kulin, M. Cohen (1965); J. Metals, Feb., 157.

P. M. Kelly, J. Nutting (1961); JISI, 197, 199.

J. S. Kirkaldy, J. Forstmann, R. Brigham (1962); Can. Met. Quart., 1, 59.

J. F. Knott (1966); JISI, 204, 104.

J. Krafft (1964); Appl. Mater. Res., 3, 88.

D. J. Latham (1970); JISI, 208, 50.

E. J. Lichy, G. C. Duderstadt, N. L. Samways (1965); J. Metals, July, 769.

J. R. Low (1968); Eng. Frac. Mech., 1, 47.

J. Malkin, A. S. Tetelman (1971); Eng. Frac. Mech., 3, 151.

F. A. McClintock, G. R. Irwin (1965); Fracture Toughness Testing, ASTM STP 381, 84.

F. A. McClintock (1968); J. Appl. Mech., June, 363.

F. A. McClintock (1969); "Crack Growth in Fully Plastic Grooved Tensile Specimens", Physics of Strength and Plasticity, MIT.

C. J. McMahon, M. Cohen (1965); Acta. Met., 13, 591.

A. Mendelson (1968); Plasticity, Theory and Application, MacMillan.

G. Oates (1968); JISI, 206, 930.

J. M. Oblak, R. F. Heheman (1967); "Structure and Growth of Widmanstätten Ferrite and Bainite", Transformation and Hardenability in Steels, Symposium.

I. Palmar, G. Smith, R. Warda (1966); "Physical Basis of Yield and Fracture", Conference Proceedings, Institute of Physics and Physical Society, 53.

N. J. Petch (1953); JISI, 174, 25.

J. L. Peterson (1963); Trans. ASM, 56, 304.

F. B. Pickering, T. Gladman (1963); Metallurgical Developments in Carbon Steels, Special Report 81, Iron and Steel Institute (London), 10.

K. Puttick (1959); Phil. Mag., Series 8, 4, 964.

J. R. Rice, G. F. Rosengren (1968); J. Mech. Phys. Solids, 16, 1012.

H. Rogers (1960); Trans. AIME, 218, 498.

A. R. Rosenfield (1968); Met. Reviews, Review 121.

A. R. Rosenfield, G. T. Hahn, J. D. Embury (1971); "Effect of Cementite Morphology on the Fracture of Steels", submitted to Met. Trans.

D.N. Shackleton, P.M. Kelly (1965); "Morphology of Bainite", Physical Properties of Martensite and Bainite, Special Report 93, Iron and Steel Institute, 126.

O. Sherby, M. Harrigan, L. Champagne, C. Sauve (1969): Trans. ASM, 62, 575.

A.K. Shoemaker (1965); Fracture Toughness Testing, ASTM STP 381, 26.

C.E. Sims (1959); Trans. AIME, 215, 367.

W.A. Spitzig (1968); Trans. ASM, 61, 344.

A.S. Tetelman, A.J. McEvily (1967); Fracture of Structural Materials, Wiley.

D.H. Timbres (1970); Ph.D. Thesis, McMaster University.

C. Tipper (1949); Metallurgia, 39, 133.

A.M. Turkalo, J.R. Low Jr. (1958); Trans. AIME, 212, 750.

J. Uvira, D.B. Clay, P. Worthington, J.D. Embury (1970); "The Structure and Properties of Warm Rolled Steel", submitted to Can. Met. Quart.

E.T. Wessel (1968); Eng. Frac. Mech., 1, 77.

T.R. Wilshaw (1966); JISI, 204, 936.

T.R. Wilshaw, C.A. Rau, A.S. Tetelman (1968); Eng. Frac. Mech., 1, 19.

V.F. Zackay, E.R. Parker (1965); Proceedings of First International Conference on Fracture, Sendai, Japan, (Preprint): BII 87.

K. Zwilsky, N. Grant (1957); J. Metals, 9, 1197.

TABLE 1

CHEMICAL COMPOSITION OF SAE 4340 (wt. %)

C	Mn	P	S	Si	Ni	Cr	Mo
0.41	0.72	0.002	0.010	0.26	1.90	0.82	0.28

Data courtesy of United States Steel Corporation.

TABLE 2

TEST NUMBER	AUSTENITIZED		TRANSFORMED	
	TEMP (^{o}C)	TIME (Min.)	TEMP (^{o}C)	TIME (Min.)
1	1000	30	650	4
2	1000	30	650	16
3	1000	30	650	30
4	1000	30	650	60

NOTE: Each test was followed by a water quench.

TABLE 3

CHEMICAL COMPOSITION OF THE STRUCTURAL STEELS

HEAT NUMBER	CHEMISTRY							HEAT TYPE	TRANSFORMATION ($^{\circ}$F) CHARACTERISTICS	
	C	Mn	Cb	Si	P	S	Al		Ar_3	Ar_1
3441	.09*	2.00*	.047	.15	.013	.016	.118	Air Induction Melt	ND	ND
3450	.13	1.64	-	.25	.013	.006	.03	Triple Slag Practice	1470	1120
3458	.19*	1.65*	.06	.34	.017	.003*	.05	ESR	1470	1120
X65	.11	1.34	.021	.32	.013	.015	.04	Open Hearth (Ce additions)	1455	1240

The figures given are weight percents.

ND - not determined

* - data checked at McMaster

Data are courtesy of the Steel Company of Canada.

TABLE 4

HEAT NUMBER	GRAIN SIZE (μ)	PERCENT PEARLITE
3441	10.2	15.0*
3450	9.4	30.7
3458	8.4	22.3
X65	10.3	17.0

* estimated from micrographs.

Data courtesy of the Steel Company of Canada.

TABLE 5

QTM DATA

HEAT NUMBER	NUMBER /mm^2 (N)	TOTAL LENGTH ($x10^{-1}mm$) (ℓ_T)	MEAN INDIVIDUAL LENGTH ($x10^{-2}mm$) (ℓ)	PERCENT TOTAL AREA	TOTAL AREA (mm^2x10^{-3}) (A_T)	MEAN INDIVIDUAL AREA (mm^2x10^{-4}) (A)
3441	174.1	.697	.470	.241	.205	.138
3450	82.1	.276	.395	.097	.083	.119
3458	36.6	.116	.370	.045	.039	.123
X65	104.4	.338	.380	.133	.113	.127

Data courtesy of the Steel Company of Canada.

TABLE 6

SAE 4340

TEMP (^{o}C)	σ_y (ksi)	K_{Ic} (ksi$\sqrt{in}$) (Load)	K_{Ic} (ksi$\sqrt{in}$) (Cod)	$(\frac{K_I}{\sigma_y})^2 \frac{1}{B}$ (Load)	$(\frac{K_I}{\sigma_y})^2 \frac{1}{B}$ (Cod)	LOAD-DISPLACEMENT CURVE TYPE (Figure 25)
AS TRANSFORMED						
25	100	64.2	61.2	1.64	1.47	4
-30	105	53.5	47.9	1.04	0.84	4
-70	110	55.7	42.3	1.00	0.60	3
-95	117	42.7	37.2	0.52	0.40	3
-120	126	36.7	31.9	0.34	0.26	3
WARM ROLLED						
25	97	77.0*	74.1	2.52	2.32	2
-30	103	81.9*	79.5	2.52	2.36	2
-70	108	81.9	79.3	2.24	2.16	1
-95	118	69.0	71.5	1.36	1.44	1
-120	130	66.0	47.6	1.04	0.52	1

* - Tests did not satisfy the ASTM 5% secant intercept requirement for plane strain.

TABLE 7

STRUCTURAL STEELS

TEMP (°C)	σ_y (ksi)	K_I ksi $\sqrt{in}$ (Load)	$(\frac{K_I}{\sigma_y})^2$ (in)	$(\frac{K_I}{\sigma_y})^2 \frac{1}{B}$	LOAD DISPLACEMENT CURVE TYPE (Figure 25)
3441-60		-	-	-	2
-75	79	79.9	1.02	4.08	2
-90	84	74.9	0.79	3.16	2
-110	91	79.5	0.76	3.04	1
-120	96	75.0	0.61	2.44	1
3450-60		-	-	-	2
-75	65	79.9	1.51	6.02	2
-90	70	68.3	0.95	3.8	2
-105	77	78.8	1.04	4.16	1
-120	85	72.1	0.72	2.88	1
3458					
-30	69	55.0	0.62	2.48	2
-60	75	55.3	0.54	2.16	2
-90	87	59.2	0.46	1.84	1
-120	101	55.6	0.30	1.20	1
X65					
-30	67	58.6	0.76	3.04	2
-60	70	62.2	0.79	3.16	2
-90	79	60.3	0.58	2.32	2
-120	92	57.6	0.39	1.56	1

TABLE 8

STEEL	TEST TEMPERATURE RANGE (^{o}C)	MODEL
as transformed SAE 4340	-120 to ~25	critical stress
warm rolled SAE 4340	-120 to ~ -50	critical stress
as transformed SAE 4340	-120 to ~25	critical strain
warm rolled SAE 4340	-120 to ~ -50	
structurals	> 25 (shelf energy range)	hole growth

TABLE 9

CRITICAL STRESS MODEL

SAE 4340 As Transformed σ_f^* = 344 ksi, ρ_o = .0025 in.
Warm Rolled σ_f^* - 364 ksi, ρ_o = .006 in.

TEMP (^oC)	σ_y (ksi)	K_{Ic} (Load) (ksi $\sqrt{in}$)	K_{Ic} (Cod) (ksi $\sqrt{in}$)	K_{Ic} Predicted (ksi $\sqrt{in}$)	$\frac{\sigma_f^*}{\sigma_y}$	G_{Ic}+ ($\frac{in.\ lb.}{in^2}$)
As Transformed						
-120	126	36.7	31.9	37	2.73	28
-95	117	42.7	37.2	41	2.94	47
-70	110	55.7	42.3	44	3.12	62
-30	105	53.5	47.9	45	3.28	86
25	100	64.2	61.2	47	3.44	121
Warm Rolled						
-120	130	66.0	47.6	65	2.80	114
-95	118	69.0	71.5	70	3.08	158
-70	108	81.9	79.3	75	3.37	185
-30	103	81.9	79.5	78	3.54	205++
25	97	77.0	74.1	82	3.75	203++

+ → G_{Ic} (plane strain) values calculated from the equation $G_{Ic} = \frac{K_{Ic}^2 (1 - \nu^2)}{E}$ (Tetelman 1967)

++ → G_I (plane stress) values calculated from the equation $G_I = \frac{K_I^2}{E}$ (Tetelman 1967)

TABLE 10

TYPE OF TEST	$\frac{\varepsilon_f}{\varepsilon_f \text{ (tensile)}}$	
	Calculated	Measured
Round Tensile Bar (Necking)	1.00	-
Plane Stress Zone	0.65	0.52[a], 0.52[b], 0.39[c]
Plane Strain Zone (Maximum constraint)	0.10	-

(a) 2219 - TA86 Al

(b) 7075 - T6 Al

(c) 4340 Steel

TABLE II

SAE 4340

TEMP (°C)	ε_f	σ_y (ksi)	K_{Ic} * (ksi$\sqrt{in}$)	G_{Ic} (in.lb/in^2)	PROCESS ZONE SIZE (μ)	
					ρ (energy)	x_1 (strain)
As Transformed						
25	.54	100	64	121	30	21
-30	.54	105	54	86	20	14
-70	.53	110	46	62	14	10
-90	.51	117	40	47	10	8
-120	.46	126	32	28	6	5
Warm Rolled						
-70	.72	108	79	185	30	23
-95	.70	118	73	158	26	18
-120	.67	130	62	114	17	12

* From Figure 26.

TABLE 12

HEAT NUMBER	STRAIN HARDENING EXPONENT (25°C) (n)
3458	0.132
3450	-
3441	0.181
X65	0.162

Data courtesy of the Steel Company of Canada.

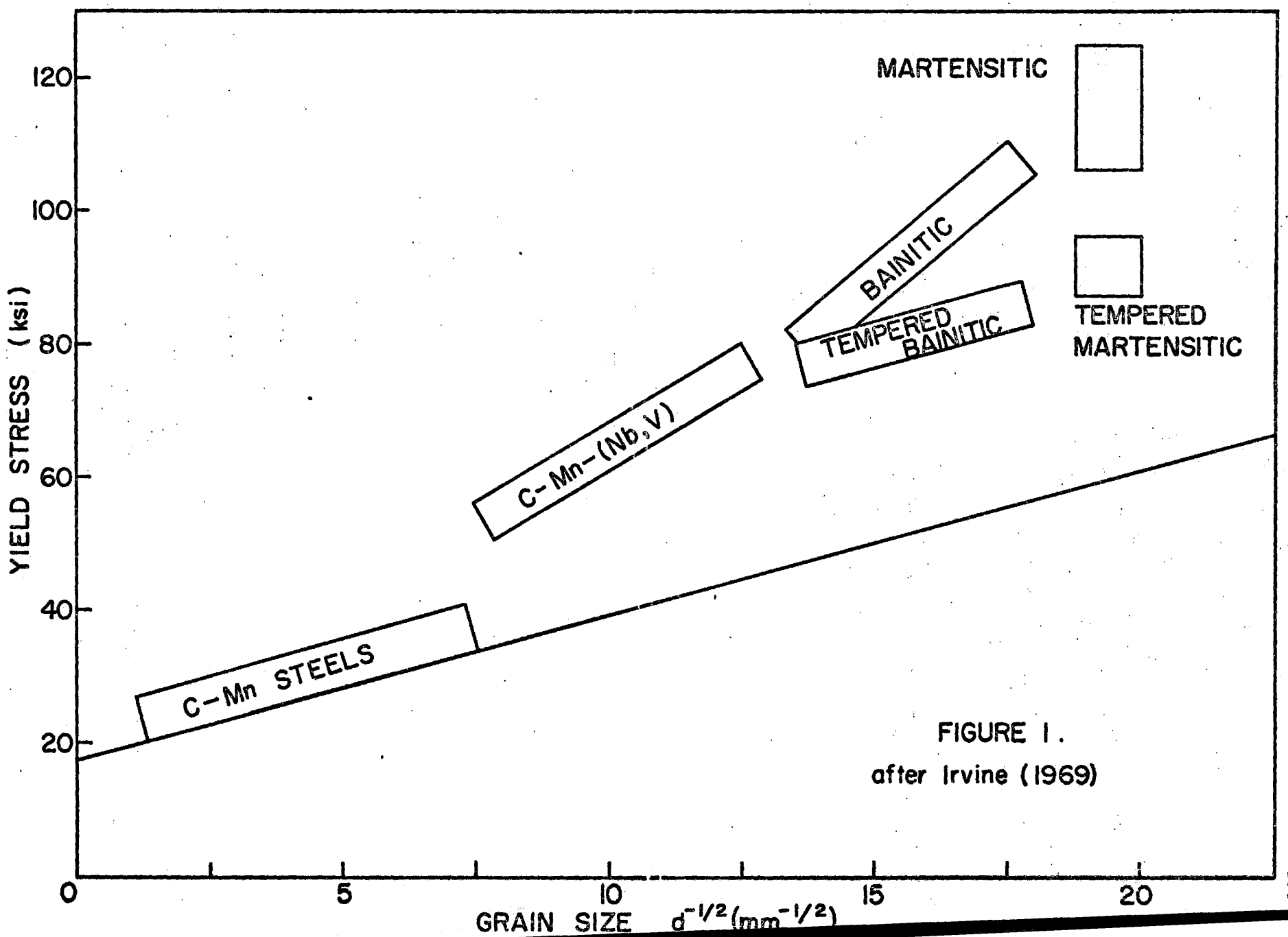

FIGURE 1.
after Irvine (1969)

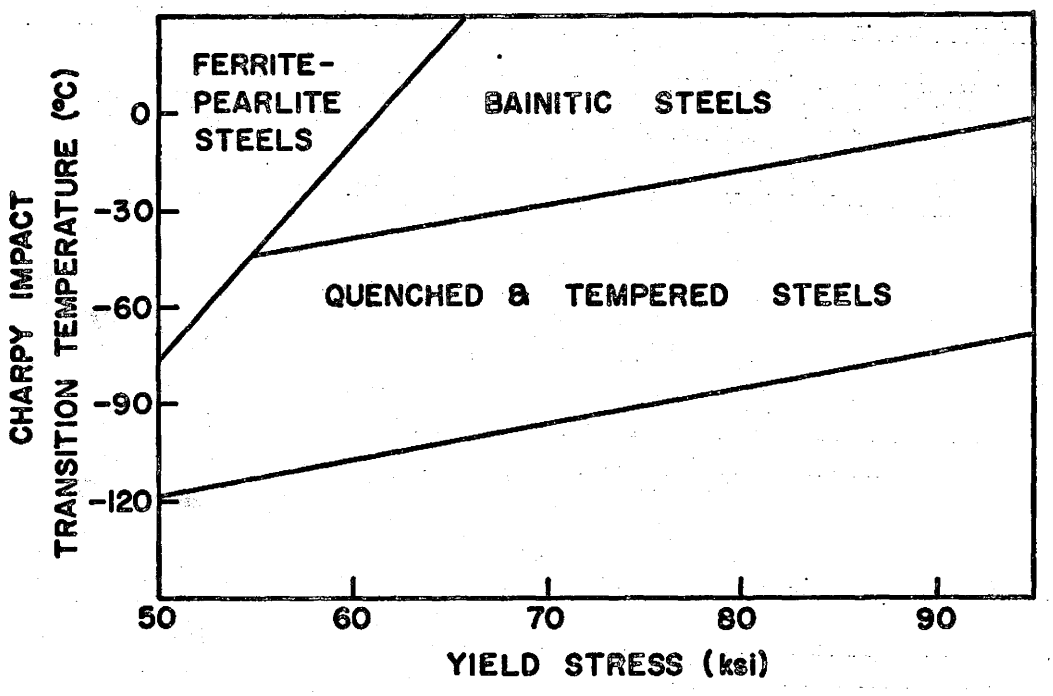

FIGURE 2. AFTER IRVINE (1969)

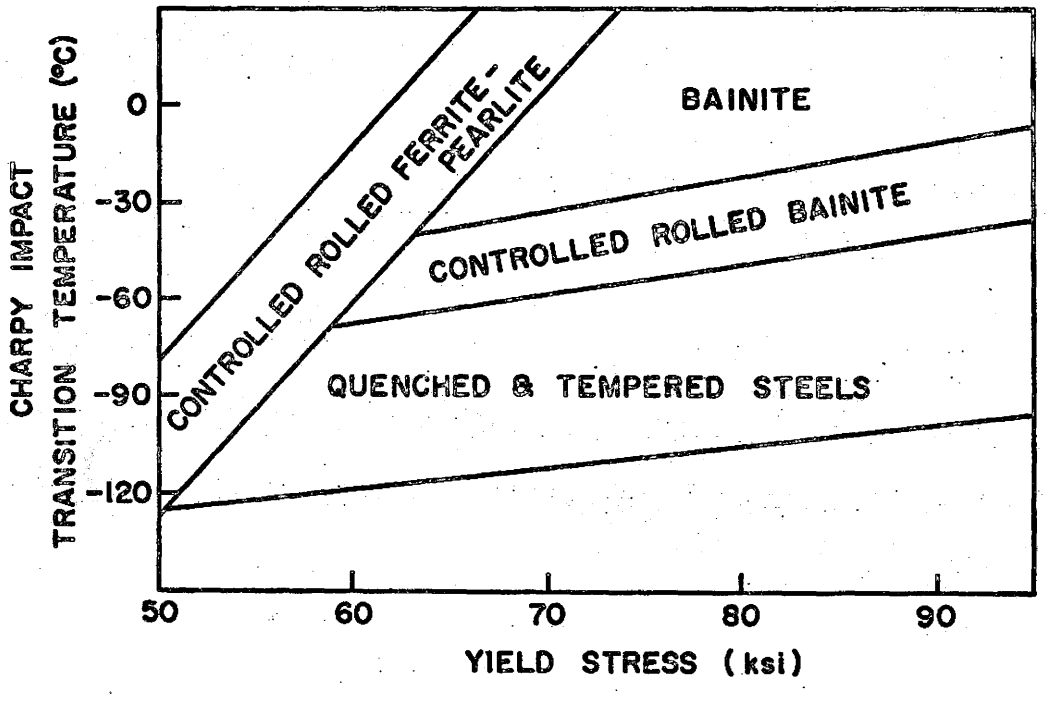

FIGURE 3. AFTER IRVINE (1969)

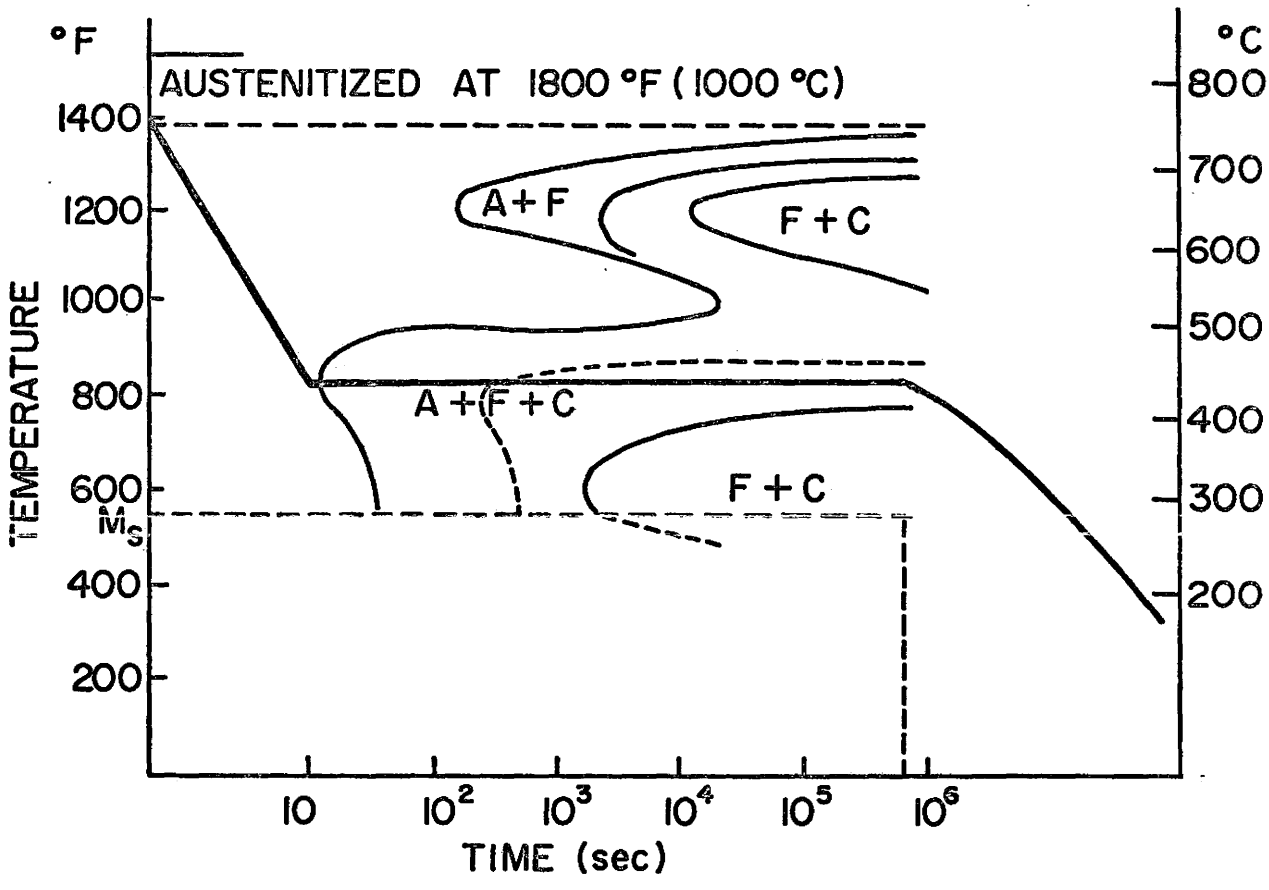

FIGURE 4. BAINITE HEAT TREATMENT CYCLE.
IT Diagram (USS 1963)

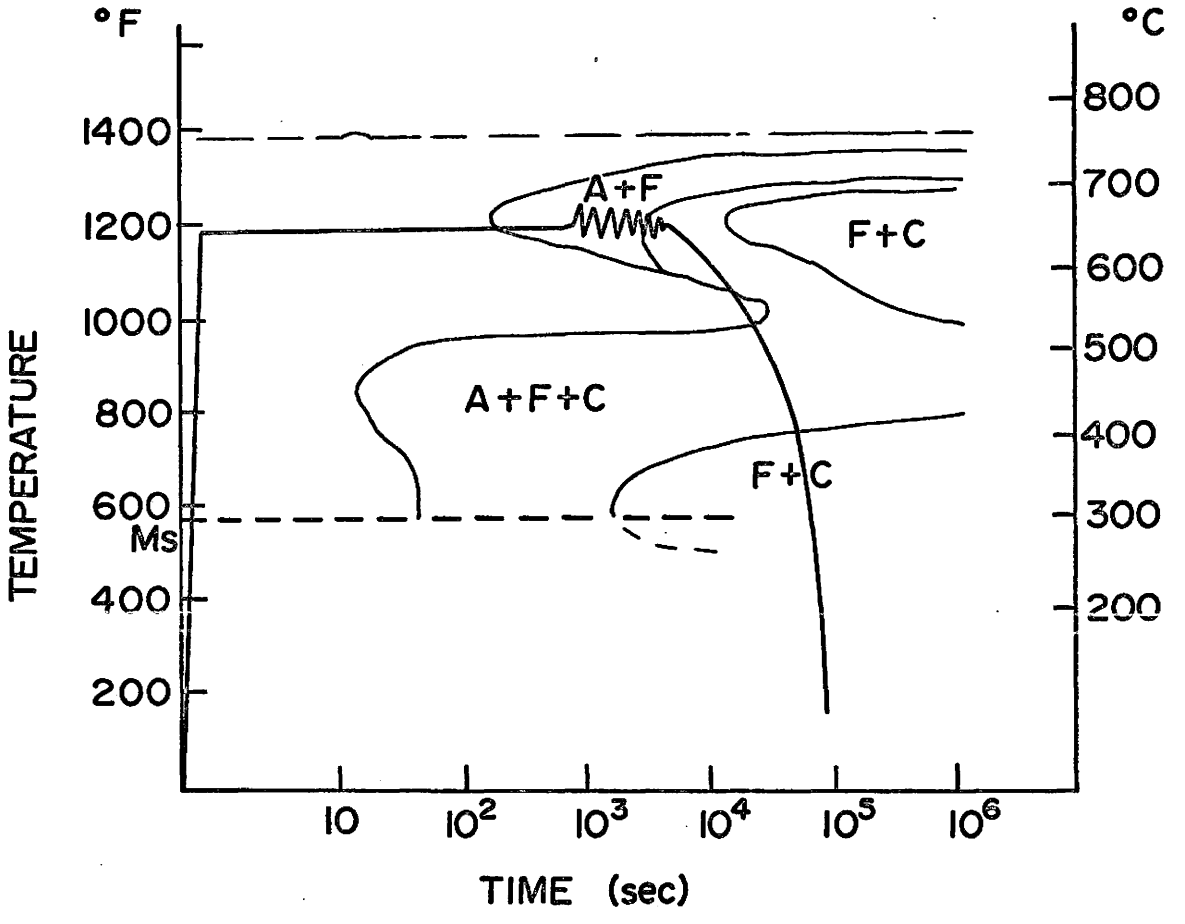

Figure 5 Thermal Mechanical Treatment Cycle
IT Diagram (USS 1963)

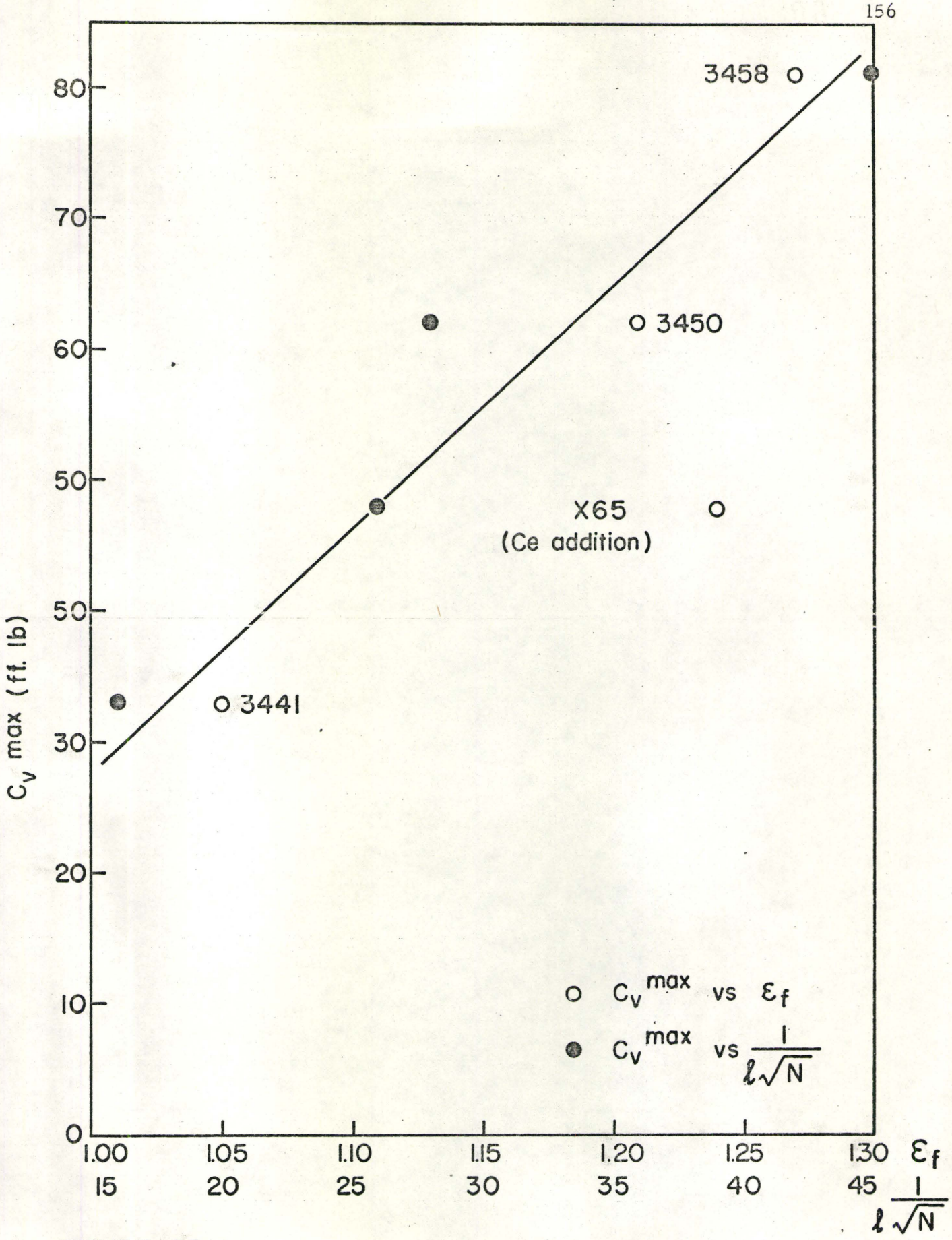
3458
3450
X65
(Ce addition)
3441
C_v max (ft. lb)
C_v^{max} vs ε_f
C_v^{max} vs $\frac{1}{\ell\sqrt{N}}$
0
10
20
30
50
50
60
70
80
1.00
1.05
1.10
1.15
1.20
1.25
1.30
ε_f
15
20
25
30
35
40
45
$\frac{1}{\ell\sqrt{N}}$

FIGURE 66.

Figure 6. SAE 4340 AS TRANSFORMED.
2000X

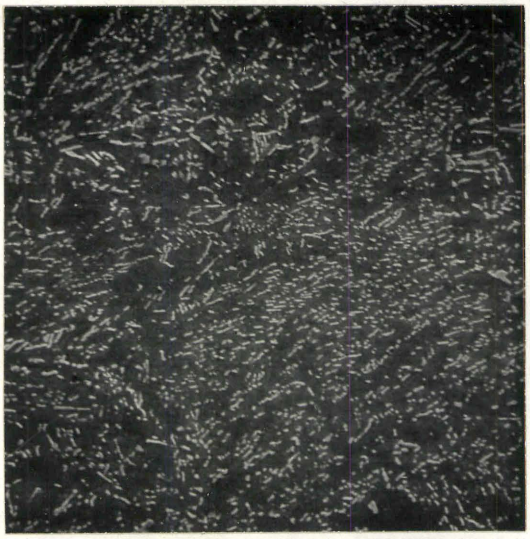

Figure 8. SAE 4340 WARM ROLLED.
2000X

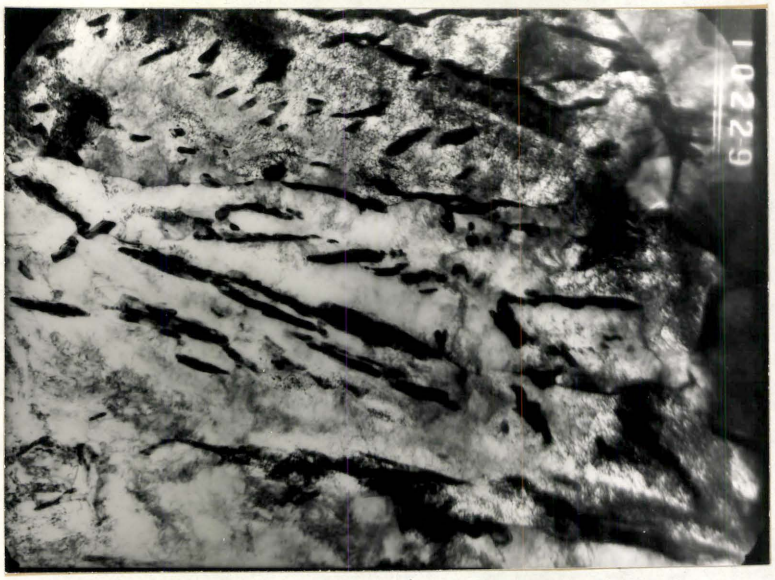

Figure 7. SAE 4340 AS TRANSFORMED. 1 μ

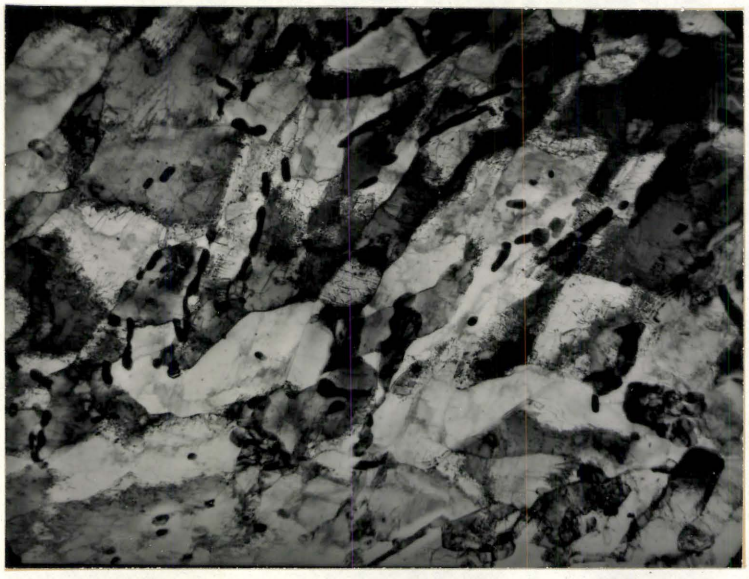

Figure 9. SAE 4340 WARM ROLLED. 1 μ

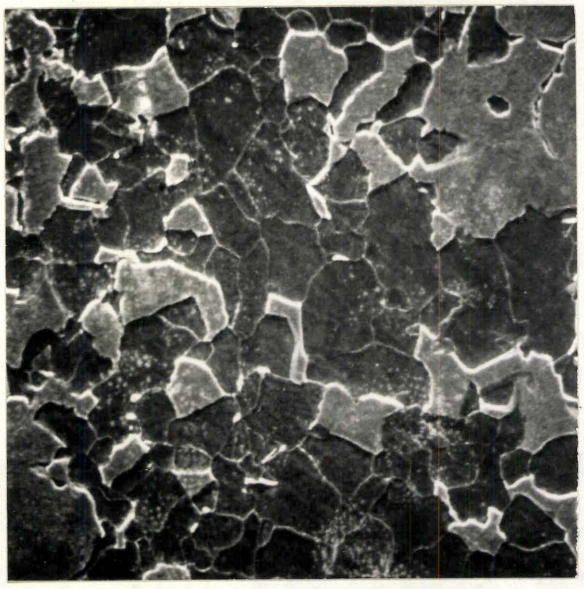

Figure 10. SAE 4340.
500X

20 μ

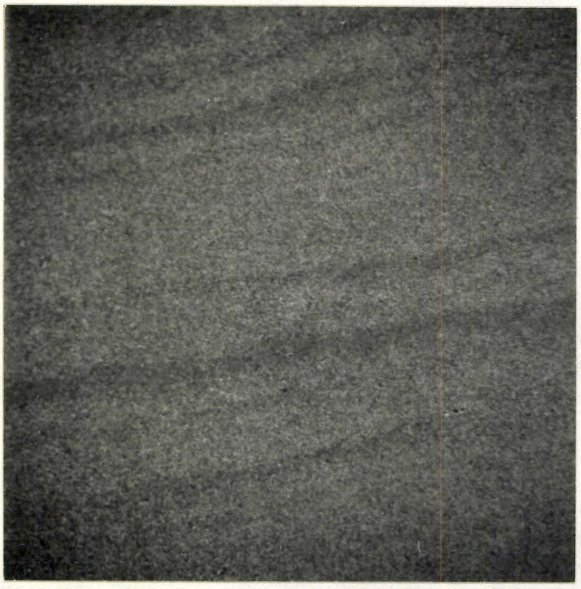

Figure 11. SAE 4340 AS TRANSFORMED.
100X

ROLLING DIRECTION

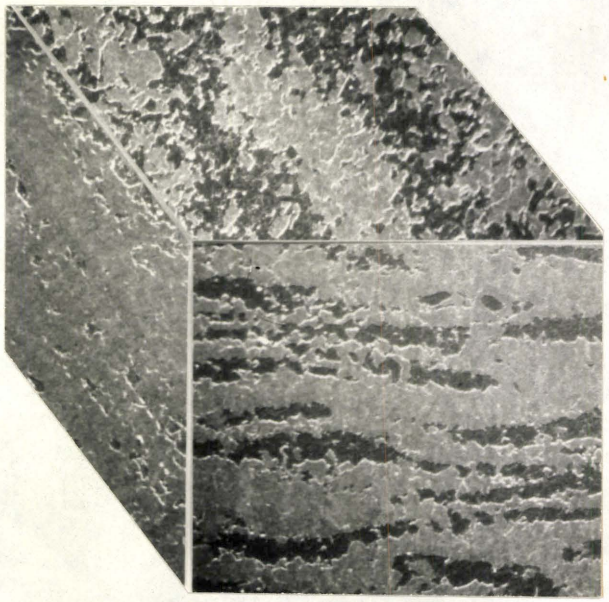

Figure 12. SAE 4340.
X100

Figure 13. SAE 4340 WARM ROLLED.
200X

ROLLING DIRECTION

Figure 14. HEAT 3441.
100X

ROLLING
DIRECTION

Figure 15. HEAT 3450.
100X

ROLLING
DIRECTION

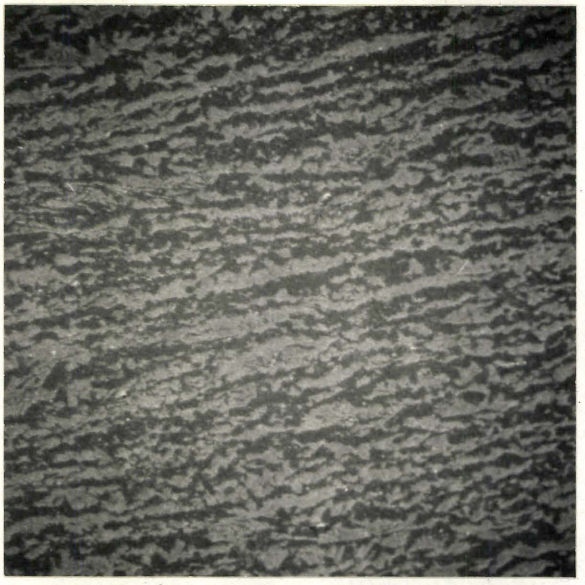

Figure 16. HEAT 3458.
100X

ROLLING
DIRECTION

Figure 17. HEAT X65.
100X

ROLLING
DIRECTION

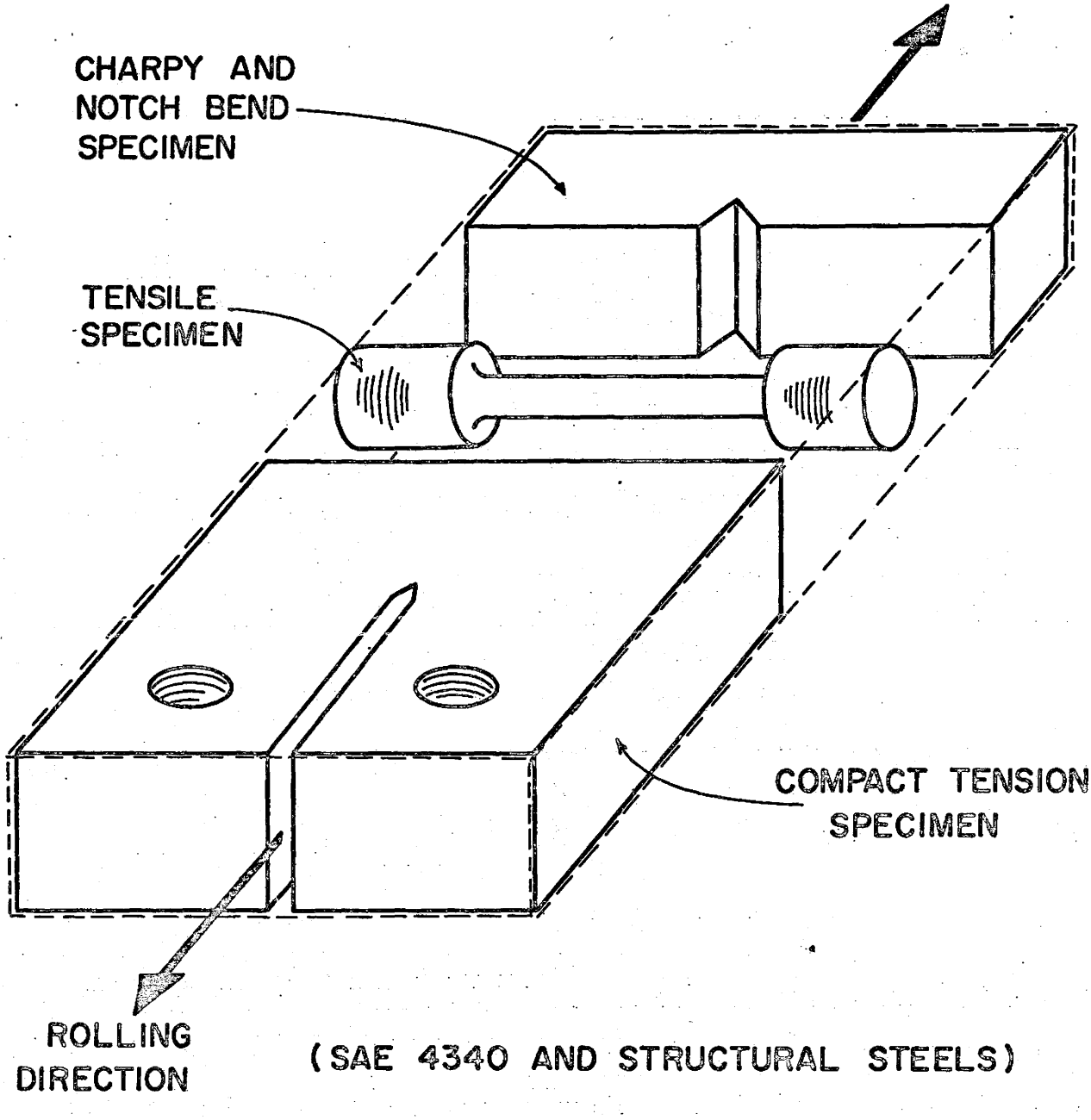
CHARPY AND
NOTCH BEND
SPECIMEN
TENSILE
SPECIMEN
COMPACT TENSION
SPECIMEN
ROLLING
DIRECTION
(SAE 4340 AND STRUCTURAL STEELS)

FIGURE 18.

FIGURE 19

CHART DRIVE AMPLIFIER
SETTING 1" = .002"

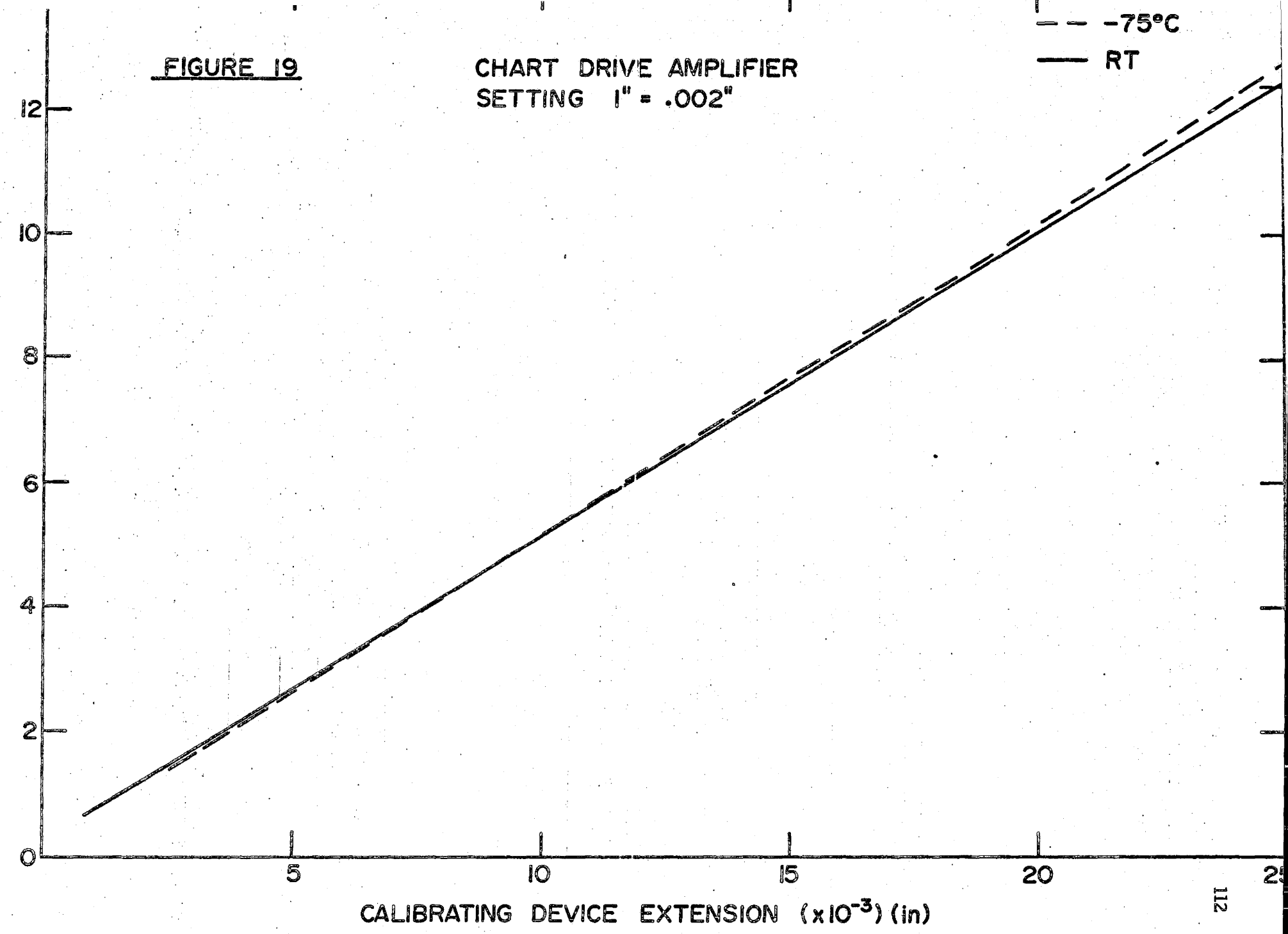

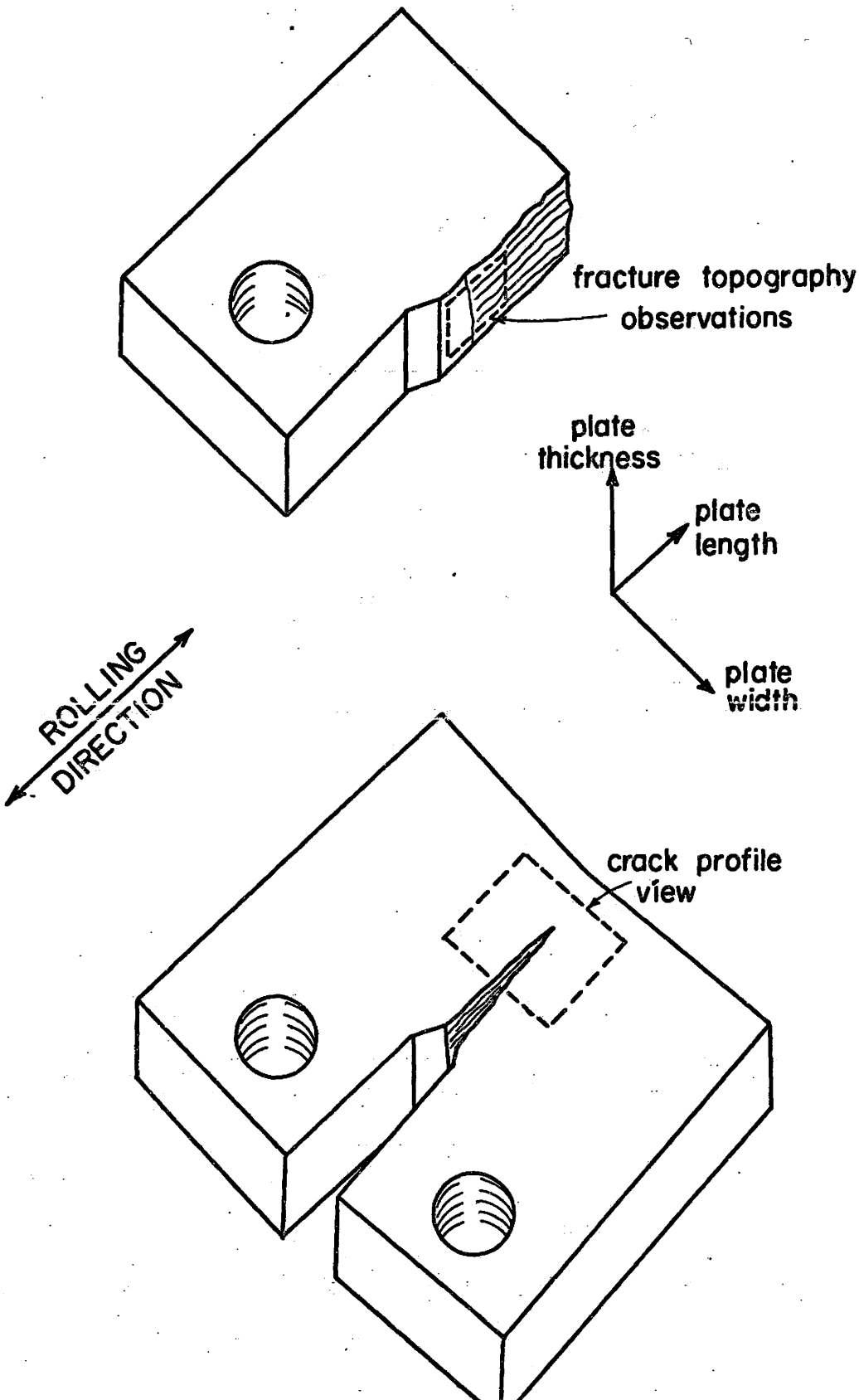

FIGURE 20. COMPACT TENSION CRACK GROWTH SPECIMEN

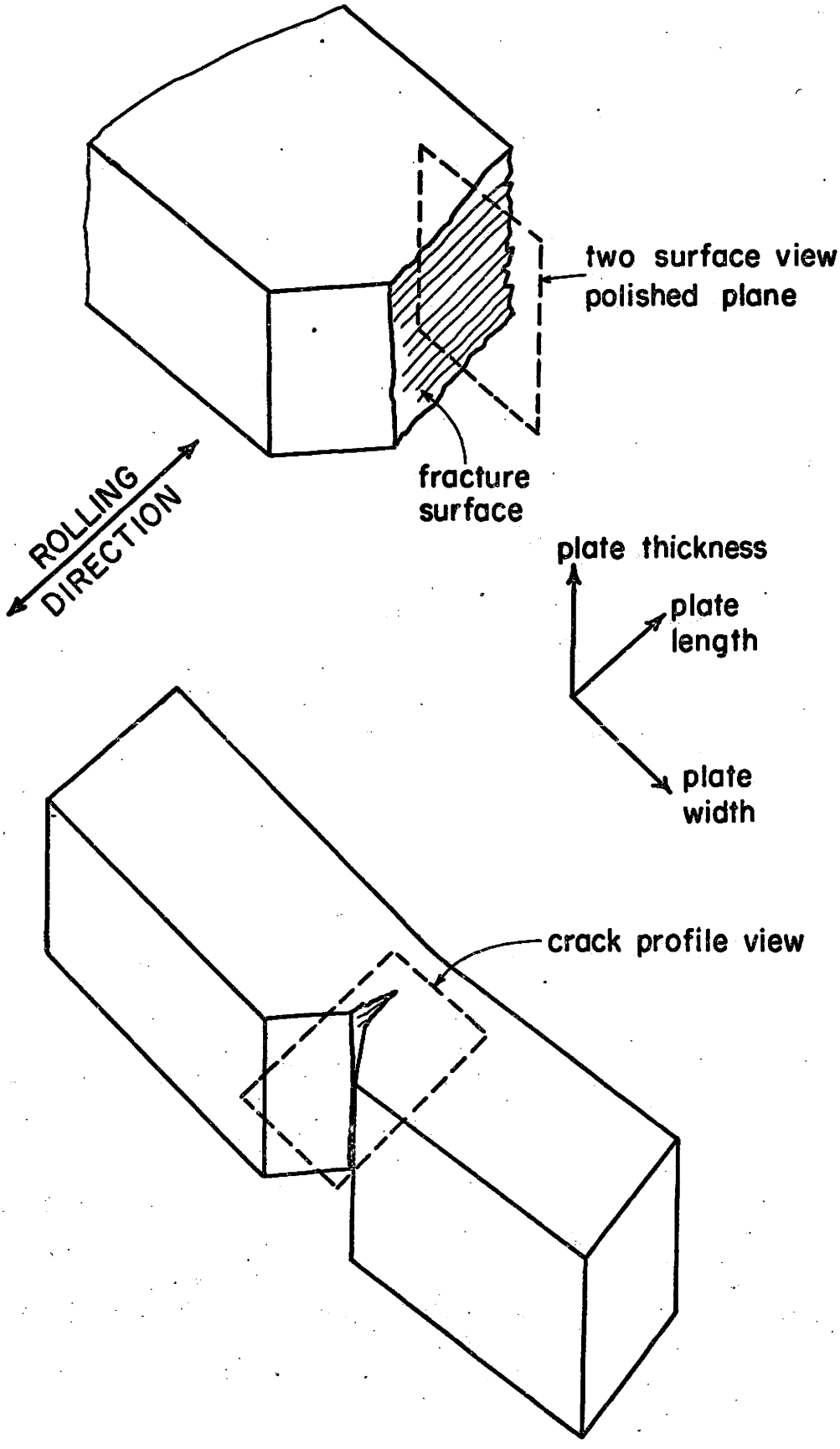

FIGURE 21. CHARPY & NOTCH BEND CRACK GROWTH SPECIMEN.

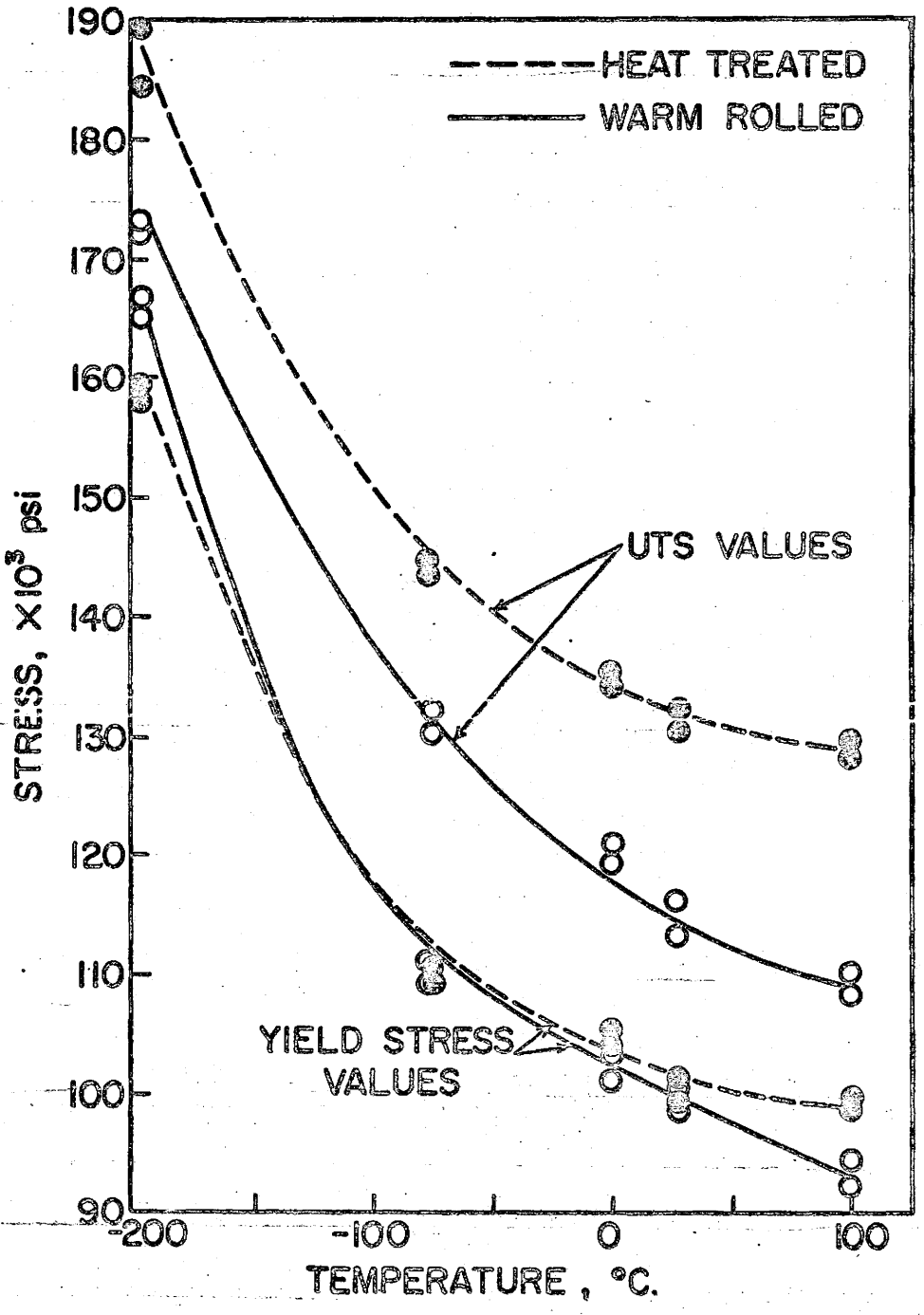

FIGURE 22. SAE 4340. TENSILE DATA.

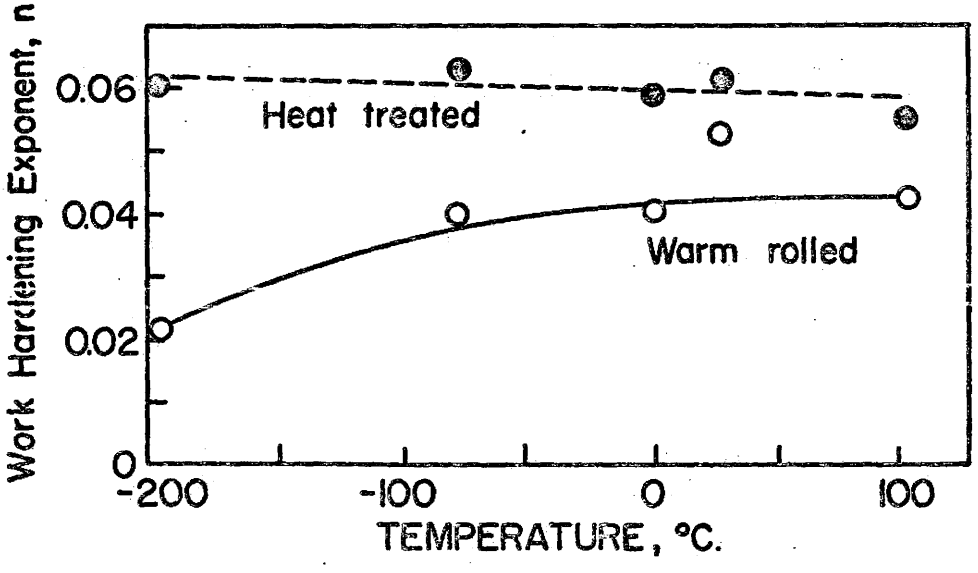

FIGURE 23. SAE 4340. WORK HARDENING EXPONENT.

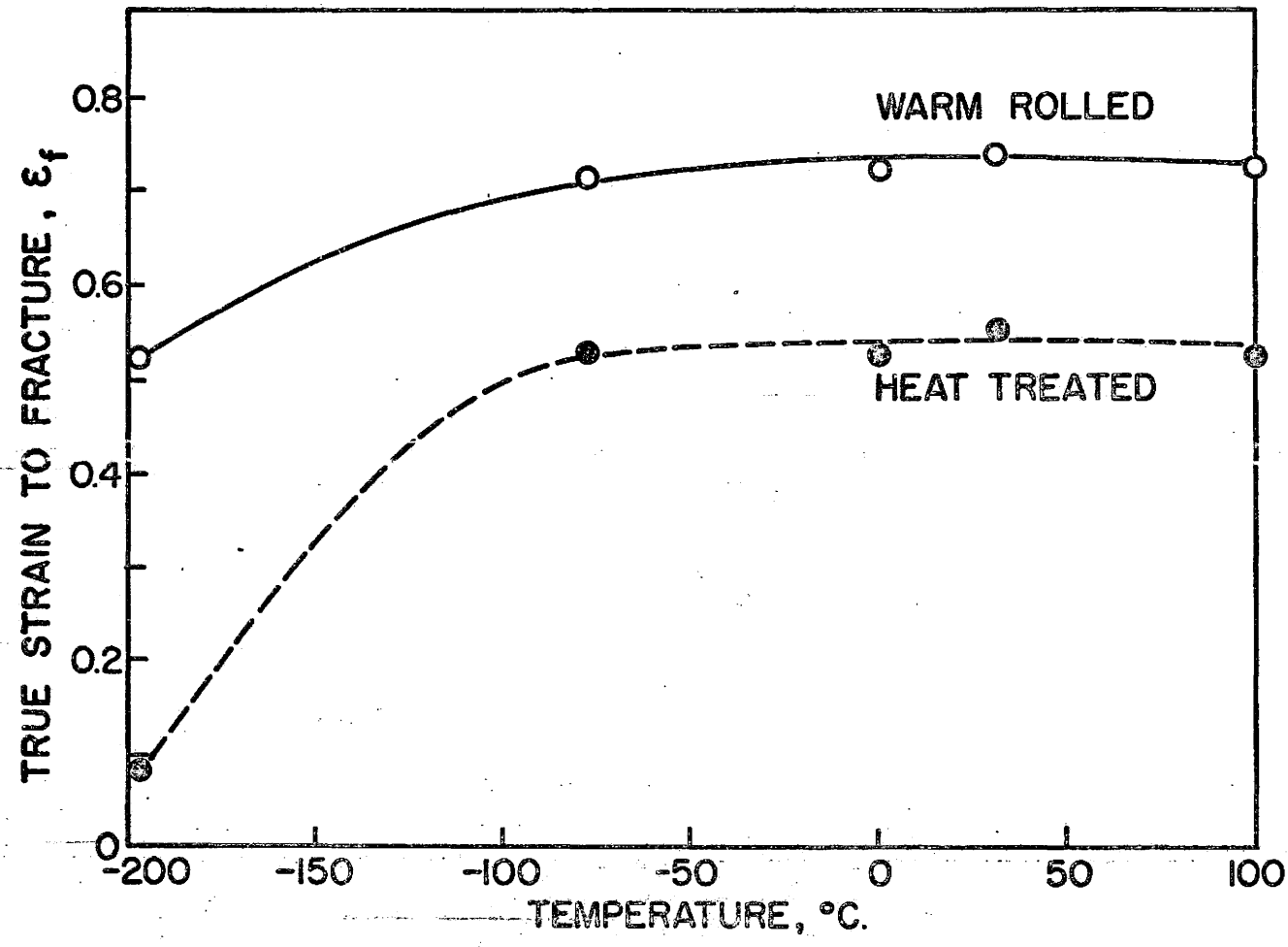

FIGURE 24. SAE 4340 .TRUE STRAIN TO FRACTURE .

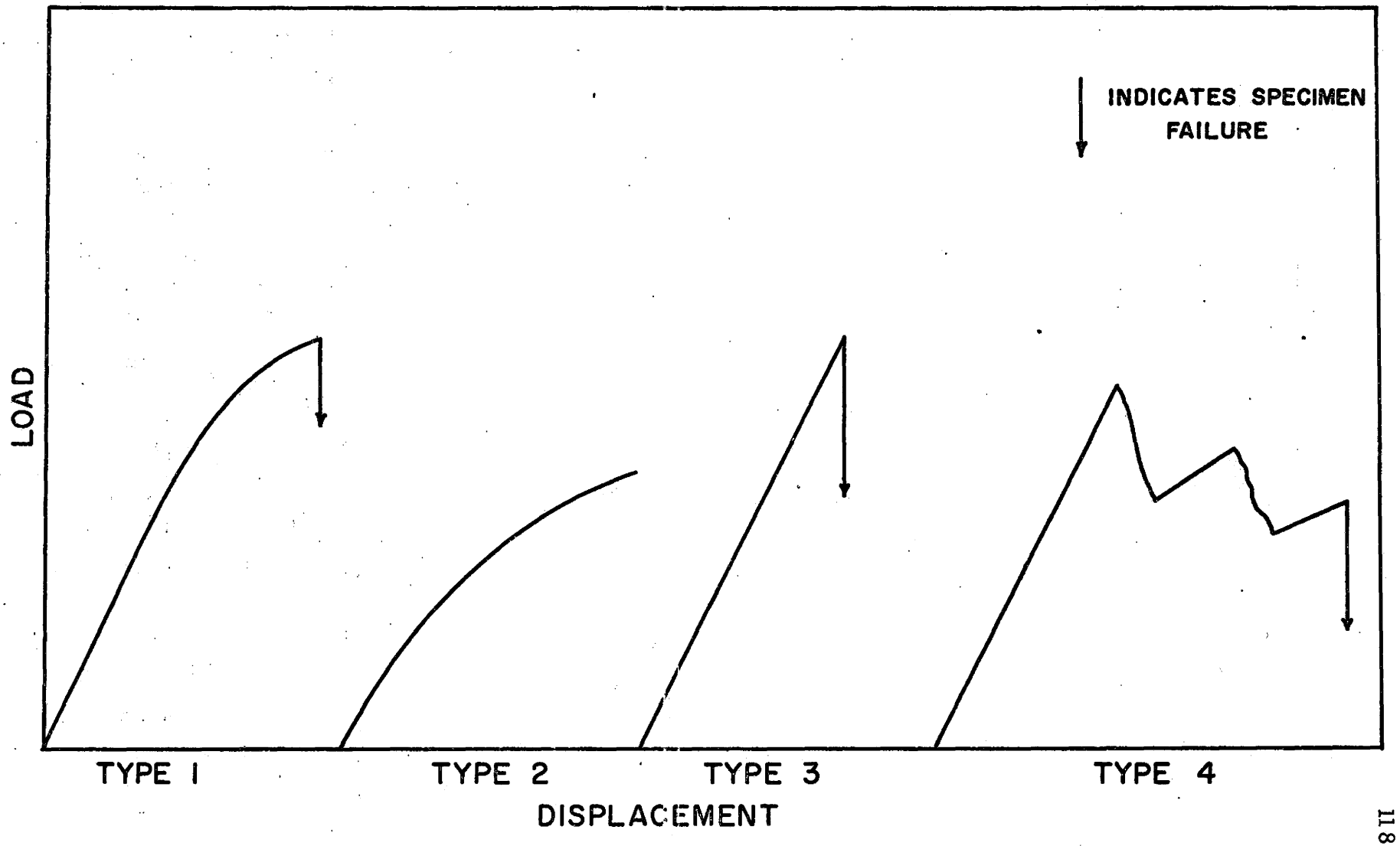

FIGURE 25. LOAD-DISPLACEMENT RECORDS.

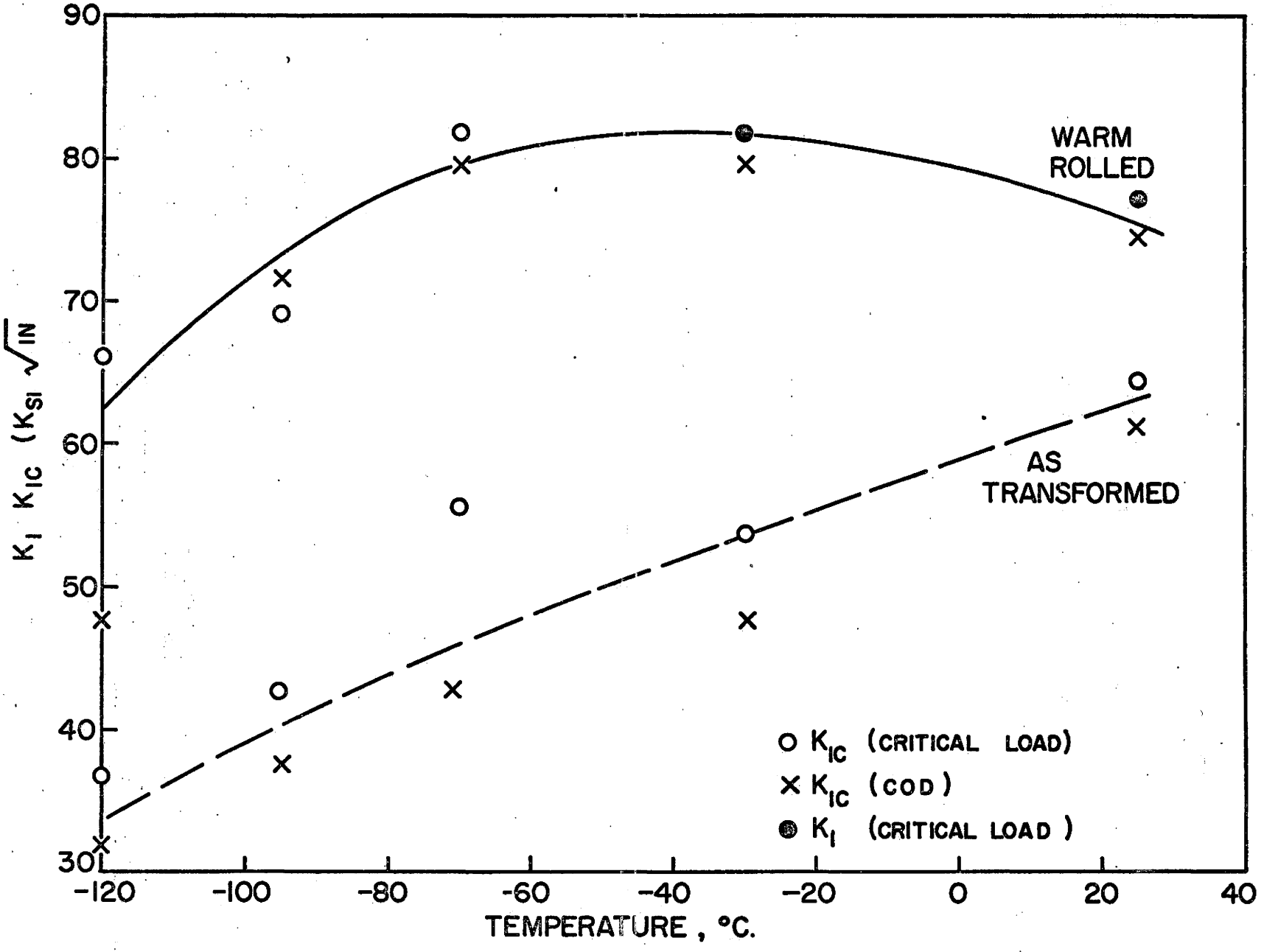
90
80
70
60
50
40
30
K_I K_{IC} ($K_{SI}\sqrt{IN}$
-120
-100
-80
-60
-40
-20
0
20
40
TEMPERATURE , °C.
WARM ROLLED
AS TRANSFORMED
O K_{IC} (CRITICAL LOAD)
× K_{IC} (COD)
● K_I (CRITICAL LOAD)

FIGURE 26 .

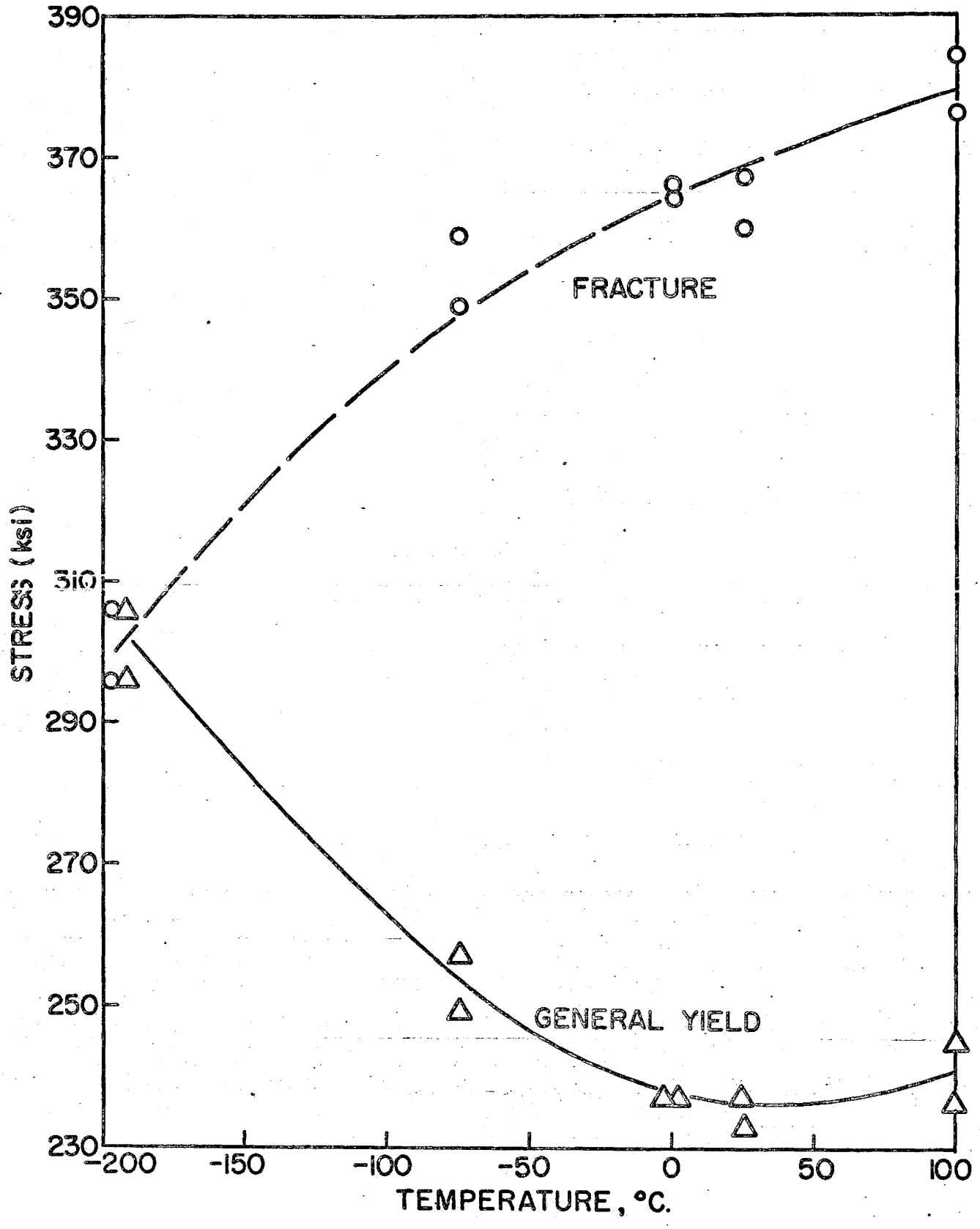

FIGURE 27. AS TRANSFORMED.

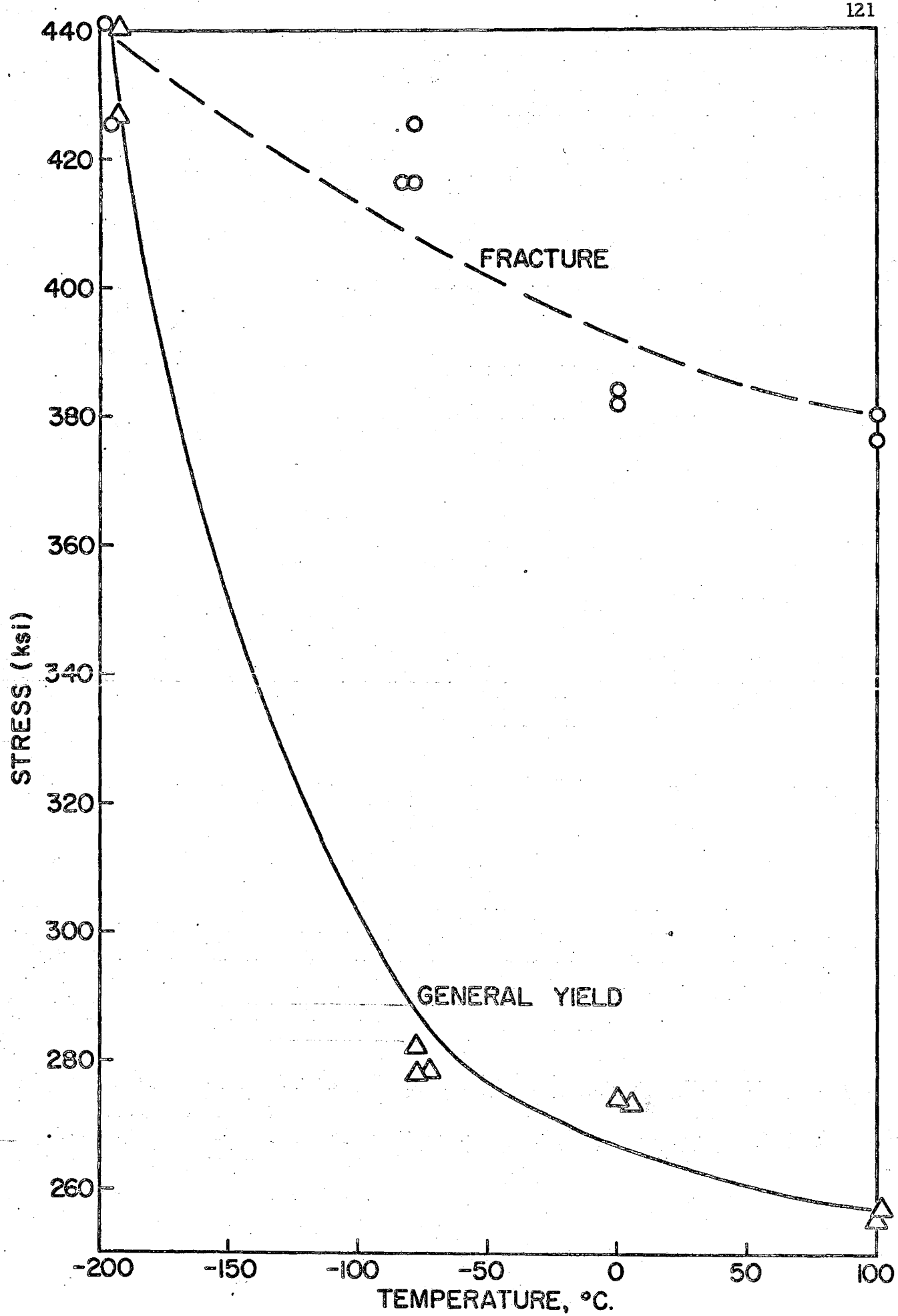

FIGURE 28. WARM ROLLED.

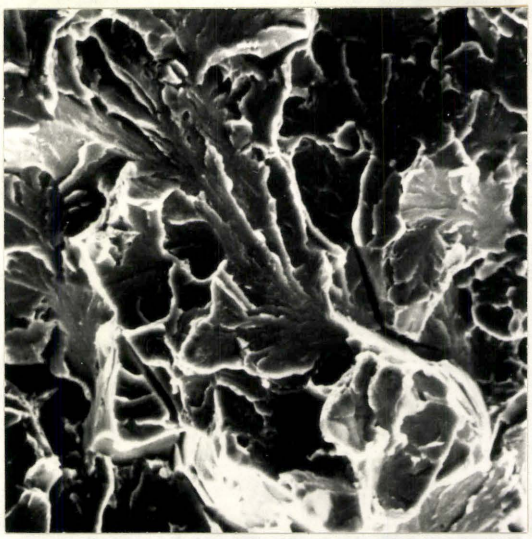

Figure 29. SAE 4340 AS TRANSFORMED
TEST TEMPERATURE -120°C
1000X
10 μ

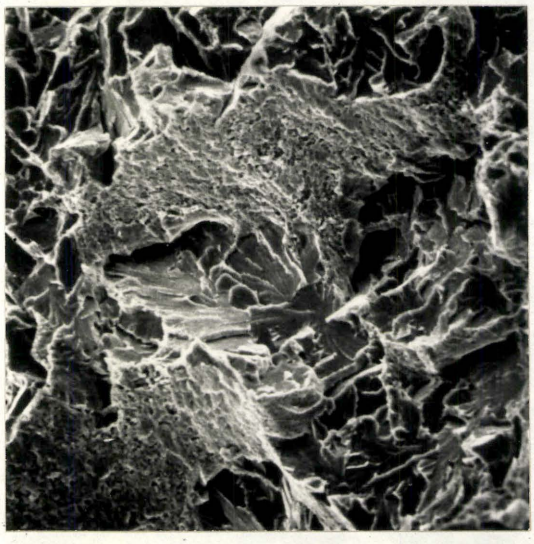

Figure 30. SAE 4340 WARM ROLLED
TEST TEMPERATURE -120°C
500X
10 μ

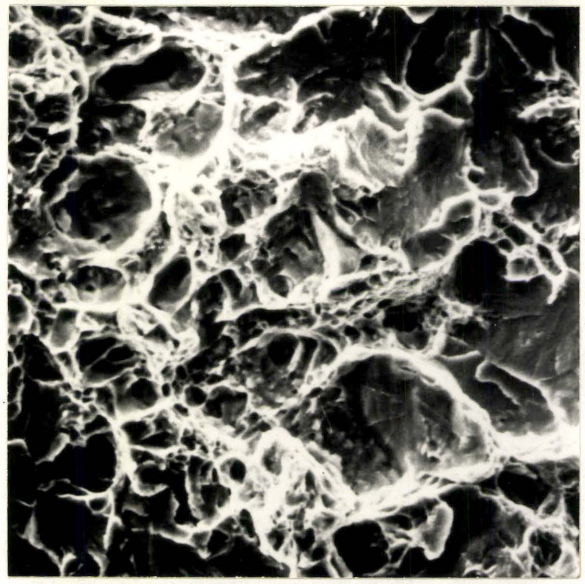

Figure 31. SAE 4340 AS TRANSFORMED
TEST TEMPERATURE 25°C
1000X
10 μ

Figure 32. SAE 4340 WARM ROLLED
TEST TEMPERATURE 25°C
200X

(a) 20X

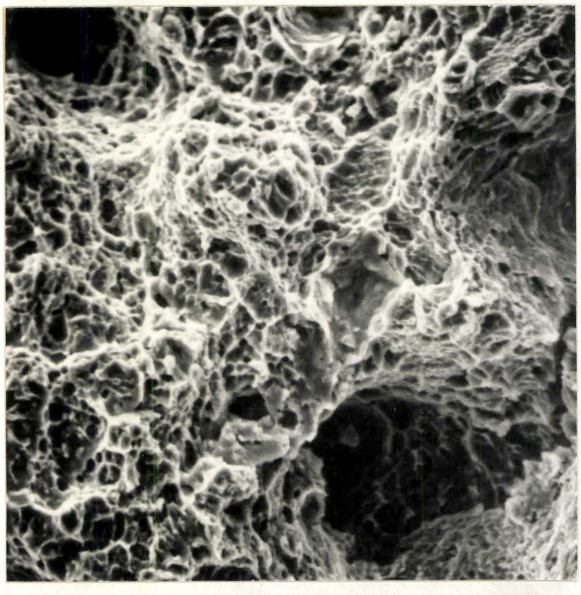

(b) 1000X

Figure 33. SAE 4340 WARM ROLLED.SLOW GROWTH REGION.TEST TEMPERATURE -70°C.

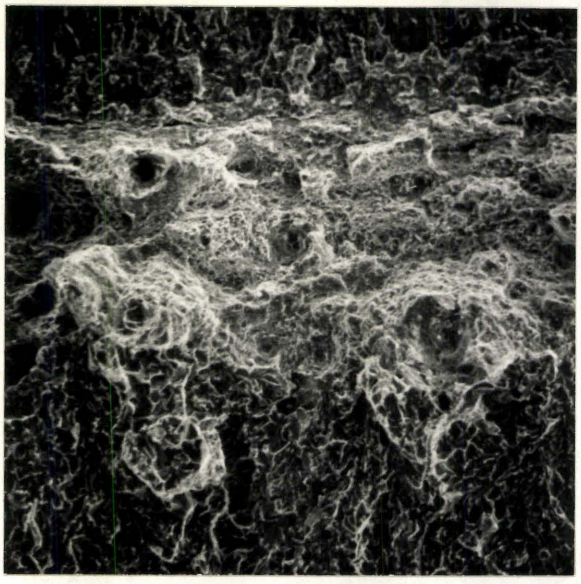

(a) 200X

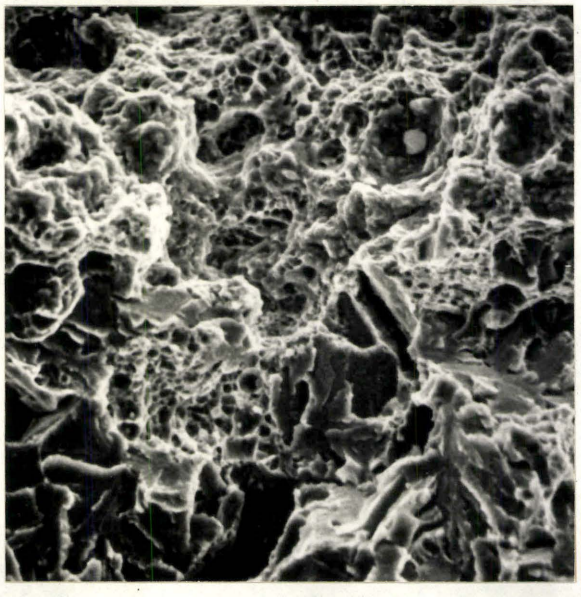

(b) 1000X

Figure 34. SAE 4340 WARM ROLLED.CRACK GROWTH SPECIMEN.TEST TEMPERATURE -70°C.

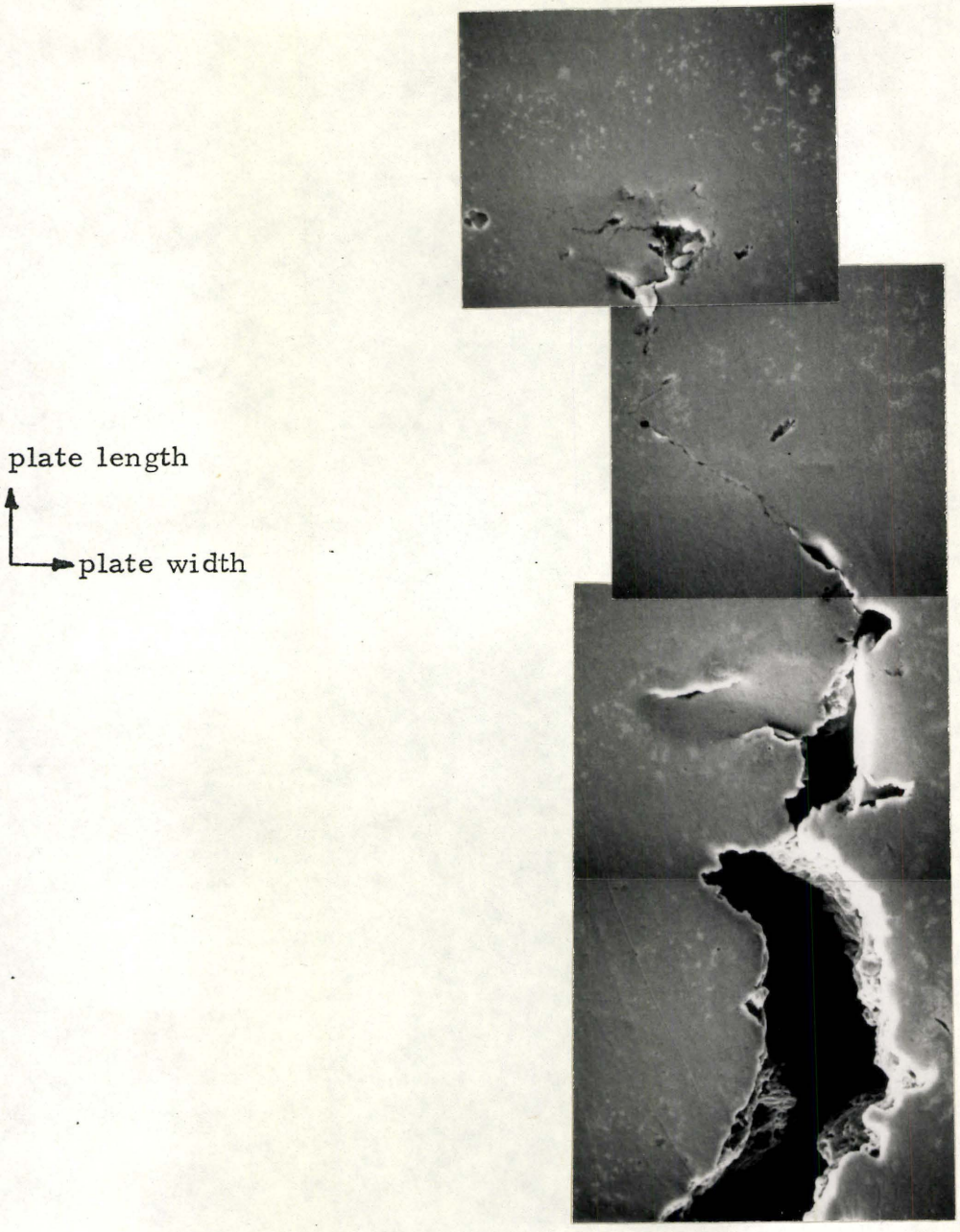

Figure 35. DEPTH: O

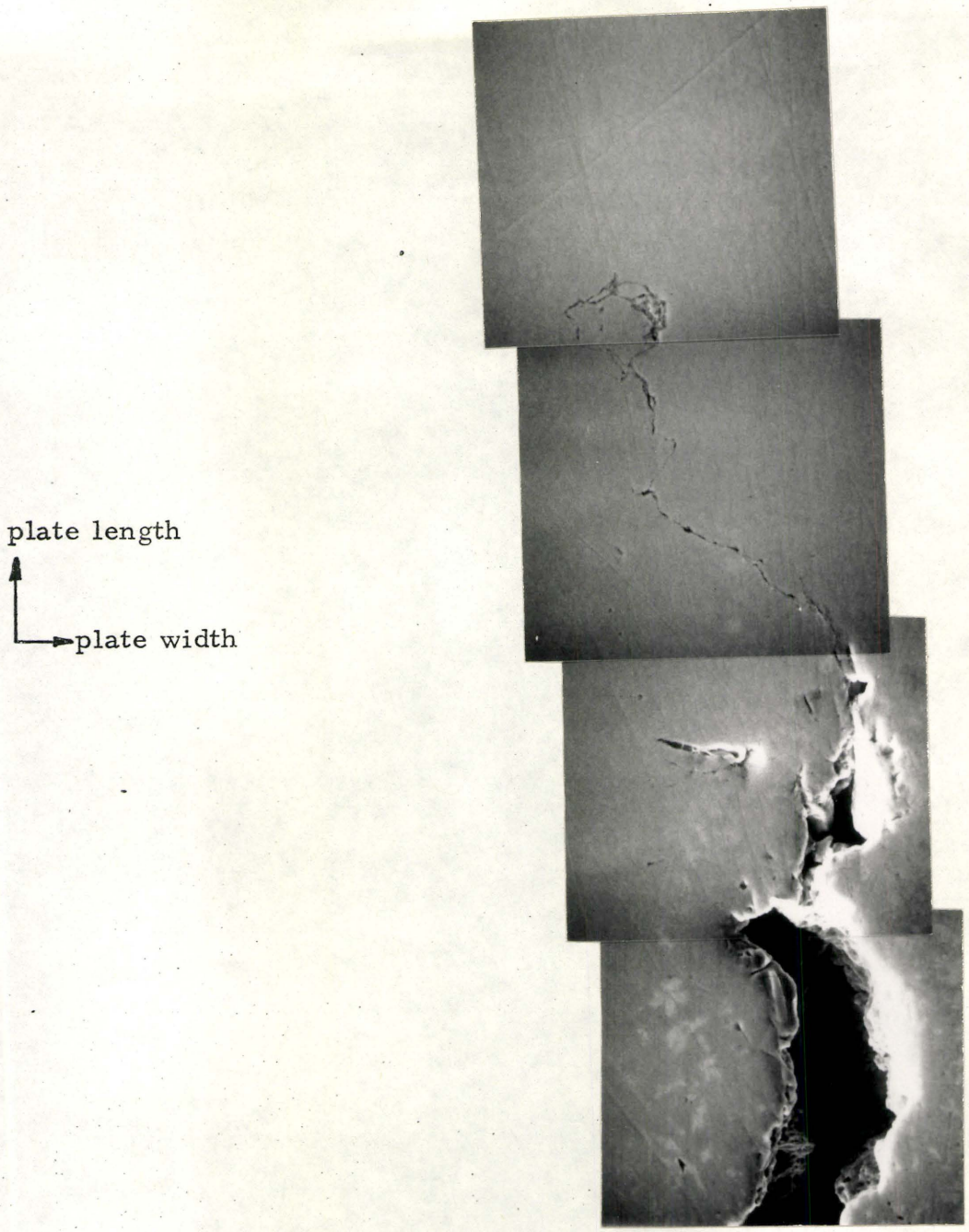

Figure 36. DEPTH: -30μ 1000X

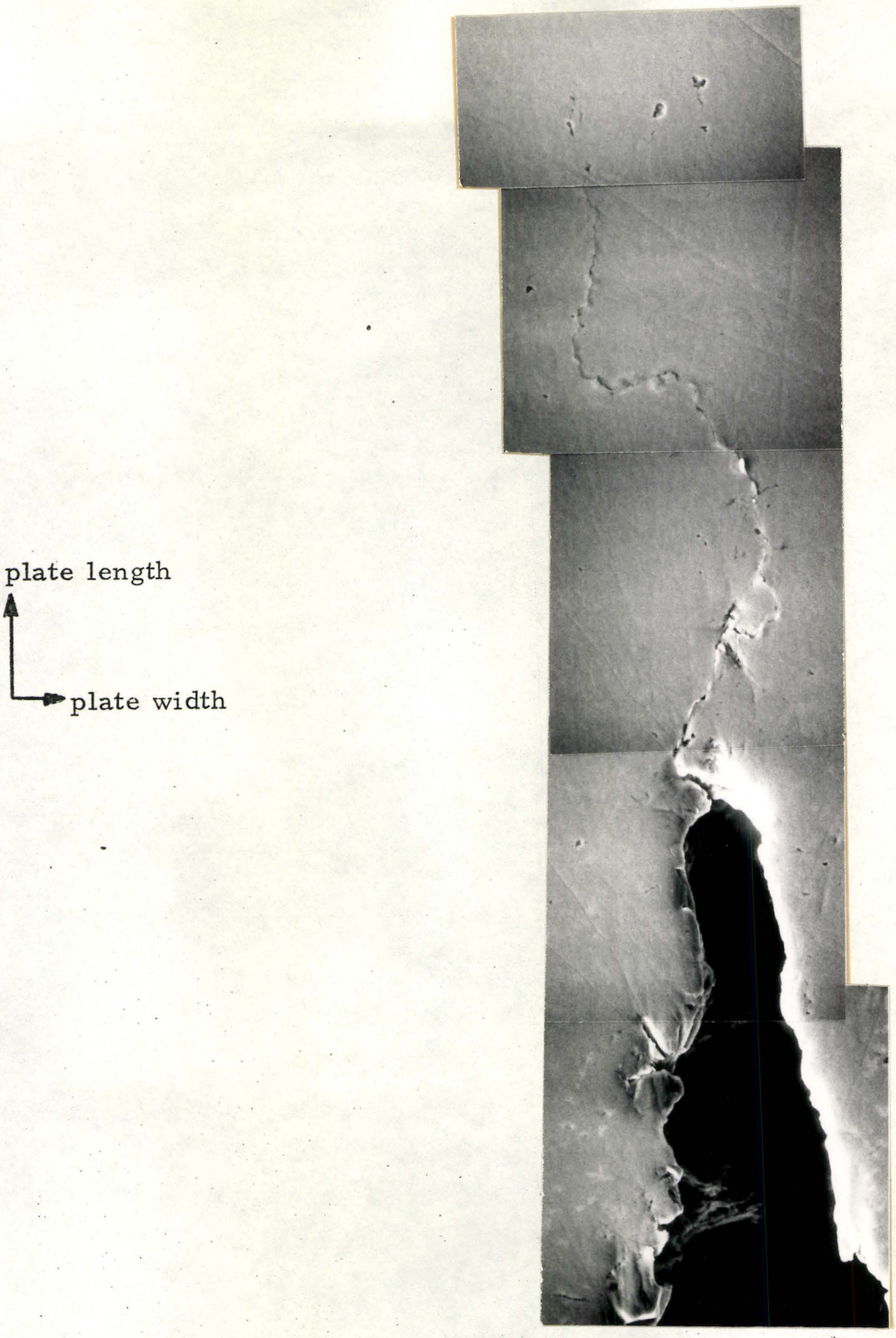

Figure 37. DEPTH: -60 μ 1000X

20 μ

Figure 38. DEPTH: -90 μ 1000X

20 μ

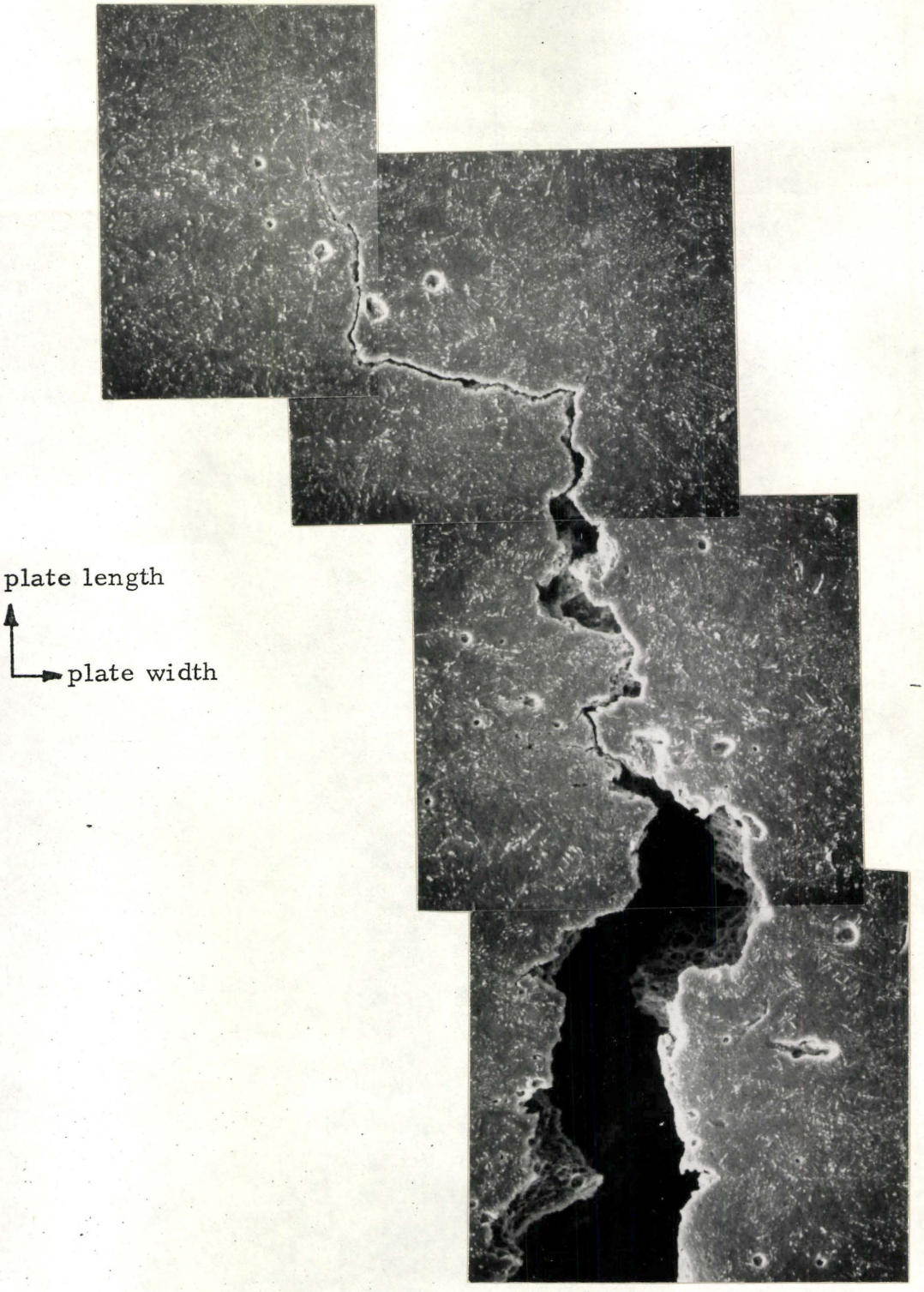

Figure 39a. DEPTH: -90 μ 1000X

20 μ

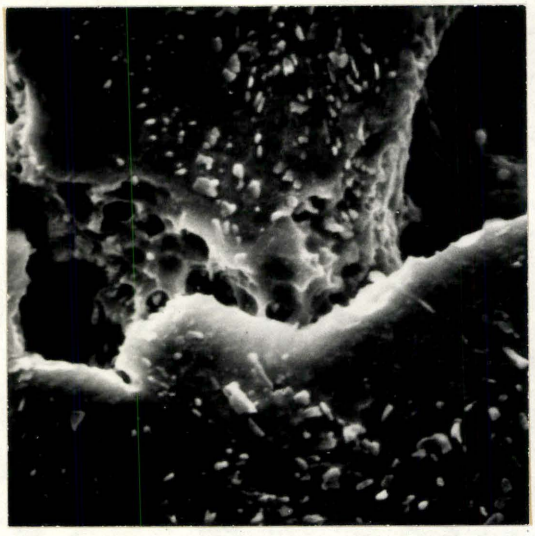

Figure 39b. SAE 4340 WARM ROLLED.CRACK GROWTH SPECIMEN. 5000X

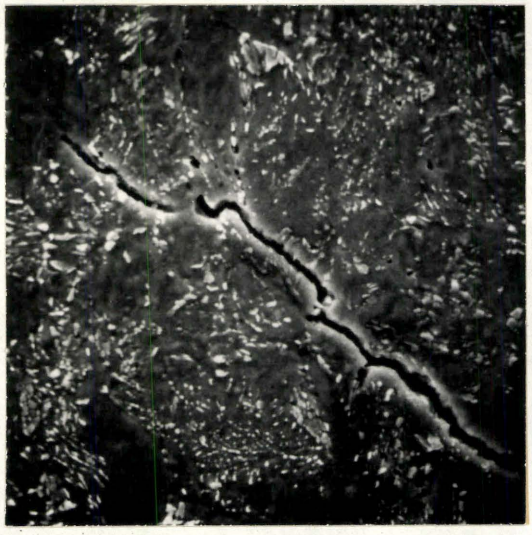

Figure 40. SAE 4340 WARM ROLLED.CRACK GROWTH SPECIMEN (NOTCH BEND), 1000X

SAE 4340
WARM ROLLED.

"TWO SURFACE" NOTCH
BEND SPECIMEN.
(TEST TEMP. -196°C)

10 μ

MICROCRACKS JUST BELOW
THE FRACTURE SURFACE.

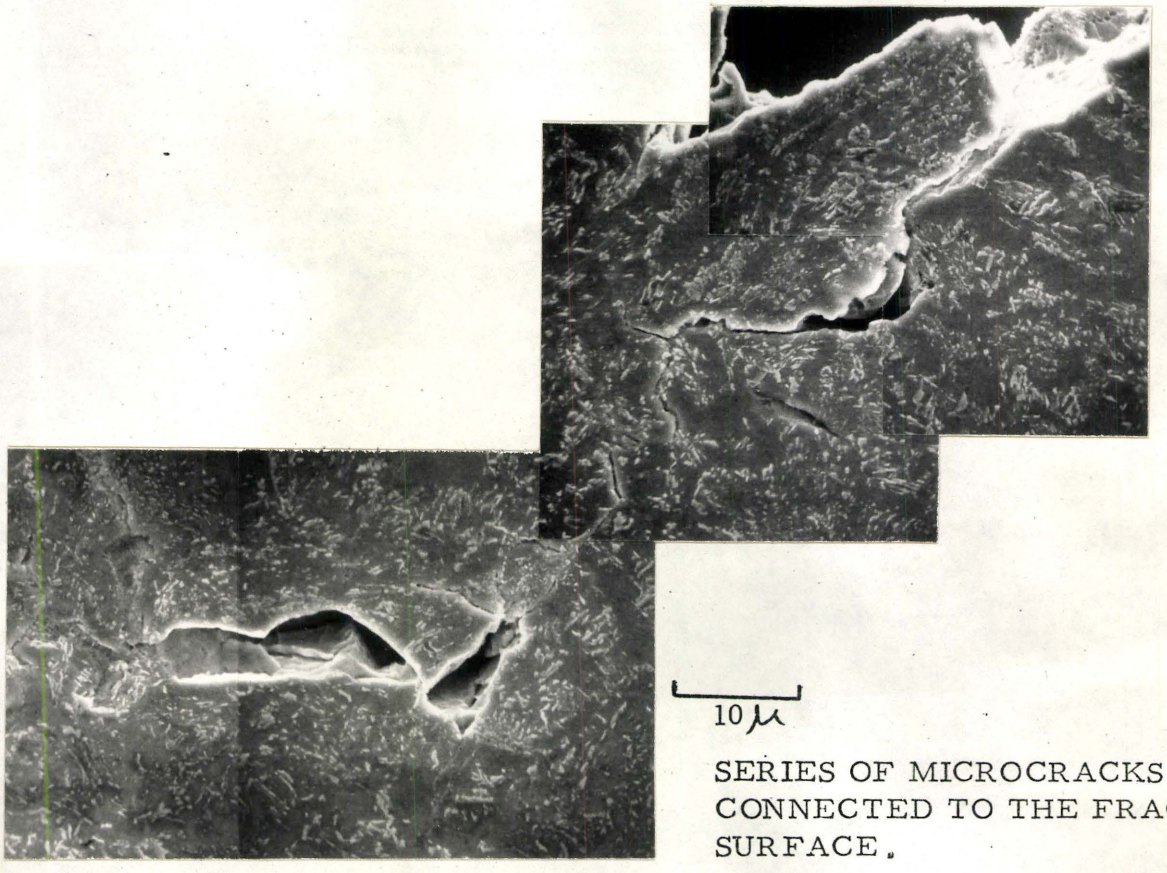

10 μ

SERIES OF MICROCRACKS
CONNECTED TO THE FRACTURE
SURFACE.

Figure 41.

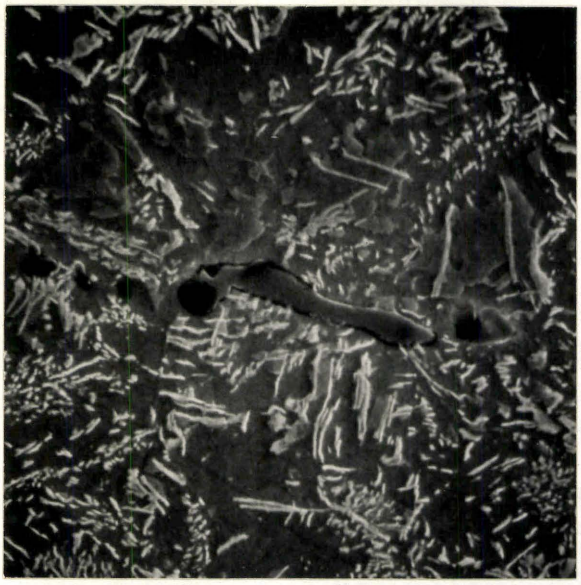

Figure 42. SAE 4340 AS TRANSFORMED. 2000X

TENSILE AXIS

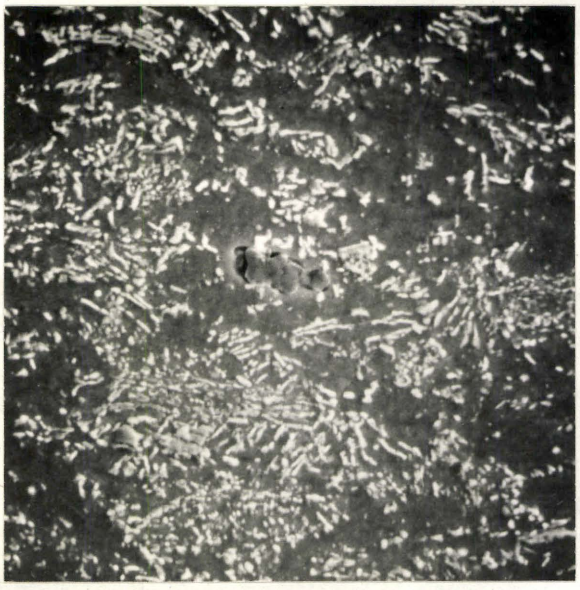

Figure 43. SAE 4340 WARM ROLLED. 2000X

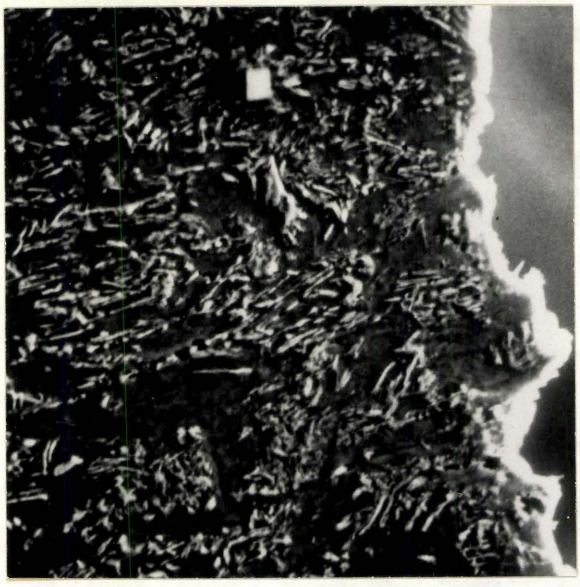

Figure 44. SAE 4340 AS TRANSFORMED.
1000X

TENSILE
AXIS

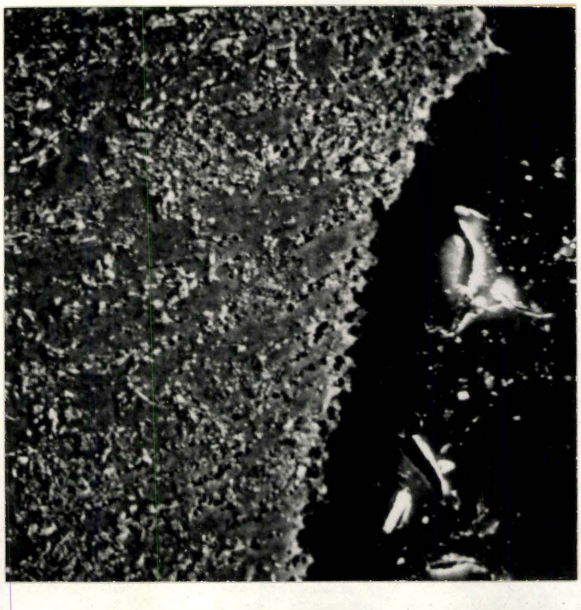

Figure 45. SAE 4340 WARM ROLLED.
1000X

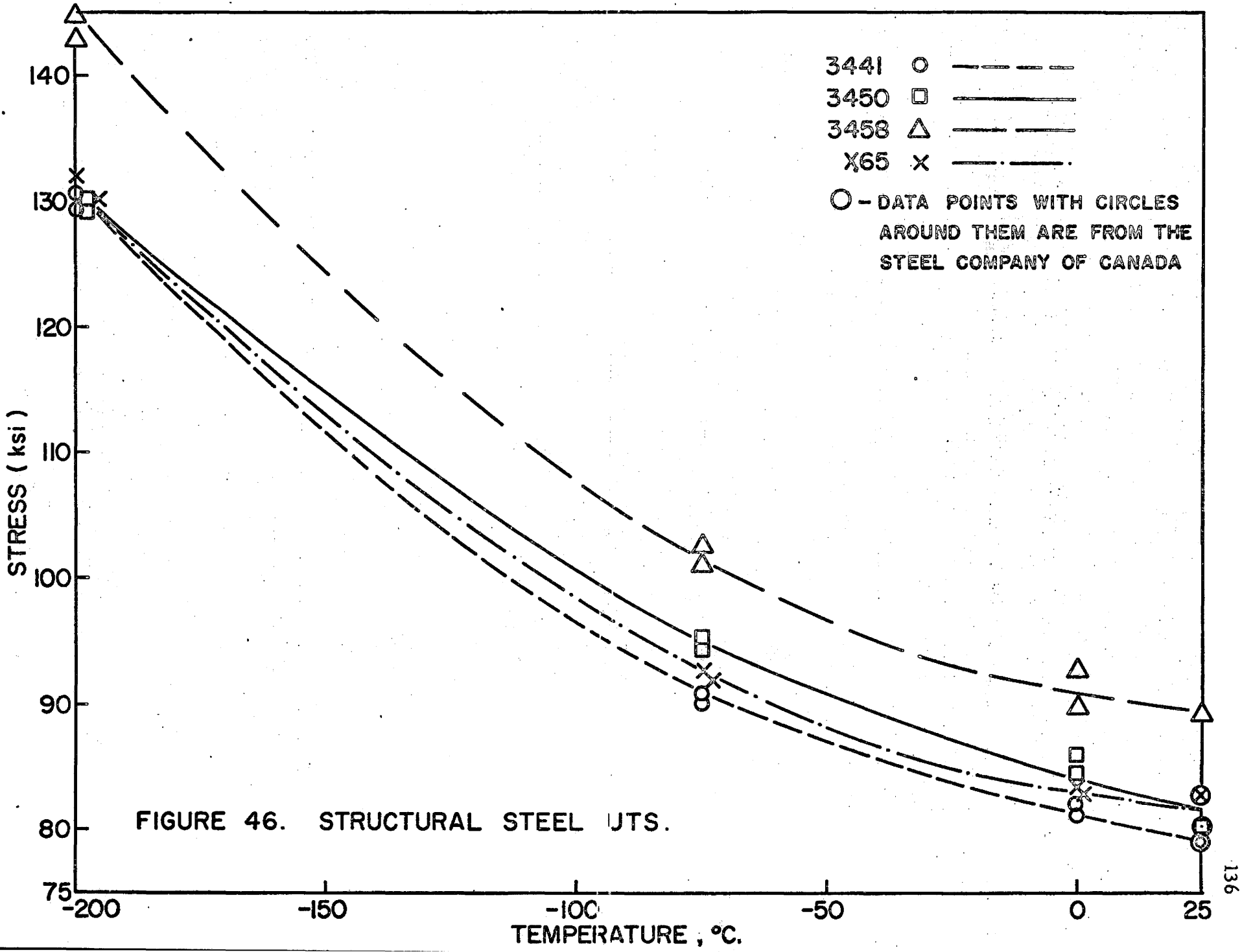

FIGURE 46. STRUCTURAL STEEL UTS.

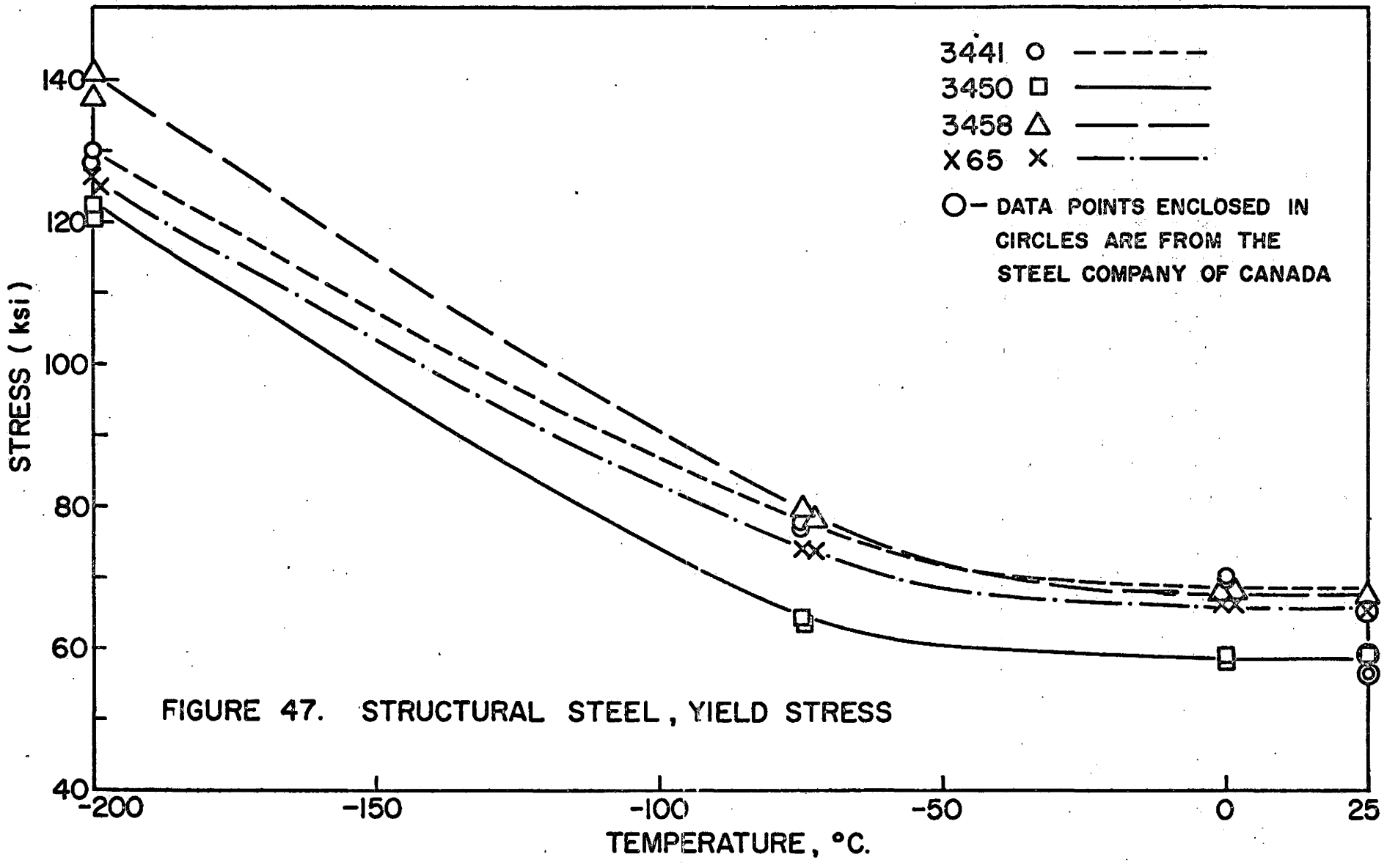

FIGURE 47. STRUCTURAL STEEL, YIELD STRESS

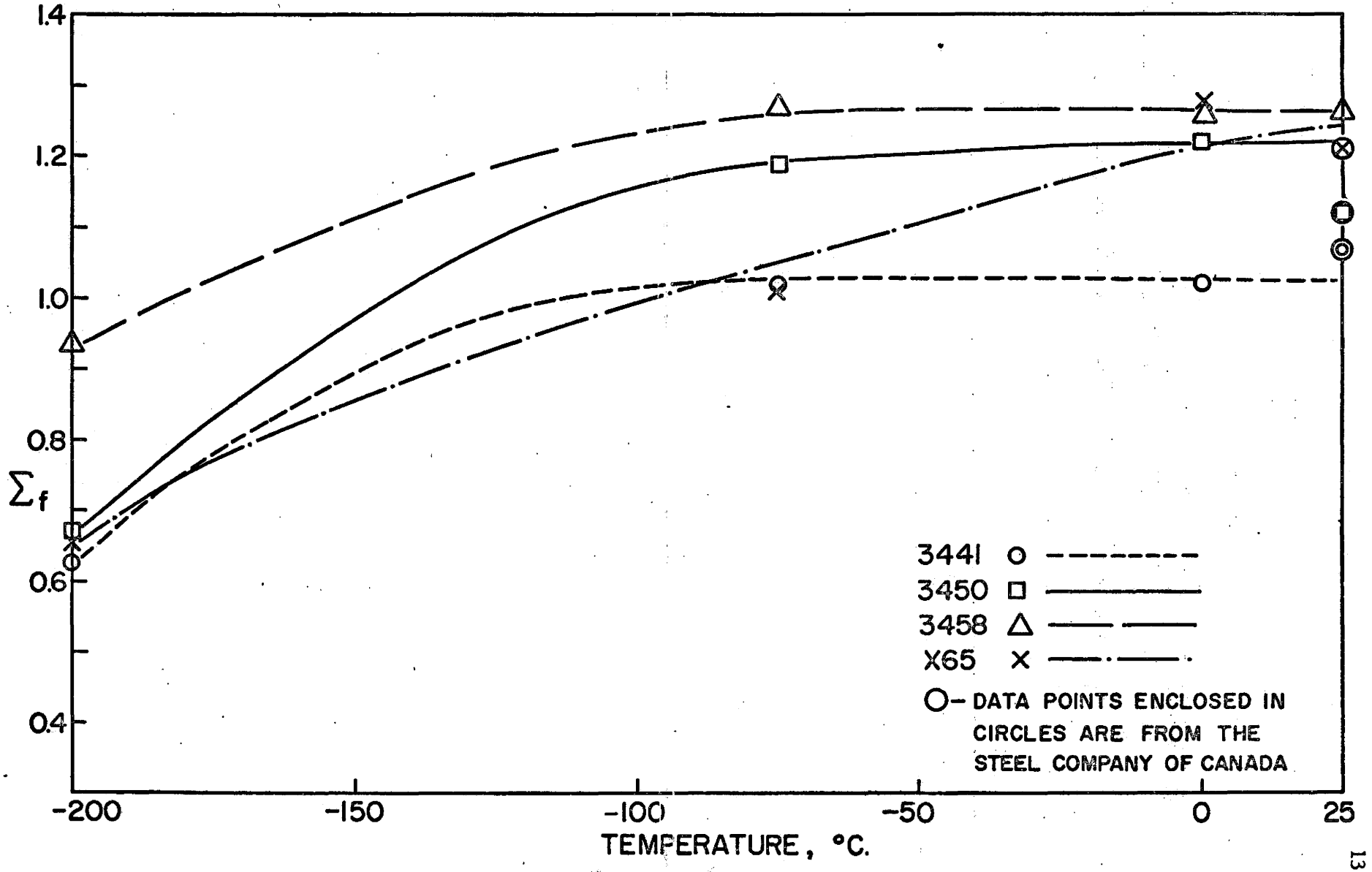

FIGURE 48. STRUCTURAL STEEL, FRACTURE STRAIN.

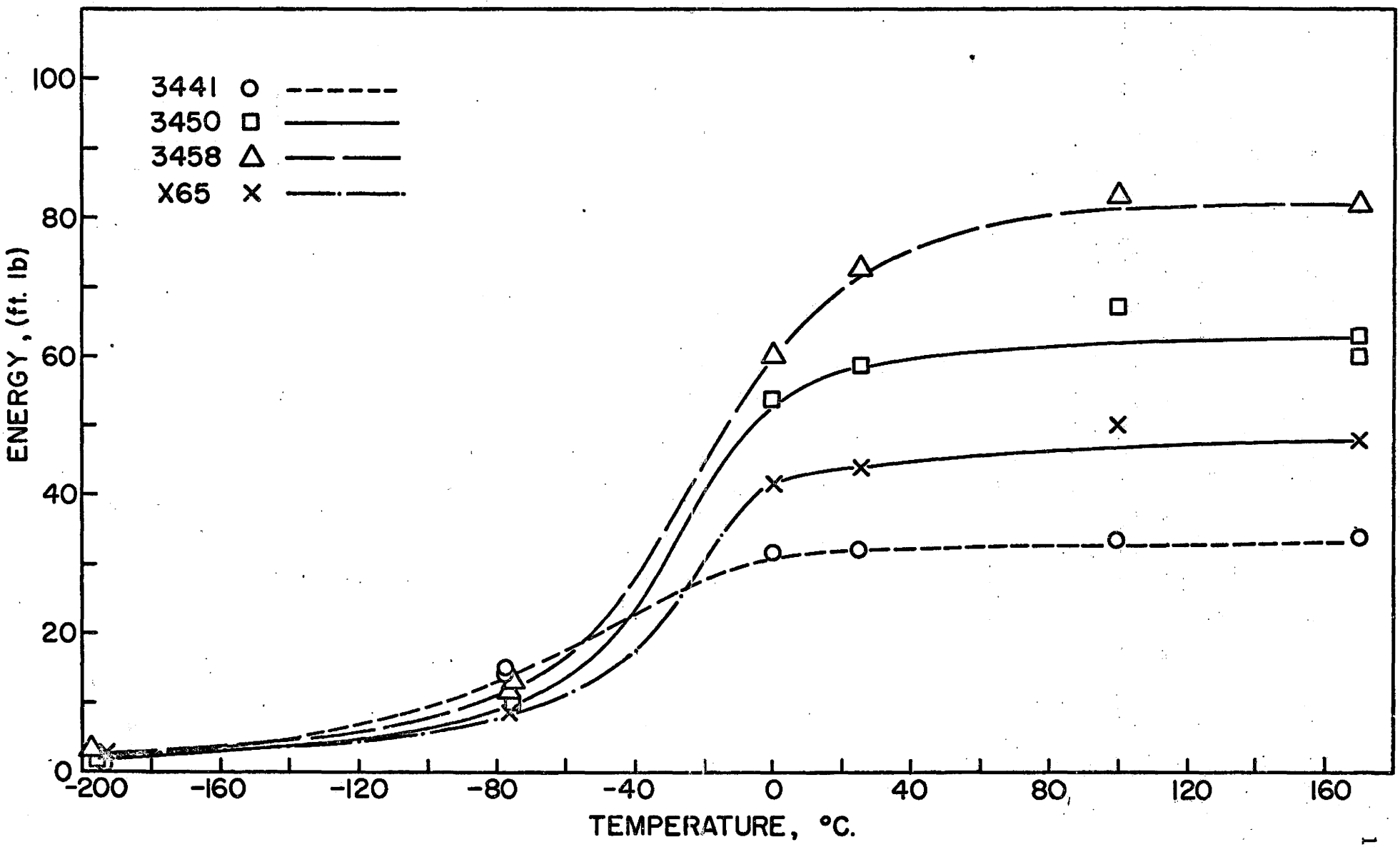

FIGURE 49. STRUCTURAL STEEL, TRANSITION DATA.

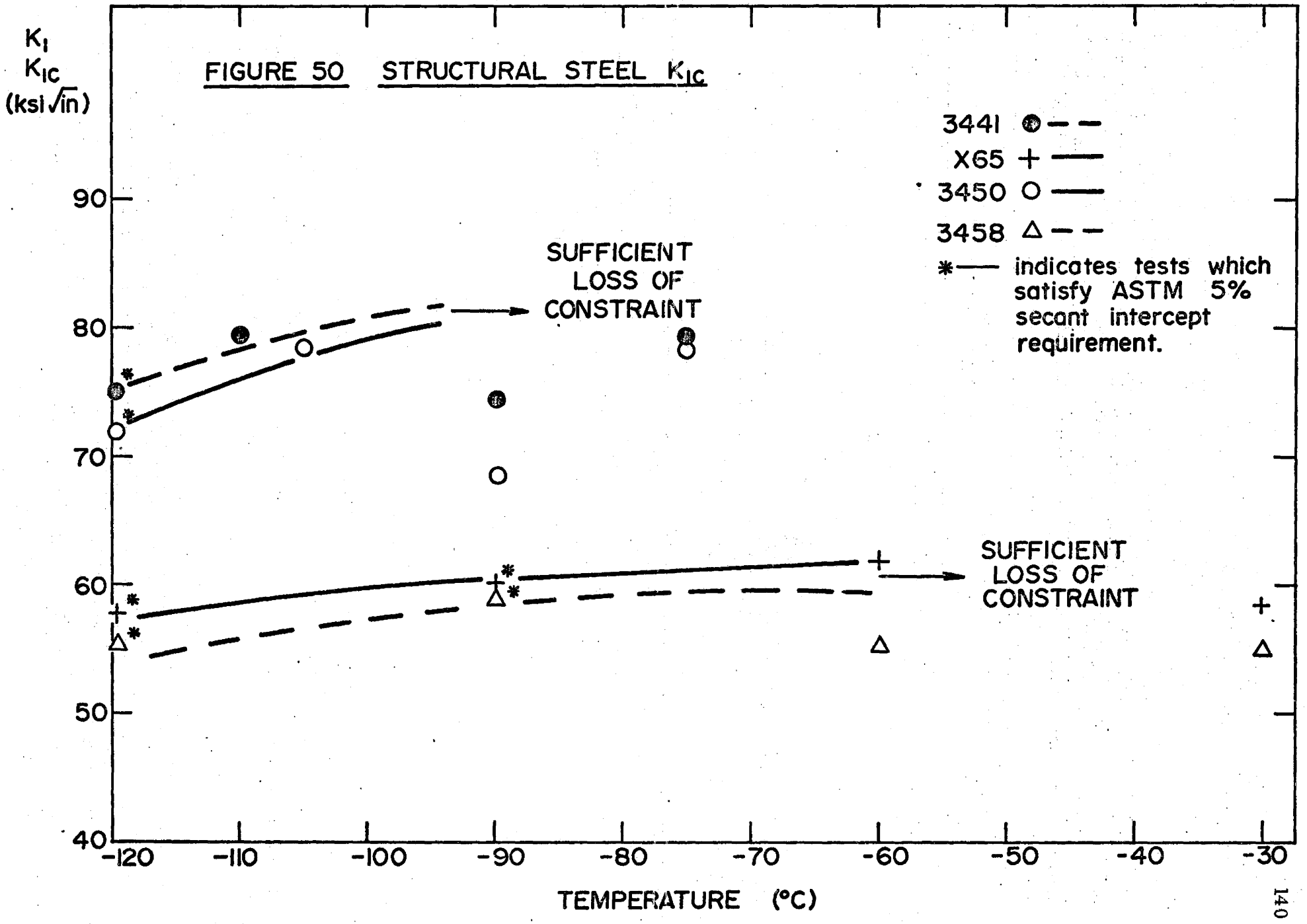
FIGURE 50 STRUCTURAL STEEL K_{IC}
K_I
K_{IC}
(ksi$\sqrt{in}$)
3441
X65
3450
3458
* indicates tests which satisfy ASTM 5% secant intercept requirement.
SUFFICIENT LOSS OF CONSTRAINT
SUFFICIENT LOSS OF CONSTRAINT
90
80
70
60
50
40
-120
-110
-100
-90
-80
-70
-60
-50
-40
-30
TEMPERATURE (°C)

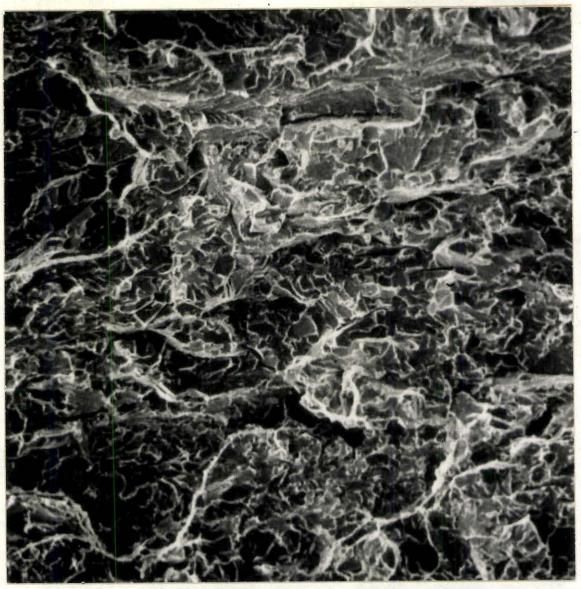

Figure 51a. HEAT 3441.
TEST TEMPERATURE -120°C.
200X

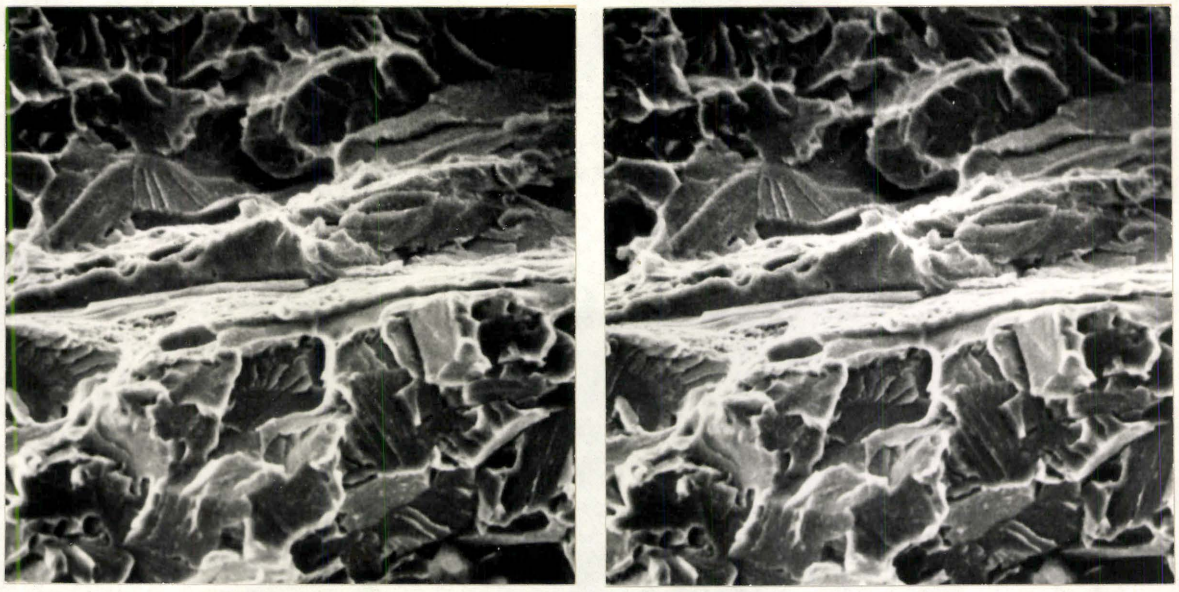

Figure 51b. HEAT 3441. STEREO PAIR. 1000X
TEST TEMPERATURE -120°C.

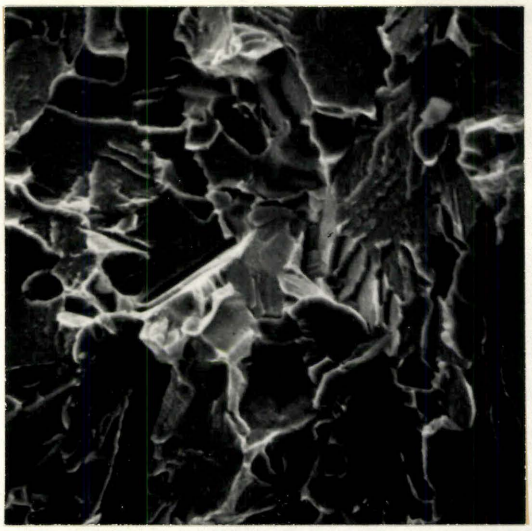

HEAT 3450.
Figure 52.

1000X

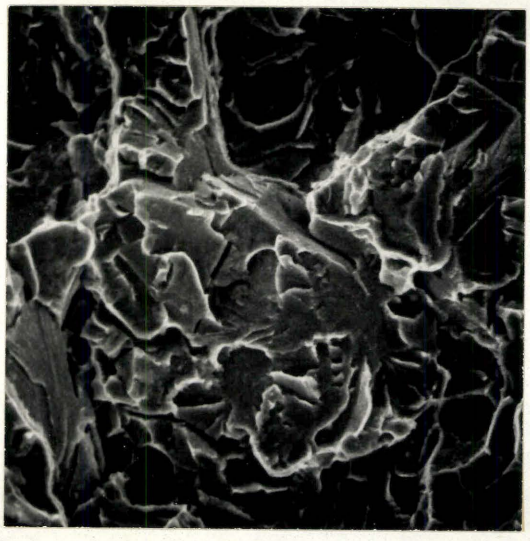

HEAT 3458.
Figure 53.

1000X

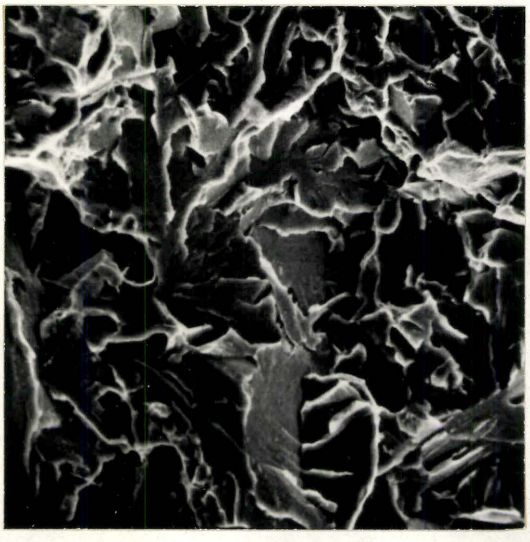

HEAT X65.
Figure 54.

1000X

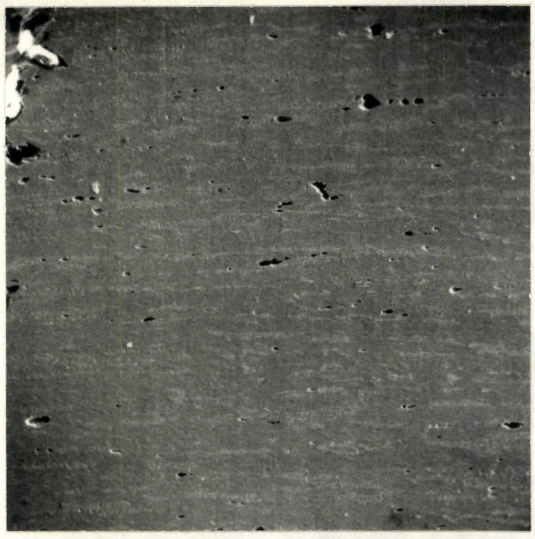

Figure 55. HEAT 3441.TENSILE SPECIMEN. TEST TEMPERATURE $0^{\circ}C$. 100X

Figure 56. HEAT 3441 . CRACK PROFILE VIEW. 500X

Figure 57a. HEAT 3441.
20X

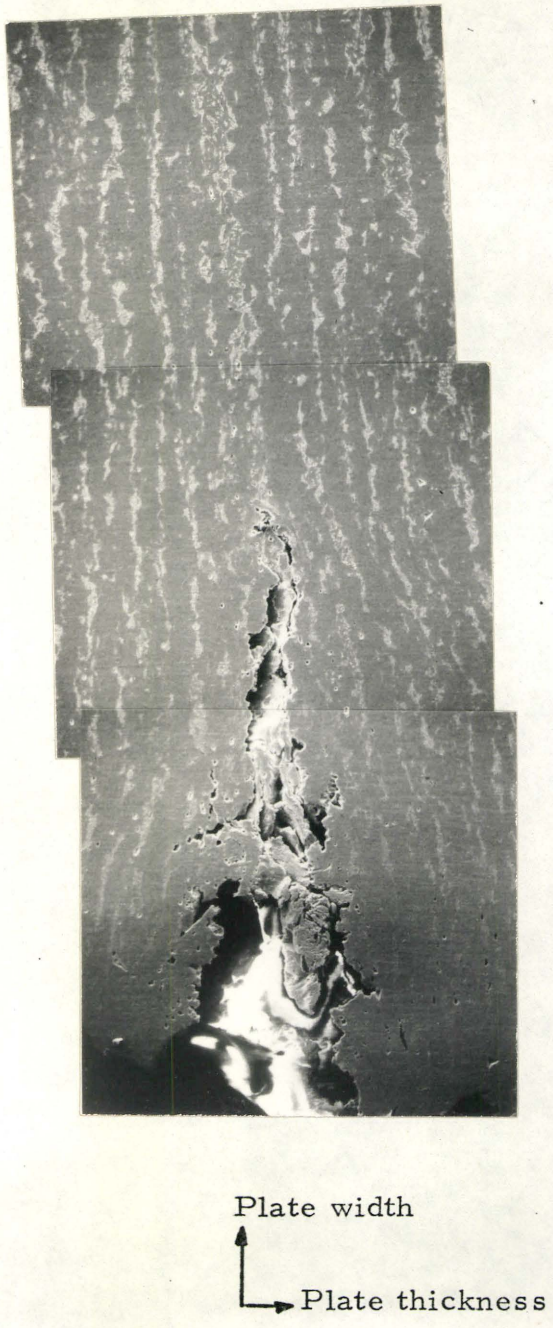

Figure 57b. HEAT 3441.
200X

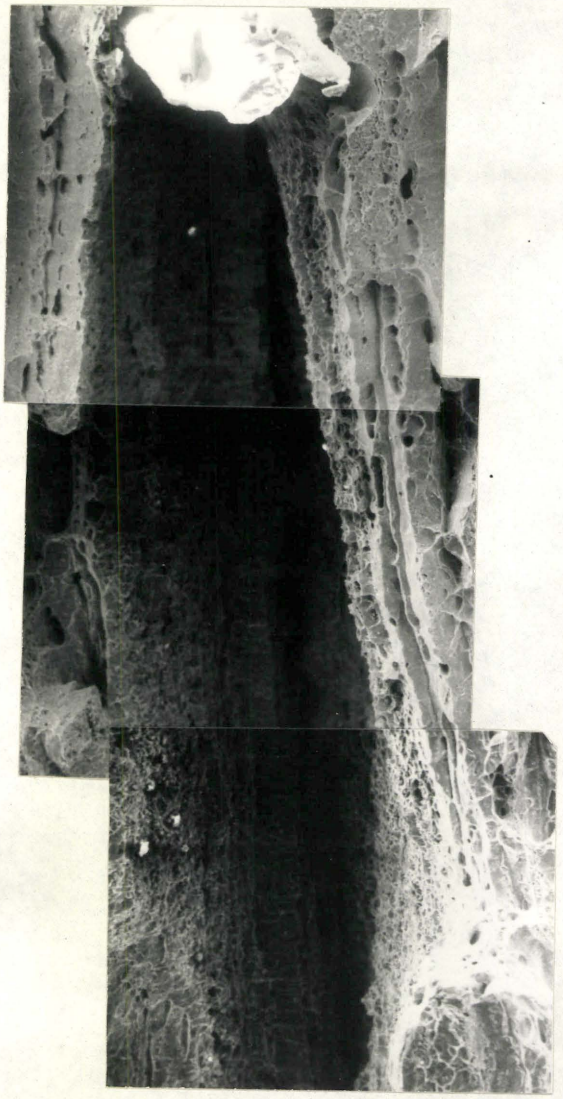

Figure 57c. HEAT 3441.
200X

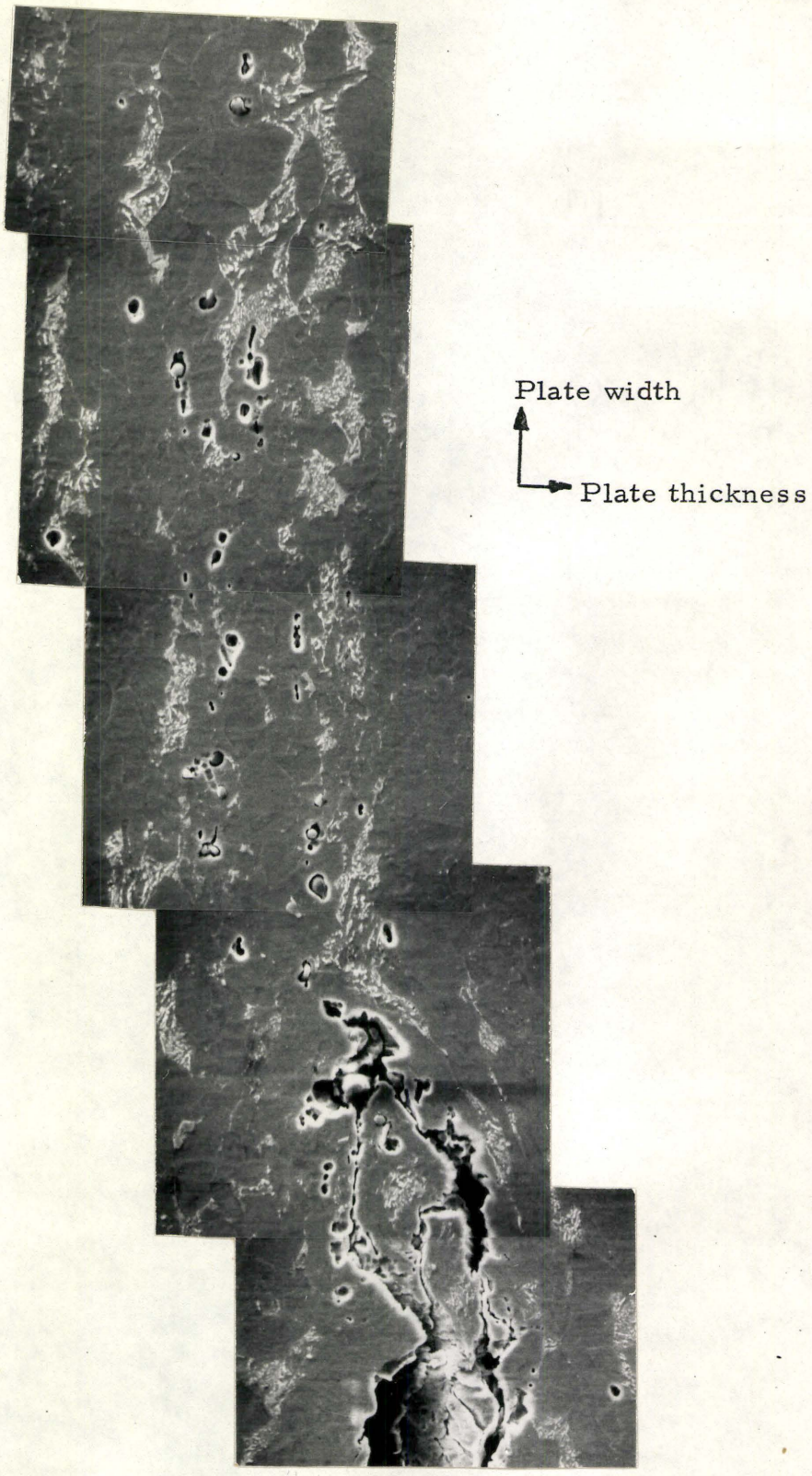

Figure 57d. HEAT 3441.
1000X

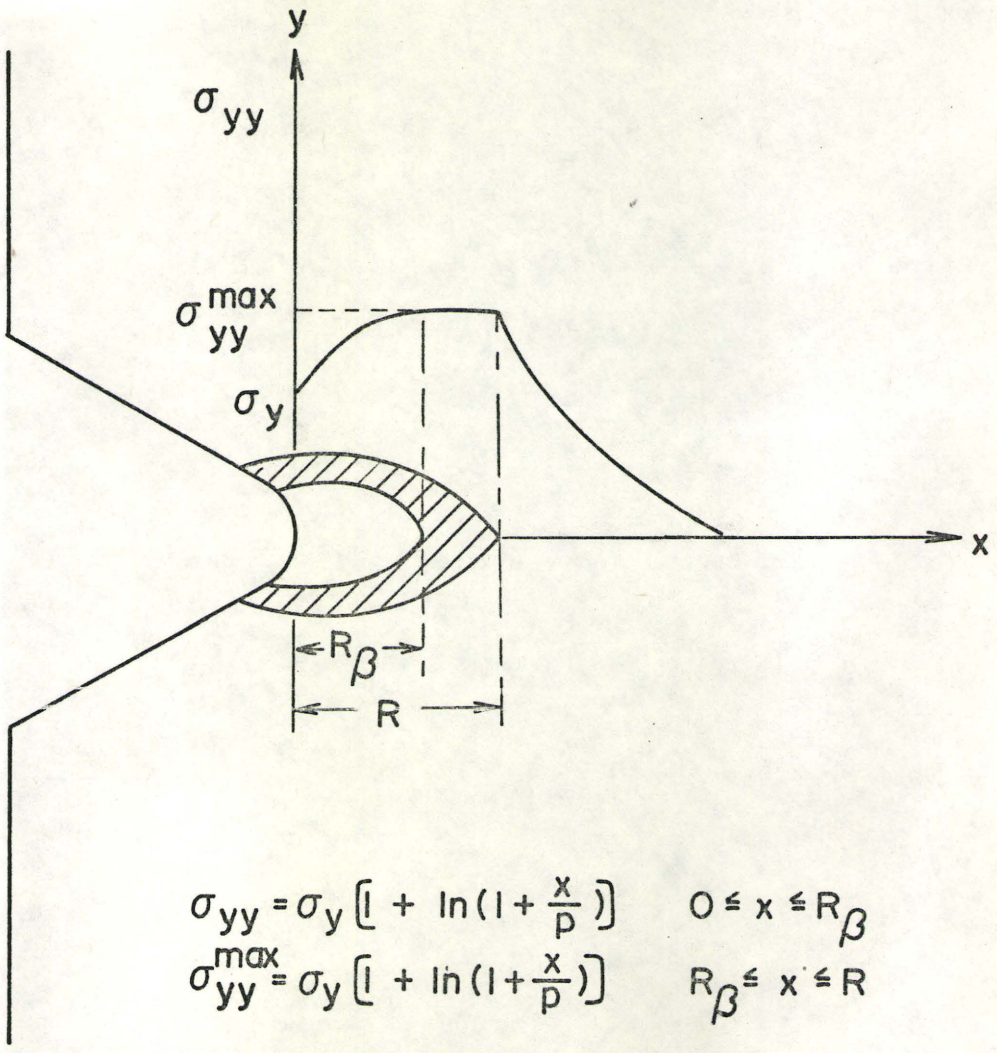

$$\sigma_{yy} = \sigma_y \left[1 + \ln\left(1 + \frac{x}{\rho}\right)\right] \qquad 0 \leq x \leq R_\beta$$

$$\sigma_{yy}^{max} = \sigma_y \left[1 + \ln\left(1 + \frac{x}{\rho}\right)\right] \qquad R_\beta \leq x \leq R$$

after Wilshaw, Rau & Tetelman (1968)

FIGURE 58

FIGURE 59 CRITICAL STRESS MODEL

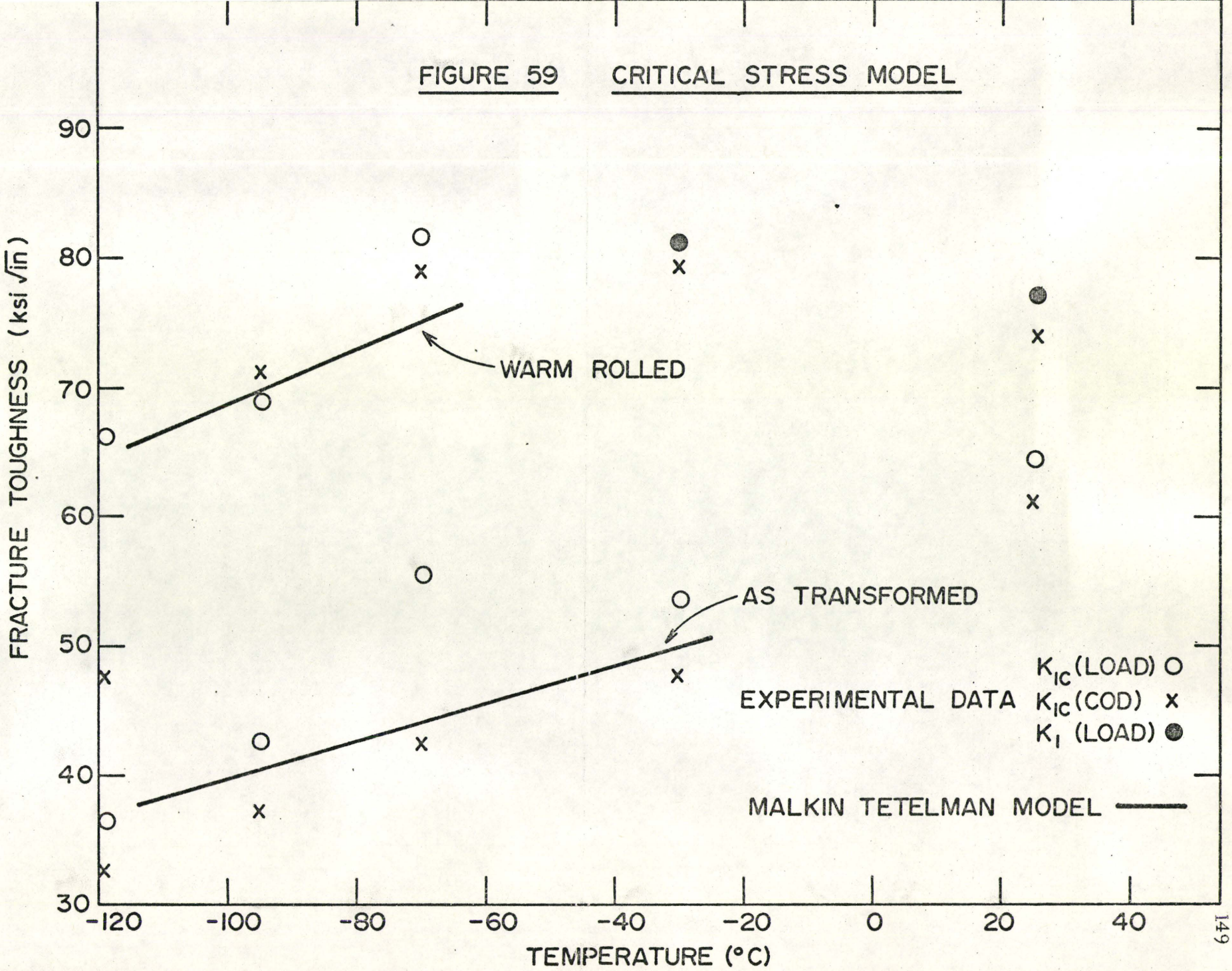

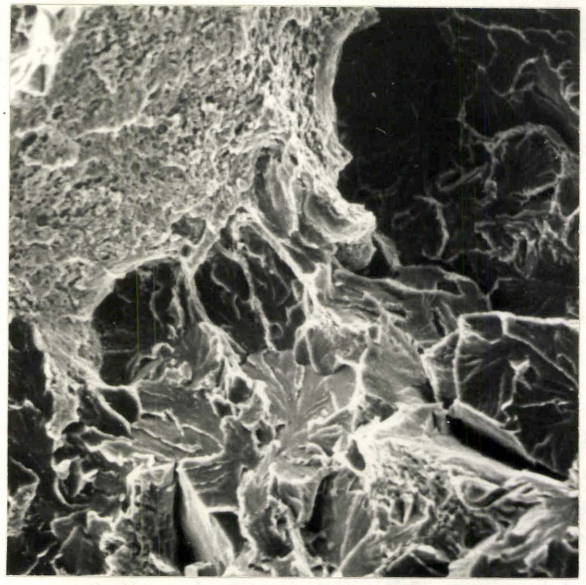

Possible microcracks

20 μ

Figure 60. SAE 4340 WARM ROLLED.
TESTED AT -120°C.